BUCKLING STRENGTH OF CIRCULAR TUBES IN SIGNS

DECEMBER 2004

COMMONWEALTH OF PENNSYLVANIA
DEPARTMENT OF TRANSPORTATION
350A07 02-01(C06)

Technical Report Documentation Page

1. Report No. FHWA-PA-2004-007-350A07-0201 (C06)	2. Government Accession No.	3. Recipient's Catalog No.
4. Title and Subtitle **Buckling Strength of Circular Tubes in Signs**		5. Report Date December 13, 2004
		6. Performing Organization Code
7. Author(s) Christopher J. Earls, Ph.D., P.E.; Brian M. Kozy, Ph.D., P.E.; and Rebecca L. Boyle		8. Performing Organization Report No. CE/ST 29
9. Performing Organization Name and Address University of Pittsburgh School of Engineering, Department of Civil & Environmental Engineering 949 Benedum Hall Pittsburgh, PA 15261-2294		10. Work Unit No. (TRAIS)
		11. Contract or Grant No. 350A07 (02-01 (C06)
12. Sponsoring Agency Name and Address The Pennsylvania Department of Transportation Bureau of Planning and Research Commonwealth Keystone Building 400 North Street, 6th Floor Harrisburg, PA 17120-0064		13. Type of Report and Period Covered Final Report, May 04, 2003 to November 30, 2004
		14. Sponsoring Agency Code

15. Supplementary Notes
COTR: Tom Macioce, P.E.

16. Abstract
The focus of this research report concerns a portion of long-span HSS trusses exhibiting geometry typical within PennDOT design contexts: the bearing region at the upright supports. In Pennsylvania, the subject standard detail involves curved steel saddle bearings and a structural Tee (ST) connected directly to a circular HSS chord wall in end bearing; both within close proximity to the open end of the HSS chord. In simple-span HSS trusses, the primary load path for the reaction force developed at the saddles is through the chord and directly into the first intermediate vertical member. Therefore, the overall bearing capacity is influenced by all of these elements. It must be noted that this region is being investigated locally without involving the global behavior of the entire truss (i.e. the more complicated member internal forces, resulting from effects of the structural system surrounding the connection detail, are not considered). The assumption here is that the effects of such additional internal forces are of small magnitude and hence will not significantly influence the local limit states under investigation. In considering this simplified loading condition, it is noted that while some research has been done on loads applied directly through the ends of open rolled sections; no previous work has been found in the literature concerning the cases of saddle-type bearings located at chord ends or an ST bearing on a circular HSS chord.

This research is executed through the application of sophisticated nonlinear finite element modeling techniques as well as full-scale experimental testing. The nonlinear finite element modeling employs experimentally verified modeling strategies (previously verified against available relevant tests on tubular structures found in the literature as well as those tests carried out as part of the current research) and forms the cornerstone for the parametric studies carried out in formulation of a design equation aimed at predicting sidewall crushing strength in circular HSS members. The full-scale tests carried out as part of the current research were executed using geometric configurations identified as either being most critical, or most germane, vis-à-vis initial parametric finite element analyses. Through the use of finite element modeling studies that are supported and verified with the judicious use of full-scale experimental testing, a very large sample space of geometric combinations are economically considered. This is of pivotal importance to the research since a design equation must be applicable to all reasonable geometric configurations that are likely to arise in practice.

17. Key Words	18. Distribution Statement
Buckling, circular tubes, HSS trusses, predicting capacity, finite element modeling, modeling techniques, bearing capacity equations.	No restrictions. This document is available from the National Technical Information Service, Springfield, VA 22161

19. Security Classif. (of this report)	20. Security Classif. (of this page)	21. No. of Pages	22. Price
Unclassified	Unclassified	155	

Form DOT F 1700.7 (8-72) Reproduction of completed page authorized

BUCKLING STRENGTH OF CIRCULAR TUBES IN SIGN STRUCTURES

FINAL REPORT

Prepared for

Commonwealth of Pennsylvania
Department of Transportation

By

Christopher J. Earls, Ph.D., P.E.
Brian M. Kozy, Ph.D., P.E.
Rebecca L. Boyle

University of Pittsburgh
Department of Civil and Environmental Engineering
Report CE/ST 29

December 2004

This work was sponsored by the Pennsylvania Department of Transportation and the U.S. Department of Transportation, Federal Highway Administration.

TABLE OF CONTENTS

LIST OF TABLES

LIST OF FIGURES

1.0 BACKGROUND

The Bridge Quality Assurance Division of the Pennsylvania Department of Transportation's (PENNDOT's) Bureau of Design has indicated concern regarding the safety and economy of certain design standards when applied to long-span tri-chord sign structures. Specifically, the Bureau of Design has expressed concern about the ability of existing specifications to accurately predict the buckling strength of circular tubes in overhead sign trusses at locations near supports where vertical web members connect to the horizontal hollow circular chord members.

While the AISC *Load and Resistance Factor Design Specification for Steel Hollow Structural Sections* (2000) treats a connection geometry related to that which is typical in long-span tri-chord sign structures, the portability of the technique, as currently promulgated by AISC, is not clear since the tri-chord sign geometries at issue fall outside the scope of the experimental testing database that was used to verify the analytical strategy adopted by AISC. Furthermore, the AISC loading condition is not precisely the same as the case of a Structural Tee (ST) bearing on a circular Hollow Structural Section (HSS) sidewall in the vicinity of the open end. Nonetheless, the AISC method holds promise as a point of departure for treating the problem at issue.

In contrast to the AISC specification (2000), is the AASHTO *Standard Specifications for Structural Supports for Highway Signs, Luminaires and Traffic Signals, 4th Edition* (2001): ASSHTO is silent regarding the issue of circular HSS side-wall buckling under the action of concentrated loads at joints or bearings. Implicit in AASHTO's lack of treatment of this potential failure mode is the notion that such a failure cannot occur. This implicit assumption on the part of AASHTO has unfortunately been shown to be in error: a recent failure in PENNDOT Engineering District 6-0 in which a tri-chord sign structure with a 180-ft span, experienced just such a crushing failure at the column connections during final erection attests to the seriousness of AASHTO's omission. As result of the failure in District 6-0, a similar sign structure (with a 140-ft span), scheduled to be erected in District 12-0 was delayed while modifications were

made to the connection region details to guard against the occurrence of side-wall crushing. While the District 6-0 and 12-0 structures were modified to address the side-wall buckling limit state, the approaches used were different. The District 6-0 design retrofit consisted of cutting out the damaged section of HSS in each lower chord connection side and installing a new piece with a 100 percent greater wall thickness than the original piece, in addition to containing a series of two annular plate stiffeners at each tower seat location. A further corrective measure within the District 6-0 retrofit was to employ curved saddles upon which the HSS bear (thus increasing overall contact area of the lower chord, at the column attachment, beyond what was originally specified). In the case of the District 12-0 sign, the HSS chord ends were filled with non-shrink grout and seated on a series of fabricated saddles instead of bearing directly on the flat surface of a standard seat connection.

While the retrofits in District 6-0 and 12-0 are believed to be adequate for preventing any additional problems with crushing and side-wall buckling of the portion of the HSS wall in bearing with the column seat, a more rigorous understanding of the mechanics in the connection region is sought in order that more economical and reliable design provisions can be prescribed, both within the context of the AASHTO Specification (AASTHO 2001) and PENNDOT's BD-644M (PENNDOT 2003). Furthermore, now that the tube crushing failure mode has to some extent been mitigated at the location of the connection seat, as a result of the retrofits discussed, the focus of concern now shifts to the reserve capacity within the lattice uprights of the chord lacing immediately adjacent to the seat region. These regions are susceptible to the same side-wall buckling failure mode as a result of the high internal shear forces being developed in the chord regions immediately adjacent to the chord-to-upright connection location.

1.1 SCOPE OF RESEARCH

The focus of the research work reported on herein concerns a portion of long-span HSS trusses exhibiting a geometry typical within PennDOT design contexts: the bearing region at the upright supports. In Pennsylvania, the subject standard detail involves curved steel saddle bearings and a

Structural Tee (ST) connected directly to a circular HSS chord wall in end bearing; both within close proximity to the open end of the HSS chord (see Figure 1-1). In simple-span HSS trusses, the primary load path for the reaction force developed at the saddles is through the chord and directly into the first intermediate vertical member. Therefore, the overall bearing capacity is influenced by all of these elements. It must be noted that this region is being investigated locally

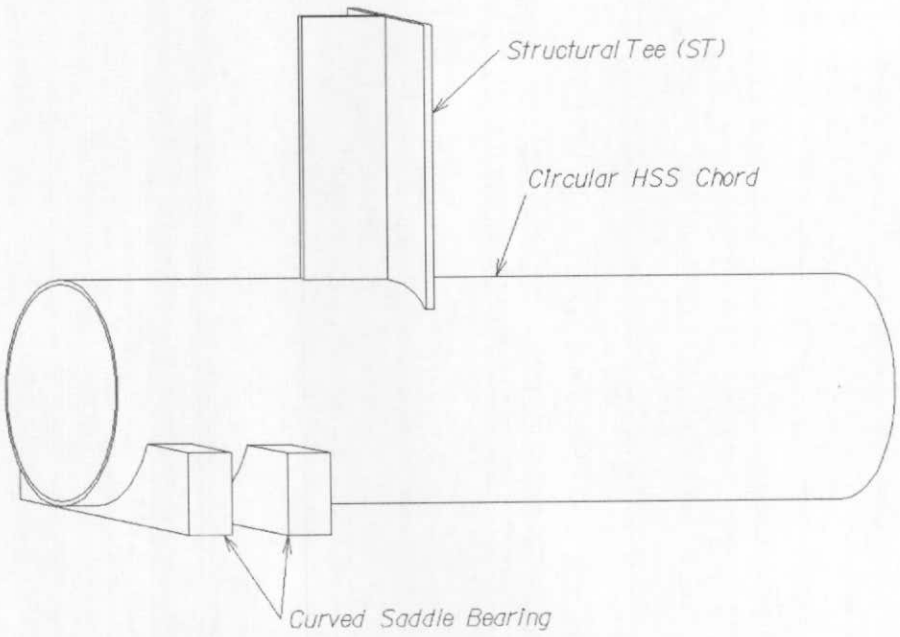

Figure 1-1: Bearing Configuration Under Investigation.

without involving the global behavior of the entire truss (i.e. the more complicated member internal forces, resulting from effects of the structural system surrounding the connection detail, are not considered). The assumption here is that the effects of such additional internal forces are of small magnitude and hence will not significantly influence the local limit states under investigation. In considering this simplified loading condition, it is noted that while some research has been done on local concentrated loads applied to HSS walls through gusset plates, very little work has been done on loads applied directly through the ends of an open rolled sections; no previous work has been found in the literature concerning the cases of saddle-type bearings located at chord ends or an ST bearing on a circular HSS chord.

This research is executed through the application of sophisticated nonlinear finite element modeling techniques as well as full-scale experimental testing. The nonlinear finite element modeling employs experimentally verified modeling strategies (previously verified against available relevant tests on tubular structures found in the literature as well as those tests carried out as part of the current research) and forms the cornerstone for the parametric studies carried out in the formulation of a design equation aimed at predicting sidewall crushing strength in circular HSS members. The full-scale tests carried out as part of the current research were executed using geometric configurations identified as either being most critical, or most germane, vis-à-vis initial parametric finite element analyses. Through the use of finite element modeling studies that are supported and verified with the judicious use of full-scale experimental testing, a very large sample space of geometric combinations are economically considered. This is of pivotal importance to the research since a design equation must be demonstrably applicable to all reasonable geometric configurations that are likely to arise in practice.

2.0 REVIEW OF EXISTING SPECIFICATIONS AND RESEARCH

Circular Hollow Structural Sections (HSS) possess a very efficient cross-section for the resistance of compressive and torsional stresses as a result of their closed, symmetrical geometry. A given circular HSS member has both a smaller surface area and greater torsional rigidity relative to a comparable open section member of the same weight. Although the material cost is higher for the grades of steel typically specified for hollow sections, this increased cost is typically offset by the lower construction weight deriving from greater structural efficiency, and the smaller coating area required for corrosion protection (paint or galvanizing) due to the enclosed nature of the section.. Combine this with the pleasing aesthetics of the HSS, and one can see why tubular members are quickly gaining popularity in structural applications. In particular, the circular HSS has become the member of choice in applications that involve wind, water, or wave loading due to its low drag coefficient. Common structures that utilize the circular HSS include offshore platforms, space trusses in buildings and stadiums, and overhead highway sign structures. It is one design aspect of the last of these applications that has motivated the current research. However, the findings will be of interest to researchers and engineers working with other applications.

One of the primary challenges in designing a safe, cost-effective tubular structure is in the detailing of the joints. Joints in tubular structures can be simple HSS-to-HSS connections, connections between an open section and an HSS, or connections made through gusset plates. The last two of these are sometimes referred to as "plate-type" connections. In the specialized case of a truss, HSS connections usually consist of one or more smaller branch members that are attached to a continuous chord that passes through the connection work point. These joints can be classified as a T-Connection, Y-Connection, Cross-Connection, or a K-Connection depending on the geometry. For design, special attention must be given to ensure that the connection does not fail by way of punching shear rupture, chord wall plastification, general collapse, or by some

other local failure mechanism. The behavior of HSS-to-HSS connections has been researched and is well understood, but less work has been done in the area of plate-type HSS connections.

In the design of tubular truss-type structures such as overhead highway signs, the desire is to have chord members of a large radius of gyration (larger diameter with thinner walls) so as to increase axial compressive resistance while at the same time reducing member weight. However, such an approach as this usually leads to a trade-off since joint capacities are typically reduced due to the decreased bearing capacity in thin chord walls. Therefore as a compromise, it is recommended that chord members be sized with relatively thick walls and branch members be sized with relatively thin walls (AISC 2000). If the joint design demands that the chord wall be excessively thick, the designer should then consider reinforcing the joint with stiffeners or grouting rather than using a greater chord thickness; in the interest of economy. Unfortunately, it is not always a simple matter to determine under what circumstances chord wall demands become excessive.

2.1 RELEVANT SPECIFICATIONS

The governing specification for the design of highway overhead sign structures in the US is the *Standard Specifications for Structural Supports for Highway Signs, Luminaires and Traffic Signals, 4th Edition* (AASHTO 2001). Currently, this specification does not address the capacity of tubular connections or bearings at all; a potentially serious omission since joint related limit states often control the overall structural capacity (Li and Earls 2002). The design engineer must look beyond this omission and recognize the need for checking joint strengths by consulting other specifications for guidance. American specifications that do address connection capacities in tubular structures are the *Load and Resistance Factor Design Specification for Steel Hollow Structural Sections* (AISC 2000), which can be found in Part 16 of *AISC LRFD Manual 3rd Edition* (AISC 2001), and *AWS D1.1 Structural Welding Code – Steel* (AWS 2004). Also, more detailed guidance and examples are provided in the *AISC Hollow Structural Sections Connection Manual* (AISC 1997a).

The *AISC Hollow Structural Sections Connections Manual* (AISC 1997a) is the definitive American design manual representing the state-of-the-art in hollow structural section connection design and detailing. This manual treats specific design topics related to: dimensions and properties of HSS members; welding practice; issues related to bolting; simple shear connections; moment connections; tension and compression connections; cap plates, base plate, and column splices; and welded truss connections. In addition, the manual contains the *Specification for the Design of Steel Hollow Structural Sections* (AISC 1997b), which deals specifically with HSS design issues related to: material properties; loads and load combinations; effective net area for tension members; local plate buckling; limiting slenderness ratios; and design for tension, compression, flexure, shear, torsion, combined loading, and the localized effects of various type of transverse loading scenarios; weld design; truss connection design; and fabrication requirements.

The *AISC Hollow Structural Sections Connections Manual* (AISC 1997a) has a Canadian counterpart in the CISC Hollow Structural Section Connections and Trusses Design Guide (Packer and Henderson 1997). This Canadian Manual treats many of the same topics of its American counterpart as well as several additional topics such as: material property and cross-sectional geometric definitions; standard truss design; standard truss welded connections; non-standard truss design; multiplanar welded connections; HSS-to-HSS moment connections; bolted HSS connections; fabrication, welding, and inspection; beam to HSS column connections; trusses and base plates to HSS connections; plate to HSS connections; HSS welded connections subjected to fatigue loading; and standard truss examples.

While it may appear from the forgoing that the Canadian and American HSS manuals are very similar, this would be an incorrect conclusion to draw. The American HSS manual (AISC 1997a) is constructed to be consistent with the format and fundamental approach contained in all other AISC design manuals and as such takes a much more general approach to the promulgation of design guidelines. In contrast, the Canadian HSS manual (Packer 1997) is much more focused on the specific design case of the HSS truss. Most of the Canadian manual is focused to support the design of variations on the HSS truss form.

To discuss the state-of-art knowledge in steel HSS construction, it would be a mistake not to also consider work that is being done outside of North America. Both the Canadian and American HSS specifications have adopted significant material from the European Comite

International pour le Developpement et l'Etude de la Construction Tubulaire (CIDECT). Founded in 1962, CIDECT is an international organization of major HSS manufacturers that was formed to combine all the resources worldwide from industry, universities, and other national and international bodies for research and application of technical data, development of simple design and calculation methods and dissemination of the results of research (Wardenier et al.. 1991). CIDECT has technical and research activities ongoing in many areas of HSS construction including: buckling behavior of columns and trusses, bending strength of members, static strength of welded and bolted joints, and fatigue resistance of joints. Most germane to the current discussion on circular HSS connections is CIDECT's publication *Design Guide for Circular Hollow Section (CHS) Joints Under Predominantly Static Loading* (Wardenier et al. 1991). This publication contains capacity equations for many of the same HSS connections addressed in the Canadian and American specifications, but it also provides data for many other types of joints which will prove valuable for predicting the bearing capacity of circular HSS chord members; the focus of the present work.

2.2 PROCEDURES FOR ANALYSIS AND DESIGN

The analysis and design of connections in tubular structures is a very complex problem in general. Many different analytical methods have been applied to address this problem including elastic shell theory, the finite element method, the method of cutting sections, and plastic yield line analysis. However, these analytical methods are often cumbersome or computationally expensive. Thus, researchers and engineers have tended toward the use of experimental methods, which can address the full range of behavior from the elastic to the ultimate limit state. The following paragraphs give a brief overview of the various methods applied to the solution of this difficult problem; a more detailed description of each can be found in Marshall (1992).

The first level of analysis that can be conducted on a tubular connection is elastic analysis. Elastic analysis can be important in fatigue design, in which the localized stresses are typically desired. Closed form solutions for elastic stresses in cylindrical shells have been developed for many simple, symmetric loading conditions (Young 1989), however even the

simplest case requires a complex solution. Some tubular connections can be approximated using these simple understood cases, but direct theoretical solutions for common connection details are impractical due the curved geometry and complex stress fields, and are generally not attempted.

Another method utilized for the calculation of elastic stresses in tubular member connection details is the finite element method, which includes thin shell finite elements or 3-dimenensional isoparametric continuum finite elements. Thin shell finite element analysis is based on constructing a mesh at the mid-surface of the plate components with the through-thickness direction being implied within the formulation, which works well for analyzing stresses away from discontinuities such as a weld toe. 3-D isoparametric continuum elements provide a solid element to model the finite thickness of the shells, which avoid the paradoxical results that are sometimes obtained from "surface" stresses at the mid-plane intersection in thin-shell analysis (Marshall 1992). Researchers have used these methods with success, but typically consulting engineers from industry are not equipped for this type of analysis.

The next types of analysis that are conducted on tubular connections are limit state methods. The most common approach used for developing capacity equations for HSS connections is the method of cutting sections, often called the "ring model." This method involves analysis of a unit strip or slice through the HSS chord using simple plastic analysis, i.e. the yield line method. Then, the effective width of the ring (length along the HSS chord) is estimated or determined using empirical test data. The ring model approach is found throughout the literature (Kurobane, et al. 1976) (Kurobane, 1981) (Wardenier, 1982) and is the basis for many of the HSS capacity equations in the current specifications.

Another limit state method applied to the analysis of tubular connections is the yield line method, which is based on the upper bound theorem of plasticity. The general approach is to assume a rigid plastic failure mechanism, and compute the load level at which internal work due to yielding equals the external work due to the applied loads (Marshall 1992). This method has been used with success for the formulation of capacity equations in symmetric tubular box connections (Kosteski and Packer, 2003), in which a kinematically admissible collapse mechanism can be developed using simple geometric considerations. For circular HSS connections, the yield line method was applied by Soh et al. (2000), but it is generally not the preferred method due to the associated complex geometry of the failure mechanisms.

Inelastic finite element analysis is another method applied to study of tubular connections. Clough (1965) described the finite element stiffness method in terms of the following steps: (1) Express element internal displacements in terms of assumed deformation patterns which approximate behavior of the continuum, are more or less compatible at the element boundaries and whose magnitude is given by generalized coordinates, one for each degree of freedom, (2-4) Express both nodal displacements and internal strains in terms of the same generalized coordinates and deformation patterns, (5) Evaluate internal stresses from the internal strains, with material characteristics represented by the stress-strain matrix, (6) In generalized coordinates, integrate over the element volume to compute internal virtual work due to internal stresses an strains, compute external work due to nodal forces and displacements; and equate these to extract the element stiffness, (7) Transform to the desired nodal point stiffness matrix for each element. The process is repeated for all the elements to assemble the global stiffness matrix for the whole structure. For linear structures, this is solved by matrix inversion of numerically equivalent methods. However, for solving non-linear problems an additional sub-procedure is required, for which two principal methods are used: incremental loading and intermediate equilibrium iteration. Because inelastic finite element analysis involves complex numerical procedures, the modeling techniques (mesh size and layout, element selection, material descriptions, and solution strategy) should be carefully calibrated and benchmarked against reliable experimental results (Marshall 1992).

When none of the previous analytical methods can be applied, then the last resort is to conduct model testing on the tubular connection. Model tests can be used to study the elastic stresses, ultimate strength limit state, and the fatigue behavior, and are considered by most to be the most reliable way for verifying capacity. However, experimental testing can be relatively expensive as compared to computerized simulations.

3.0 EXPERIMENTAL TESTING PROGRAM

The experimental research program is aimed at quantifying the physical response of the bearing connection region in long-span tubular sign trusses. The given connection detail selected for study is one which is considered susceptible to bearing failure (i.e. a detail with a slender chord cross-section). The scope of the current experimental work is threefold: to determine the capacity of a particular truss bearing configuration through physical testing, to evaluate the accuracy of existing provisions for predicting the bearing capacity of tubular truss chords; and to produce a data set of physical testing results for the purposes of validating nonlinear finite element modeling techniques to be used for the parametric studies.

3.1 DESCRIPTION OF TEST SPECIMEN AND SETUP

The basis for the geometry of the specimens considered in the experimental tests is the *Standard Drawings for Bridge Construction [and Design]* (PennDOT 2003a,b). In these standards, the bearing configuration selected for consideration can be found in many of the long-span highway sign structure truss details. In an effort to maintain reasonable geometric parameters for testing, the experimental specimens are proportioned to exactly match the design and details emanating from BD-644M and BC-744M (PennDOT 2003a,b) for the case of a tri-chord truss spanning greater than 197 ft; which calls for three (3) - ½ in. x 26 in. diameter HSS chords laced together with ST10x48 intermediate members.

At the truss ends, the first ST intermediate (branch) member is oriented vertically and thus is normal to the sidewall of the HSS chord, and the chord end is seated in a curved saddle bearing assembly in close proximity to the ST. As a result of the ST orientation, and the fact that

this location is highly stressed from the reaction forces, the ST was detailed to bear directly upon the HSS chord side wall through a full-penetration welded connection. In order to simulate this connection condition in the laboratory set-up, two curved saddles were proportioned and positioned within a specially built load frame whose proportions were consistent with those called out in BD-744M (PennDOT 2003b). In general, the schematic testing condition depicted in Figure 3-1 was adhered to in the design of the specimens and load frame. Two (2) specimens having the same dimensions and loading conditions were tested in order that repeatability of results within the testing program might be ascertained.

Fully nonlinear shell finite element based models of potential specimen geometries and the general testing configuration were first constructed and analyzed using ABAQUS (ABAQUS 2003) as a means of identifying proportions that permitted economy in material and fabrication costs while at the same time preserving the integrity of the structural response and failure modes germane to the current work. In the end, the 26 in. circular HSS component of the specimens

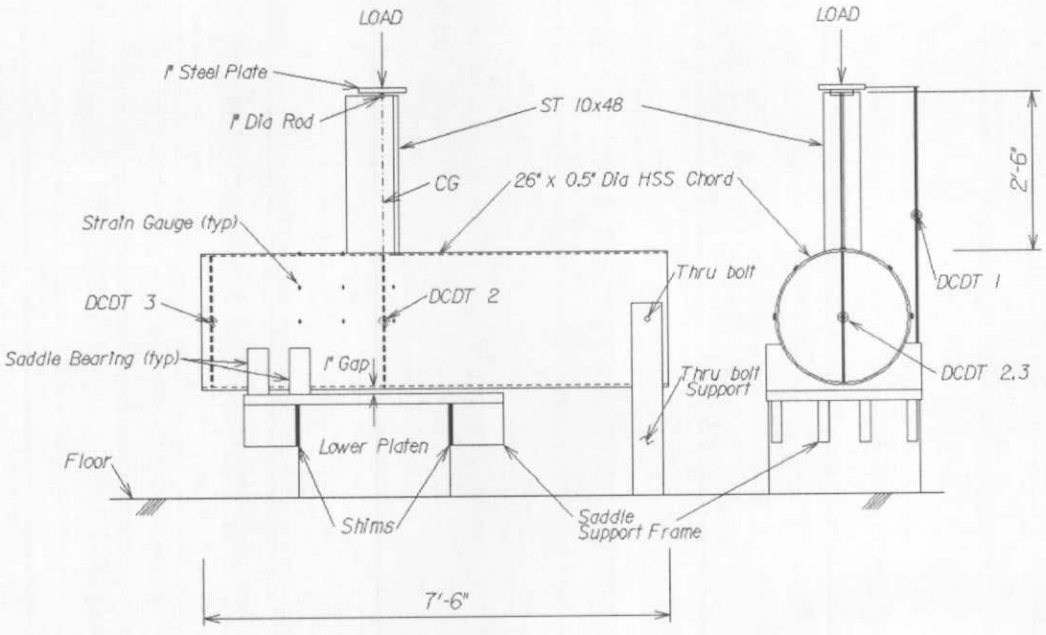

Figure 3-1: Schematic of Experimental Test Setup.

was selected to be 7 ft-6 in. long and the ST10x48 was specified to be 2 ft-6 in. long (as shown in Figure 3-1). The HSS length was selected to provide a sufficiently long specimen such that continuity effects of adjacent HSS material would be preserved (i.e. the specimen had to be long enough to capture the local effects of continuity in HSS sidewall provided by the 197 ft + long piece as would be used in the field). The finite element models indicated that the 7 ft-6 in. length would be more than adequate for this purpose. Another consideration impacting on the selection of the HSS specimen length was related to the desire to have the end of the circular HSS bear firmly against the saddles and not "lift-off" as a result of pivoting around the support of an excessively short HSS section. Finite element modeling indicated that the 7 ft-6 in. HSS length was sufficient to ensure realistic kinematics in the test. Similarly, the length of the ST10x48 specified was arrived at through finite element modeling that indicated 2 ft-6 in. of member length would be sufficient to attenuate local effects from the point load applied to the top of the ST member by the loading frame actuator (i.e. 2 ft-6 in. was sufficient for St. Venant's principle to take effect and disperse stress concentrations at the load point). In terms of boundary conditions on the circular HSS, at the end away from the saddle, a single thru-bolt was positioned close to the end of the HSS end in order to serve as a "pinned end." The grade of steel used for the HSS was ASTM A53 Grade B and the steel used for the ST10x48 was ASTM A709 Grade 50. The general behvaior of the material stress-strain response obtained from coupon tests are shown in Figure 3-2.

In order to compare the experimental test results to the finite element modeling results, the strains at certain critical points on the HSS section needed to be accurately measured. After reviewing the preliminary finite element models of the specimen geometries considered herein, it was decided that three rows of strain rosettes on the HSS section were required to capture the needed information. The first row fell directly over the saddle closest to the ST; the third was directly under the ST, aligned with the center of the flange; the second row of rosettes was oriented at the midpoint between the two. Five rosettes were circumferentially placed in each row, one at each 90 and 45 degree angular position around the outside of the cross-section, and one located at the top of the HSS section as seen in Figure 3-3. The third rosette row, located under the ST, did not have a rosette on top since the ST occupied the required location for

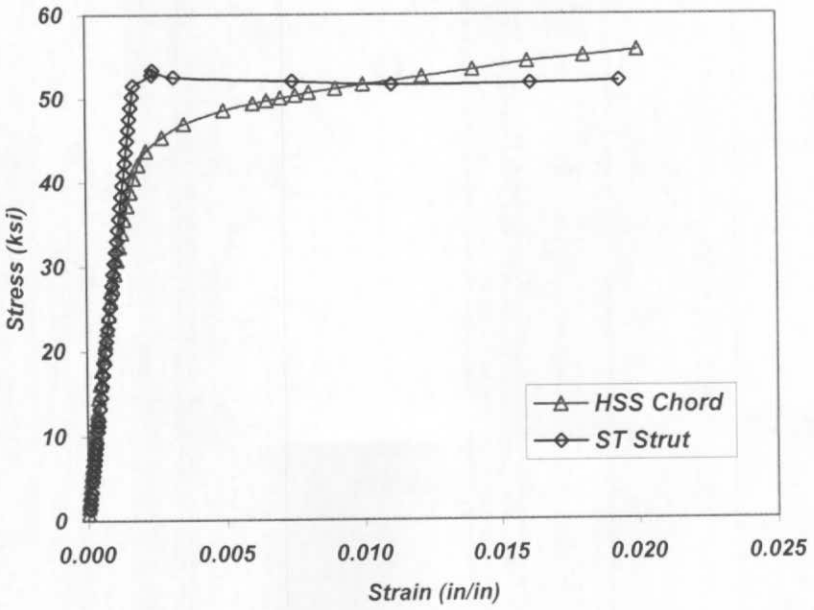

Figure 3-2: Material Response of Steels Used in Test Specimens.

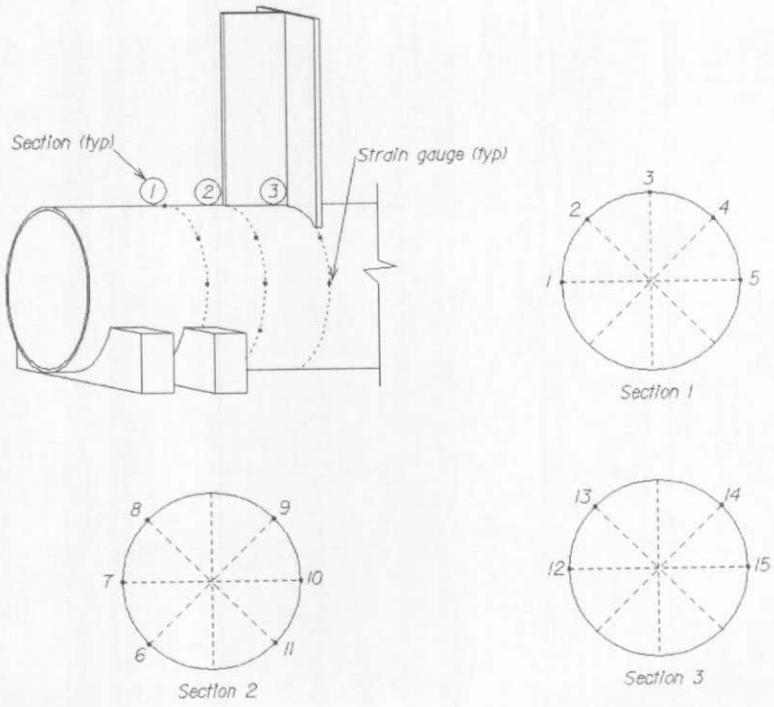

Figure 3-3: Rosette strain gauge locations on chord wall

installation. Three uniaxial strain gauges were also placed at the midpoint of the ST on each of the flange tips as well as on the web tip to measure the strains in the ST section.

In an effort to monitor deformations and cross-sectional distortion, three displacement transducers (DCDTs), identified as DCDT 1, 2, and 3 were used to measure displacements at different locations as shown in Figure 3-1. The locations were selected to reveal the portion of the overall specimen deformation that results from local wall distortion and the portion that results from global bending. The DCDT 1, was mounted externally to a bar that was attached to the lower platen of the loading frame, which served as a ground (fixed) point. This DCDT extended to the upper platen of the testing machine and thus it measured the total displacement including both global and local deformation effects within the specimen (i.e. both overall bending of the chord and ovalization of the chord cross-section). The DCDT 2 was positioned inside the HSS directly under the flange-web junction of the ST. This DCDT measured the relative displacement of the top and bottom walls of the HSS, which is the deflection due to local wall distortion (ovalization) under the ST. The final DCDT 3 was oriented in a similar fashion to DCDT 2 inside the HSS, but in this case at the open end of the HSS over the saddles. The results of DCDT 3 will reveal if any ovalization occurs at the open end, thus indicating to what extent the applied load is dispersed longitudinally.

As previously mentioned, the load was applied to the top of the ST using an actuator. The load was applied in 5 kip increments, which were held for approximately two minutes as the instrumentation was scanned and recorded using a computer controlled data acquisition system. In order to ensure minimal eccentricities at the point of load application, a semicircular notch was cut into the stem of the ST directly at the centroid of the cross section where load application occurred. A steel plate with a 1 in. diameter rod (which fit directly into the notch) welded to the center was positioned into the notch; the load cell bore on the plate as the actuator applied the load. In this way, any incidental moment was released and not transmitted to the load cell.

3.2 TEST RESULTS

The two (2) full-scale experimental tests were conducted in the Watkins-Haggart Structural Engineering Laboratory at the University of Pittsburgh in August 2003 (see Figure 3-4). The load versus deflection responses as recorded by DCDT 1, 2, and 3 for both experimental tests are shown in Figure 3-5 and Figure 3-6. The complete test data including the raw strain gauge results is available in the report by Boyle and Earls (2004). Based on the deflection data alone, there are a number of important observations that can be made.

Both tests were completed without any significant problems. However, during the testing of Specimen #1, the thru-bolt at the right end yielded due to a bending overstress. Approximately midway through the test, the bolt began to sag, allowing the HSS end to drop slightly (less than 0.25 in.). This allowed the HSS chord to rotate, and thus caused some undesired eccentricity (and moment) to be applied to the joint. The test was continued until failure, but it is believed that the ultimate load was reduced somewhat by the additional moment introduced into the ST as a result of the slight sagging associated with the thru-bolt. For Specimen #2, the thru-bolt size was increased and stiffening bars were added to decrease the span length for the bolt. As a result, the second test was completed without any plastic deformation of the thru-bolt. This is apparent by observing the smooth shape of the load-deflection plot for Specimen #2 as compared to Specimen #1.

Upon review of the DCDT measurements of both tests, it is observed that the majority of the displacement is due to local distortion or ovalization of the HSS cross-section. This is apparent by observing the small difference in the measured displacements of DCDT 1 and DCDT 2 at any load. Recall that DCDT 1 measured the total displacement at the ST including both global and local deformation effects within the specimen and DCDT 2 measured the local deformation only. Since the difference between these two measurements remains relatively small for all loads, this indicates that there is little global deformation. This makes sense physically since the ST and saddles are in such close proximity and the internal moment arm generated between these two elements is quite small when considered from a practical standpoint.

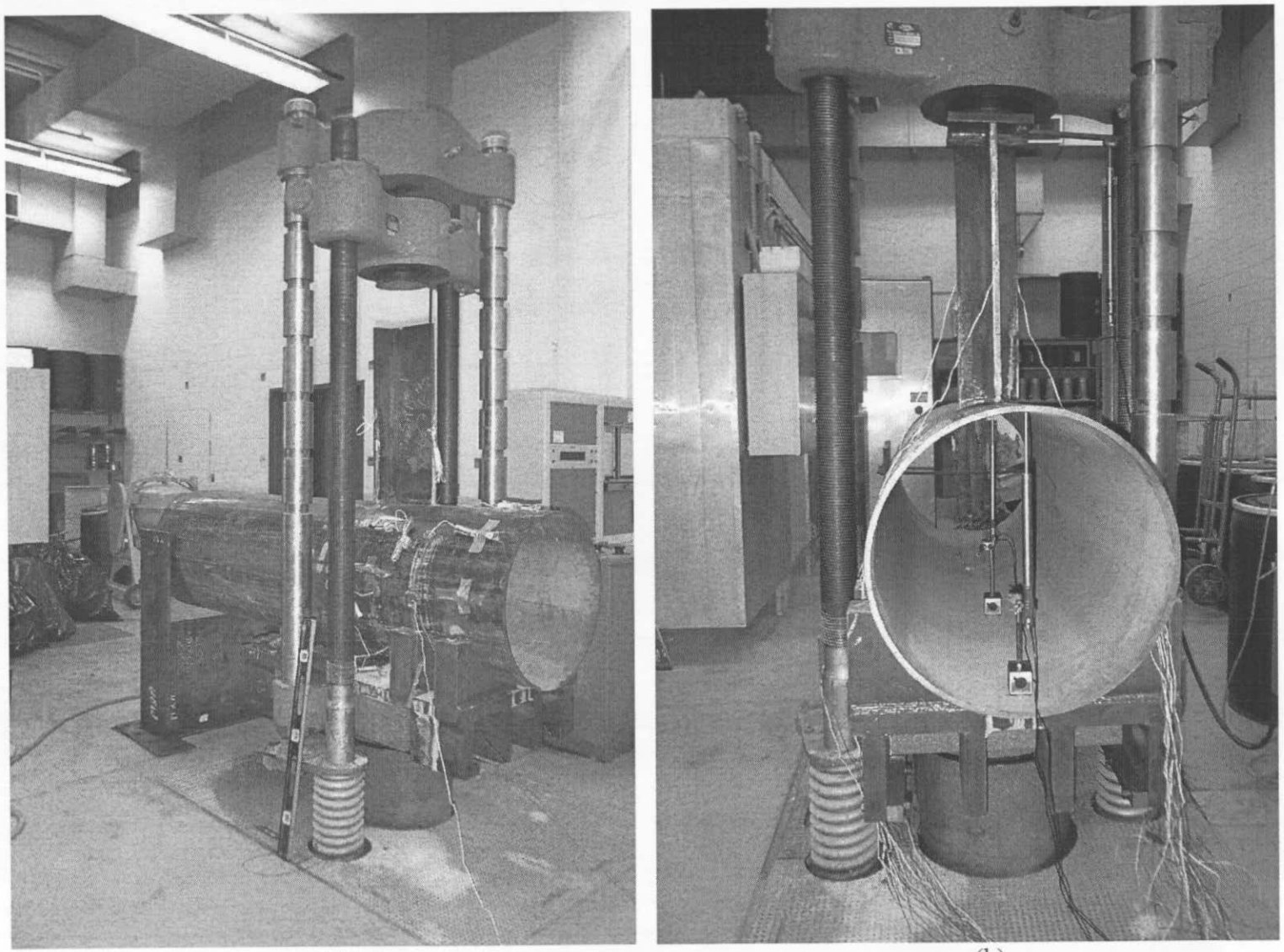

(a) (b)

Figure 3-4: Photographs of Experimental Test Specimens

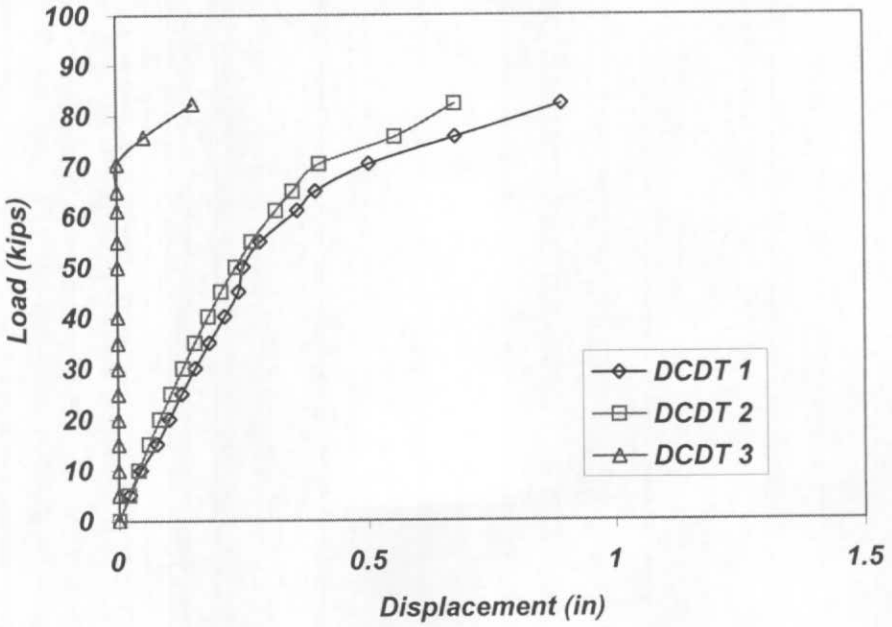

Figure 3-5: Experimental displacement measurements for Specimen #1.

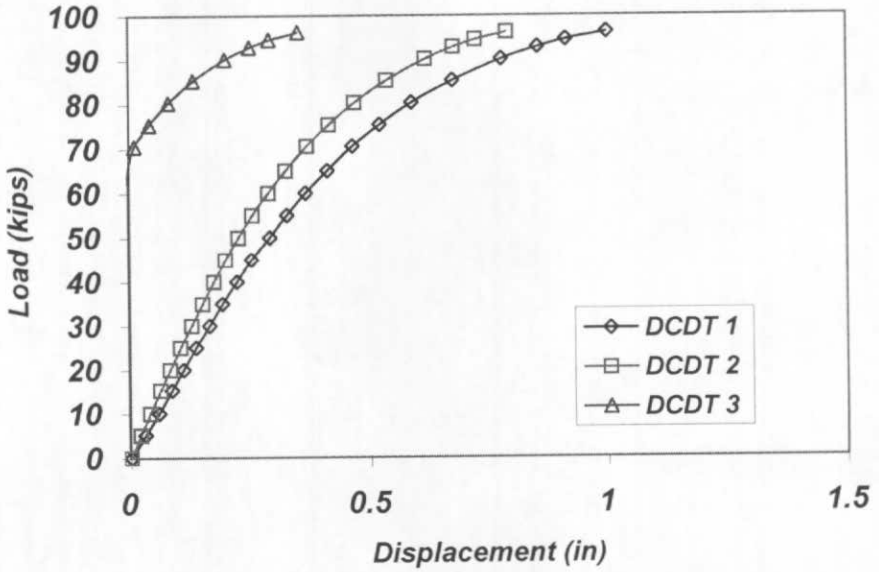

Figure 3-6: Experimental displacement measurements for Specimen #2.

The next observations made are relevant to the various limit states of failure for the bearing region. Three response features in the load-deflection response are identified that may be of importance in standard design practice. They are: 1) the yield load, P_y 2) the ultimate load, P_u and 3) the nominal capacity load, P_n.

By analyzing the measurements of DCDT 1 and DCDT 2, it appears that both specimens began to yield at a load of approximately 40 kips. This is the load at which the non-linear behavior appears to have initiated in the load deflection response, but a precise value is difficult to ascertain from the experimental data set since the loading was increased in 5 kip increments. Based on observations of the specimens during testing, it was noted that this yielding occurred in the HSS wall adjacent to each ST flange tip in the form of small "dimples." Depending on the structural application, this dimpling may not be considered objectionable. Since this yielding occurs at such a low load level and there is so much reserve capacity in the joint beyond this load, it is likely to be too costly to design the connection to prevent any yielding whatsoever.

The ultimate load of this connection is significantly higher than the yield load: Specimen #1 achieved an ultimate load of 82 kips and Specimen #2 achieved an ultimate load of 96 kips. As mentioned previously, during testing of Specimen #1 a small moment was believed to be introduced in the specimen due to shifting occurring at the pin - support end; it is suspected that this reduced the ultimate load for the test. Therefore, it is believed that the ultimate capacity should be considered as 96 kips rather than the average of the two tests until further testing is conducted. It should be noted that 96 kips is consistent with the ultimate load predicted by FEM analysis (see Chapter 5.0).

For defining the nominal capacity for the purposes of design in the context of LRFD, some judgment must be exercised. AISC has formulated many of its provisions so that a deformation limit state is not exceeded at service loads (AISC 1997a). A similar approach might be applied to the present results by analyzing the DCDT 3 response, which is located at the open end of the HSS. At the open end, no distortion was observed as the load increased through most of the test. But when the load reached 70 kips, the deflection began to increase quickly at the open end of the HSS adjacent to the saddles and the ultimate load for the specimen was realized soon after this point. This indicates that a collapse mechanism began to form at a load of 70 kips and the stability of the failure mechanism was in question once the open end began to deform. It

should also be noted that this behavior was observed to be repeatable across both tests. In the context of preventing excessive deformations, the point of initiation of the collapse mechanism might be considered as the nominal capacity. This is a slightly different approach than that utilized by AISC, but it may be warranted due to the apparent unstable nature of the failure. This is discussed further in Chapter 8.

For analysis of the strain gauge data, conversion to equivalent von Mises stresses is one way to quickly assess the mechanical response within the HSS chord. These are shown graphically for each gauge location in Figure 3-7 and Figure 3-8. From these plots, it can be seen that location 3 is subject to the largest state of stress, with locations 13 and 14 close behind. Noting that the yield stress of the HSS steel is 47 ksi reveals that the additional locations experiencing yield are: 1, 5, 8, and 9. These yielded locations will be considered within the context of the verification portion of the finite element modeling as discussed in Section 5.3. Despite the minor incident that occurred at the pinned end support in Specimen #1, it is encouraging to note that the stress histories for the strain rosettes are still very consistent between the two tests (i.e. Specimen #1 and #2).

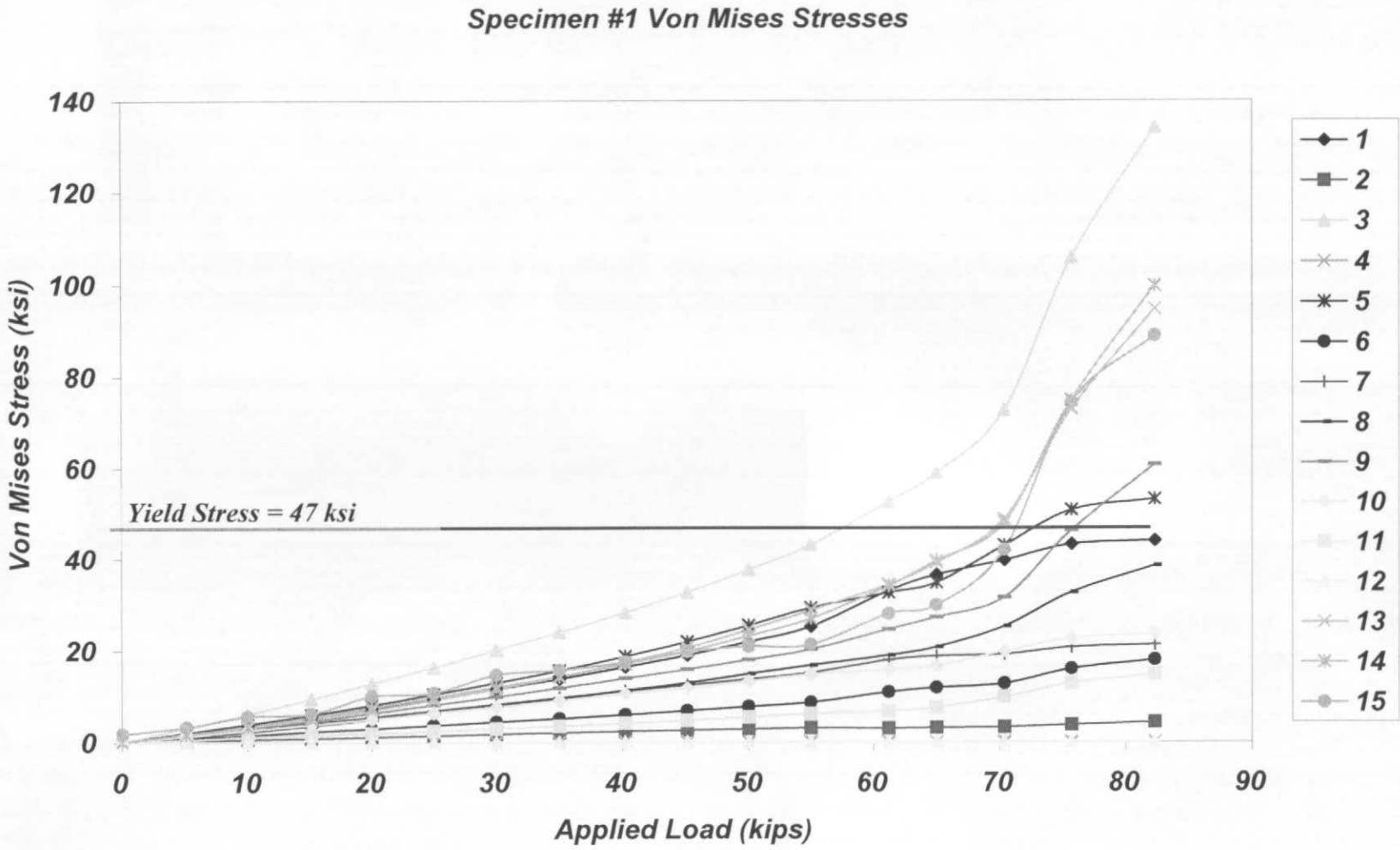

Figure 3-7: von Mises stresses in chord wall for Specimen #1

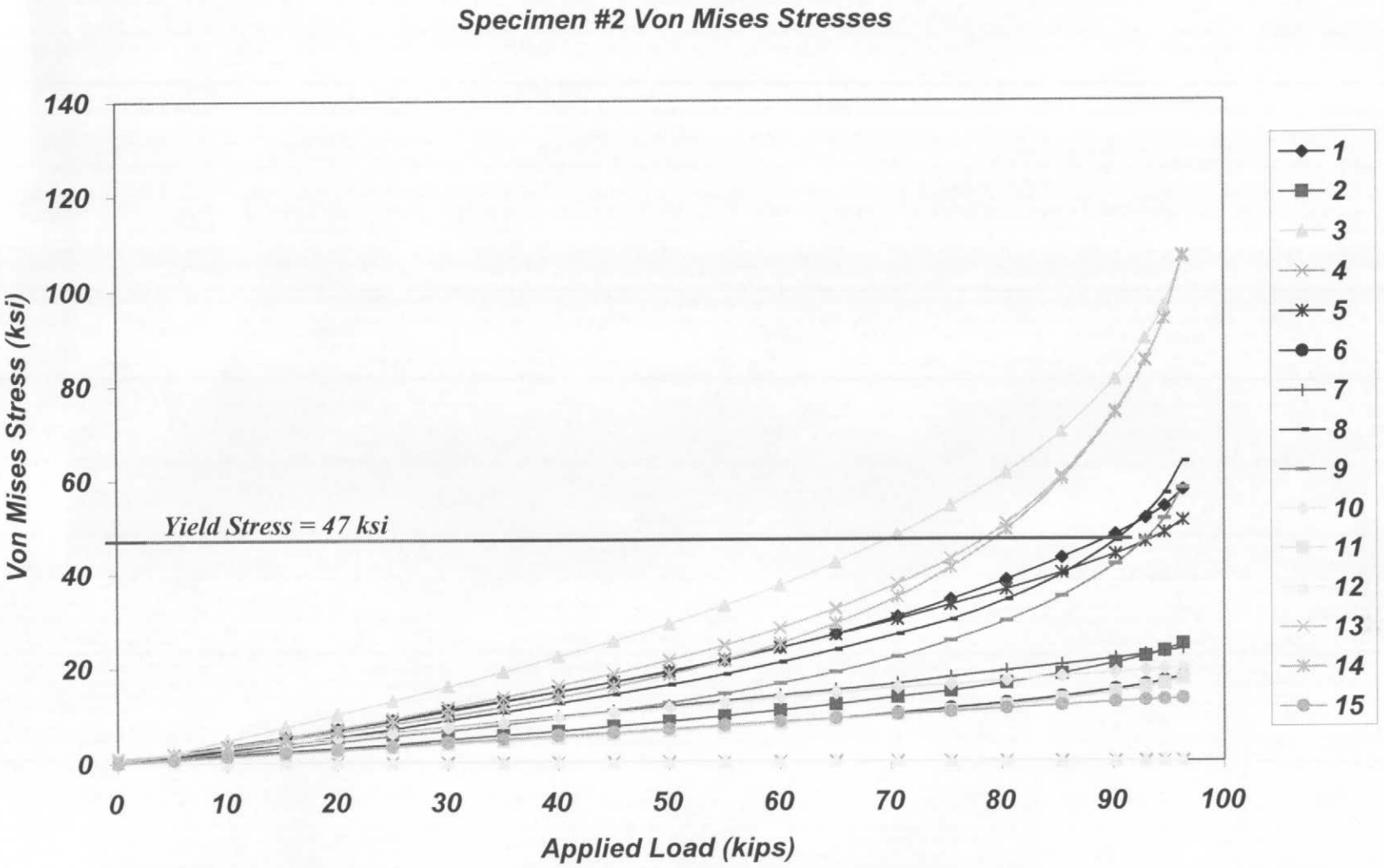

Figure 3-8: von Mises stresses in chord wall for Specimen #2

4.0 APPROXIMATE METHODS FOR PREDICTING CAPACITY

As mentioned previously, none of the referenced publications in the literature specifically address the bearing capacity in circular HSS truss chords. However, research has been done, and capacity equations published, for many HSS connections that are related (to various degrees) to this particular case of interest. An attempt is made to identify existing provisions that are based on a similar failure mode that governs for this bearing configuration, and that could be adapted for the purposes of estimating the chord bearing capacity.

The proposed methods are based on the assumption that the ST-to-chord joint is the "weak link" in the system and that overall capacity is governed by this detail alone. That is, the saddle bearings are assumed to adequately transfer the reaction force to the chord without compromising the overall capacity and the failure mode takes place in the chord wall locally at the ST. However, in applying this assumption it is quickly noted that even the ST joint itself is not covered directly by existing specifications; and thus, existing provisions must be adapted further. All the methods described below are based on the limit state of plastic flexural collapse of the chord wall, which is consistent with the observed failure mode in the experimental test specimens.

4.1 DESCRIPTION OF METHODS

4.1.1 Method 1: Modified application of AISC HSS Specification Section 8

In Section 8 of the LRFD HSS specification (AISC 2000), capacity equations are provided for the case of a concentrated force applied to an unstiffened HSS wall through a single bearing plate. To utilize these provisions, the ST member could be analyzed as two individual plates;

one transverse and one longitudinal to the HSS axis. Section 8.1 addresses the case of a *Concentrated Force Distributed Transversely at the Center of the HSS Face*, and Section 8.2 addresses the case of a *Concentrated Force Distributed Longitudinally at the Center of the HSS Face* (see Figure 4-1 and Figure 4-2). These provisions may be applied by assuming that the ST connection will have a total capacity equal to the transverse plate capacity plus the longitudinal plate capacity, or direct superposition of the capacities. (Since this approach neglects any interaction between the two plates, this will prove to be unconservative; as will be discussed later.)

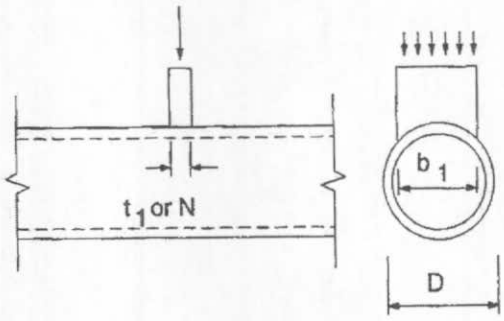

Figure 4-1: Concentrated Force Distributed Transversely

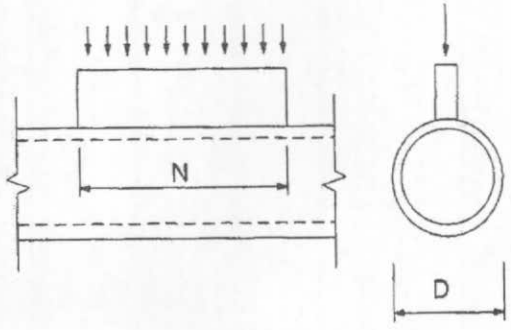

Figure 4-2: Concentrated Force Distributed Longitudinally

Using this approach, the capacity of the transverse component (flange) is first calculated using the provision for a circular HSS subjected to a uniformly distributed transverse line load as shown in Section 8.1 (and reproduced below as Equation 4-1):

$$R_n = \frac{5F_y t^2}{1-0.81b_1/D} Q_f \qquad (4\text{-}1)$$

where,

$b_1 \equiv$ the width of the ST flange
$Q_f \equiv 1.0$ for tension in the HSS (for compression see eqn. 8.1-1 in AISC (2000))
$F_y \equiv$ specified minimum yield strength of the HSS
$t \equiv$ HSS Chord wall thickness
$D \equiv$ HSS Chord diameter

Similarly for the longitudinal component (stem), the capacity is based on the provision for a circular HSS subjected to a uniformly distributed longitudinal line load as shown in Section 8.2 (and reproduced here as Equation 4-2):

$$R_n = 5F_y t^2 \left(1+0.25N/D\right) \cdot Q_f \qquad (4\text{-}2)$$

where,

$N \equiv$ the depth of the ST
$Q_f \equiv 1.0$ for tension in the HSS (for compression see eqn. 8.1-1 in AISC (2000))
$F_y \equiv$ specified minimum yield strength of the HSS
$t \equiv$ HSS Chord wall thickness
$D \equiv$ HSS Chord diameter

Both of these equations (including the subsequent equation for Q_f) are identical to the "Factored Connection Resistance" equations presented in table 11.2 of the Canadian HSS manual (Packer 1997) and the "Design Strength" equations shown in Figure 25 (Types XP-1 and XP-2) of the CIDECT Design Guide (Wardenier et al. 1991). Unlike the American LRFD specification, the Canadian manual also provides additional insight for consideration of a cruxiform detail, which is an X-shaped open section with plates in both the longitudinal and transverse directions. It states that since the transverse plate connection is so much stronger than

the longitudinal one, the cruxiform variation is not considered to be significantly stronger than the simple transverse connection (Packer 1997). Applying this same logic to the case of an ST would suggest that a reasonable conservative estimate of the capacity could be obtained by considering the transverse plate component only. However, it should be noted that this is based on the assumption the longitudinal component is smaller or of similar size to the transverse component (Wardenier 1982). This notion will be further investigated in light of the experimental test results and calculations.

4.1.2 Method 2: Modified application of AISC HSS Specification Section 9

A second type of joint that is similar to the ST connection, and for which published data is available, is the HSS-to-HSS Truss Connection (see Figure 4-3). This case is well researched and capacity equations are published in all of the previously mentioned references: American, Canadian, and CIDECT. Although at first glance it would seem that a ST and HSS are not very similar in geometry, the limit state that governs the capacity of both joints is chord wall plastification. Both the ST and HSS will actually generate similar yield line mechanisms at failure of the chord wall (see Figure 4-4).

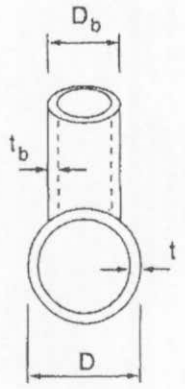

Figure 4-3: HSS-to-HSS Truss Connection

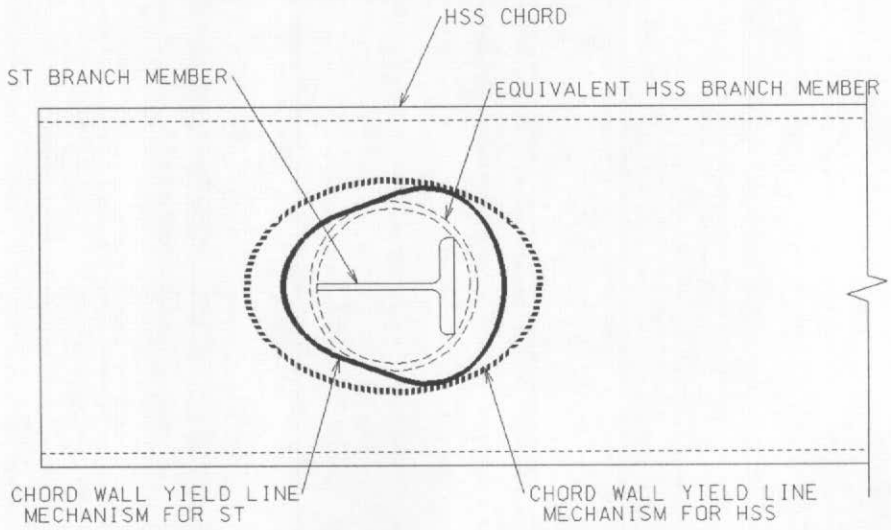

Figure 4-4: Yield Line Mechanisms for ST and Equivalent HSS Branch Members

The provisions that apply to axially loaded circular HSS-to-HSS Truss connections are published in Section 9.4 of the LRFD HSS specification (AISC 2000). Under subsection 2b, for branches with axial loads under the limit state of chord wall plastification, the capacity equation is given as:

$$P_n \sin\theta = t^2 F_y \left(6\pi \cdot \beta \cdot Q_q\right) \cdot Q_f \qquad (4\text{-}3)$$

where,

$\theta \equiv$ Angle between the branch and chord
$\beta \equiv$ Branch Diameter / Chord Diameter
$Q_q \equiv$ see Eqn. 9.4-3 in (AISC 2000)
$Q_f \equiv$ see Eqn. 9.4-3 in (AISC 2000)

In this case, the ST flange width b_f should be used as the equivalent HSS branch diameter.

4.1.3 Method 3: Modified application of CIDECT Design Guide

A third HSS joint that is similar to the ST connection for which published data is available is the case of a wide flange I-shape end-connected to a circular HSS (see Figure 4-5). This case is covered only in the CIDECT Design Guide (Type XP-4), where a capacity equation is provided. The capacity equation for this case combines Equations (4-1) and (4-2) to yield the following (recast in LRFD format):

$$P_n = \frac{5F_y t^2}{1-0.81 \cdot b_f / D} \cdot (1+0.25 \cdot d/D) \cdot Q_f \qquad (4\text{-}4)$$

Intuitively, a joint with a W shape branch member should yield a higher capacity than an ST member of the same depth due to the simple fact that there are two flanges (not just one as in an ST) oriented transversely to the HSS axis. And as stated previously, the Canadian manual suggests that transverse plate components have the greatest effect on the overall strength of the connection. However, the case of a W shape connected to a circular HSS may actually behave like the ST connection more than the case of a concentrated load applied through a single transverse plate; as will be seen subsequently. As noted for the HSS-to-HSS joint, the geometry of the chord wall yield lines at failure for both the W and ST joints should be similar.

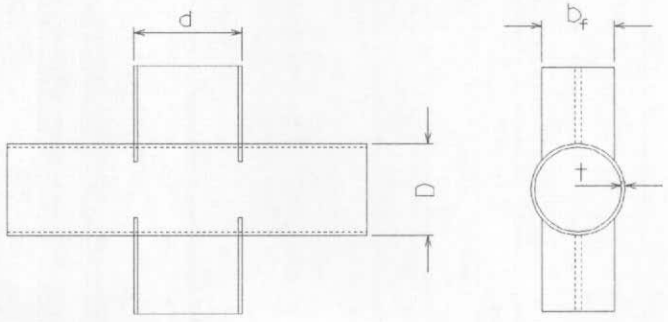

Figure 4-5: WT-to-HSS Joint Covered by CIDECT

4.1.4 Method 4: Modified application of AWS Section 2.24

Another approach to defining the capacity of the ST joint is in terms of punching shear in the chord wall. At first glance, one may argue that punching shear is not the limit state observed in the experimental tests, which is true in an academic sense. However, the term "punching shear" is used somewhat loosely in the context of tubular connection design. The actual failure mechanism involves a complex combination of local shell bending, warping, arching, and large deflection membrane effects and some researchers have chosen to quantify this in terms of a punching shear failure (Marshall, 1992). This approach is the basis for the provisions in AWS Section 2.24 (AWS 2004) and it is based on an applied stress approach. That is, the acting punching shear stress is first calculated by:

$$V_p = \tau \cdot f_n \sin\theta \qquad (4\text{-}5)$$

where:

$\tau \equiv$ branch thickness/chord diameter
$f_n \equiv$ nominal stress in branch member

However, it should be noted that for an open, plate-type branch member such as an ST, the punching shear area is doubled due to the fact that each plate component must punch through two (2) planes of the chord wall (i.e. double shear). Thus, the acting punching shear stress is cut in half in this case. Next, AWS specifies that the punching shear stress shall not exceed the allowable punching shear stress given by:

$$V_p = Q_q \cdot Q_f \cdot F_y / (0.6\gamma) \qquad (4\text{-}6)$$

where $\gamma \equiv$ chord radius / chord thickness

By setting these two equations equal to each other, substituting P/A for f_n, applying the double shear multiplier, and solving for P produces the following equation for axial load capacity:

$$P_n = 2 \cdot Q_q \cdot Q_f \cdot F_y \cdot A/(0.6 \cdot \gamma \cdot \tau) \qquad (4\text{-}7)$$

4.1.5 Additional Notes

It should be noted that there are a number of limits of applicability listed in Section 9.4 (2a) of the LRFD HSS specification (AISC 2000) that should be considered. Most relevant to the ST joint are the limits on wall stiffness and the limit on width ratio. The limit on wall stiffness states that the ratio of diameter to wall thickness must be less than or equal to 50 for chords and branches in T-, Y-, and K-connections and less than or equal to 40 for chords of Cross-connections. Members that exceed this limit would be classified as thin-walled sections. The limit on width ratio states that the ratio of branch diameter to chord diameter be within the range: $0.2 < D_b/D < 1.0$.

These limits are specified since some of the published limit state expressions (or their calibrations) are partly empirical. Although the design recommendations have been developed based on many experimental tests and related research that has been carried out worldwide, the formulas may not be reliable outside the parametric range for which they have been validated (AISC 1997a). Thus, it is prudent to use a set of parameter limits that reflect the bounds of most test results.

It is interesting to note that many of the experimental tests that are the basis for the capacity equations described above were conducted in the 1960's and early 1970's in different locations throughout the world. These tests were compiled and used to formulate the equations in 1976 by Y. Kurobane at Kumamoto University (Kurobane, et al. 1976) and the equations have remained mostly unchanged since that time. Equation (4-1) is based on a mere three (3) tests, all using a chord diameter of 6.5 in. Equation (4-2) is based on only eleven (11) tests with chord diameters of 4 in. and 4.5 in. Equation (4-4) is based on only six (6) tests with chord diameters of 6.5 in. and 4.5 in. Equation (4-3) is based on fifty-nine (59) tests with chord diameters of 4 in. to 18 in. Thus, it can be justifiably hypothesized that the range of usefulness for these equations may not include cases where extrapolations to geometries of more than two times the tested dimensions are considered.

It should also be noted that for all capacity calculations described above, a design wall thickness "t" is needed. When the actual wall thickness is not known, a value of 0.93 times the nominal thickness is permitted to be used as recommended by AISC (AISC 2000). This recommendation arises out of the fact that the American Society of Testing Materials (ASTM) permits the wall thickness in HSS fabrication to be as much as 10% below the nominal thickness.

4.2 VALIDITY OF PROPOSED METHODS

To assess the validity of the proposed methods, the various capacity equations have been applied to the geometry of the experimental test and these theoretical results are then compared to the results obtained from the experimental testing program reported on in Chapter 3. The relevant detail geometry that is considered in the application of the capacity equations is the diameter, thickness, and material strength of the HSS chord and the section dimensions for the ST10x48. This data is summarized below:

ST 10x48	HSS Chord
$b_f = 7.2$"	D = 26"
$t_f = 0.92$"	t = 0.50"
d = 10.15"	F_y = 47 ksi*
$t_w = 0.8$"	*from coupon test results
A = 14.1 in^2	

To apply the proposed equations to the experimental test, some assumptions will have to be made. The first assumption is with respect to the Q_f factor, which is relevant to all proposed methods. Since the ST is slightly offset in the longitudinal direction from the saddle support below, some flexural stress will develop in the HSS causing tension in the bottom face and compression in the top face. Compression in the chord wall at the ST will likely cause some reduction in the joint capacity. However, due to the close proximity of the ST and saddle, most of the load will likely be transferred by direct shear, or so-called "deep beam" action. Thus, it

seems reasonable to neglect any capacity reduction resulting from bending stress and assume Q_f = 1.0.

The second assumption to be made is whether this connection should be classified as a T-connection or a Cross-Connection, which is relevant to Method 2. The AISC HSS specification states that when the branch load is equilibrated by beam shear in the chord member, the connection shall be classified as a T-Connection, but when the branch load is transmitted through the chord member and is equilibrated by branch members on the opposite side, the connection shall be classified as a Cross-Connection (AISC 2000). Unfortunately, the tested configuration falls somewhere in between these two ideals, as mentioned before. Due to the close proximity of the ST and saddle bearing below, it seems reasonable to assume that most of the load is transferred directly through the HSS by shearing action with little bending stress developing. Thus, the connection might be seen to behave more like a cross-type connection.

Before applying the proposed methods, the limits of applicability mentioned in the previous section should also be considered in light of the test specimen geometry. First, the limit on wall stiffness ratio is 40 for cross connections as specified in the LRFD HSS Specification (AISC 2000). This ratio for the test specimens is 26/0.5 = 52, which is, in fact, slightly outside of the specified limit. Second, the width ratio should fall within the specified limits of 0.2 to 1.0 (AISC 2000). Utilizing the ST flange width (b_f) as the branch diameter yields a width ratio of 7.2/26 = 0.28, which is within the specified limit. Although the wall stiffness ratio has been exceeded, this does not disqualify the use of the provisions as proposed. The limits are merely being considered to evaluate how the specimen geometry compares to joint configurations studied previously.

Utilizing these assumptions and the known geometry, the capacity of the bearing detail in the experimental test has been calculated using the proposed methods developed earlier:

Method 1: Applying the provision for a concentrated force distributed transversely at the center of the HSS Face (Equation 4-1) yields:

$$R_n = \frac{5(47ksi)(0.5"\cdot 0.93)^2}{1-0.81(7.2")/(26")}(1.0) = 66kips$$

Applying the provision for a concentrated force distributed longitudinally at the center of the HSS Face (Equation 4-2) yields:

$$R_n = 5(47ksi)(0.5"\cdot 0.93)^2(1+0.25(10.15")/(26"))\cdot(1.0) = 56kips$$

Method 2: To apply the provision for a HSS-to-HSS truss connection, the Q_q factor must first be calculated using LRFD Equation 9.4-3:

$$Q_q = \left(\frac{1.7}{2.4} + \frac{0.18}{(7.2"/26")}\right)\cdot(1.0)^{0.7(2.4-1)} = 1.36$$

The capacity is now calculated using Equation 4-3 as follows:

$$P_n(1.0) = (0.5"\cdot 0.93)^2(47ksi)(6\pi\cdot(7.2"/26")\cdot(1.36))\cdot(1.0) = 72kips$$

Method 3: Applying the provision for a W-to-HSS joint (Equation 4-4) yields:

$$P_n = \frac{5(47ksi)(0.5"\cdot 0.93)^2}{1-0.81(7.2")/(26")}\cdot(1+0.25\cdot(10.15")/(26"))\cdot(1.0) = 72kips$$

Method 4: Applying the punching shear provision (Equation 4-7) yields:

$$P_n = 2\cdot(1.36)\cdot(1.0)\cdot(47ksi)\cdot(14.1in^2)/(0.6\cdot(13"/0.5")\cdot(0.79"/0.5")) = 73kips$$

The theoretical results from each proposed method along with the experimental results are summarized in Table 4-1.

Table 4-1: Accuracy of Approximate Methods

Experimental		Theoretical			
Nominal	Ultimate	Method 1	Method 2	Method 3	Method 4
70 k	96 k	66 k/56 k	72 k	72 k	73 k

4.3 DISCUSSION

In comparing the experimental and theoretical results, it is important to note that there is a fundamental assumption in using the proposed methods for predicting the capacity of the bearing in this geometric configuration. All of the existing specifications that were used in the development of the proposed methods were based on research done on a typical interior joint with a continuous chord member (i.e. not near an end). However, the vicinity of the connection to the open end of the HSS chord has influenced the geometry of the yield line failure mechanism observed experimentally and so too then, the overall capacity based on observations of the test data. Without further investigation, it is unknown to what extent the open end has affected the capacity of the joint. However, it is also pointed out that ovalization of the open end did not develop until load level of greater than 75% of ultimate capacity were achieved; an observation somewhat refuting the notion of significant effects being present. In any case, it can be surmised that the open end can only serve to *reduce* the capacity from that of an interior connection detail as compared to the capacity at an interior location.

For the bearing detail under consideration, the flange of the ST member was located a distance 33 in. from the end of the HSS, or a distance of 5/4 x D. If the proposed methods are shown to be accurate for this geometry, they will most likely *underestimate* the capacity of another joint with an end distance greater than this. Similarly, the proposed methods will likely *overestimate* the capacity of joints located in closer proximity with the open end. The parametric studies, using validated modeling strategies, are used to explore this point further in Chapter 6.0.

Method 1: The theoretical capacity predicted by Method 1 is 66 kips for the transverse component (flange plate) and 56 kips for the longitudinal component (stem plate). As mentioned above, the recommendation given the Canadian HSS manual is that only the transverse component should be considered in this case. Applying this notion to the ST joint yields a net theoretical capacity of 66 kips, which agrees well with the nominal capacity of 70 kips (within 6%) and provides a safety margin of 1.45 with respect to the ultimate capacity (not including the material yield bias). Adding the capacities of the individual components by direct superposition would result in a net theoretical capacity of 122 kips, which is a significant overestimate of the nominal capacity, and therefore considered inaccurate in this case.

Although superposition of the individual plate component capacities is unconservative for calculating the nominal capacity, it may apply to the calculation of the ultimate capacity. This recognizes that there is some increase in the ultimate connection capacity attributable to the presence of the longitudinal plate component. However, direct superposition once again overestimates the ultimate capacity of 96 kips obtained from the experimental results by a significant margin (27%). Assuming that the transverse plate component dominates the overall capacity as before, then it may be reasonable in this case to add the transverse component capacity plus a fraction of the longitudinal component capacity. Using a somewhat arbitrary 50% factor on the longitudinal plate component yields a theoretical capacity of 66 + (0.50 x 56) = 94 kips, which compares well with the experimental results.

Method 2: The capacity predicted by Method 2 is 72 kips, which agrees with the nominal capacity from the experimental results (to within 3%). This method provides a safety margin of 1.33 with respect to the ultimate capacity (not including the material yield bias). It should be mentioned that there is significant motivation for using Method 2 since it is the most portable of all the proposed methods. That is, it can be applied to many different connection geometries such as T-, Y-, K-, and Cross-connections, and it also treats the case wherein the branch member(s) experience flexure in addition to axial load. However, since the current testing has only considered the axially loaded 90° cross-connection, extending this method to other connection types should be done with care.

Method 3: The capacity predicted by Method 3 is 72 kips, which agrees with the nominal capacity from the experimental results (to within 3%). This method provides a safety margin of 1.33 with respect to the ultimate capacity (not including the material yield bias). As described earlier, this method is based on the CIDECT provision for a wide-flange connection, which is similar to the ST joint being studied except for the additional flange. This seems to imply that the additional flange does not significantly increase the overall strength of the joint.

Method 4: The capacity predicted by Method 4 is 73 kips, which also agrees with the nominal capacity from the experimental results (to within 4%) and provides a safety margin of 1.31 with respect to the ultimate capacity (not including the material yield bias). This indicates that the punching shear approach produces similar results in this case.

In summary, all of the proposed approximate methods provide a safe estimate of the bearing capacity as compared to the experimental results. However, the safety margins may be considered too low depending on the nature of loading, consequences of failure, etc. This is discussed further in Chapter 8.

5.0 FINITE ELEMENT MODELING

5.1 HSS MATERIAL BEHAVIOR

Since the failure of the bearing region involves a concentrated load which essentially "crushes" the HSS chord, the overall response of the connection is very sensitive to the HSS material behavior. If the HSS material is not modeled correctly, then agreement between the experimental and finite element analysis results will be poor. Therefore, a number of issues relevant to HSS members and their potential influence on the steel material behavior are discussed below.

5.1.1 Standard Mill Practice

A common method for manufacturing circular steel HSS members, and the method used for the manufacture of the test specimen chords, is the "formed-from-round" process. This involves conversion of a flat steel plate into an HSS through a series of forming operations. As illustrated in Figure 5-1, a flat strip of steel plate is bent continuously around its longitudinal axis to form an open-seam round by passing it through a progressive set of rolls. The resulting open-seam round is then closed with a continuous longitudinal weld. After welding, the section is cooled and then run through an additional set of sizing rolls to achieve the desired final shape (AISC, 1997a). This is important to note since the cold working in these operations causes changes in stress-strain behavior from the basic steel material properties. A metal which has undergone a severe amount of deformation, as in rolling or drawing, will develop a preferred orientation, or "texture," in which certain crystallographic planes, or mechanical fibers, tend to orient

themselves in a preferred manner with respect to the direction of maximum strain (Dieter, 1986). Researchers confirmed that this effect can be significant in tubular members by comparing the stress-strain behavior in steels from tubular columns with and without annealing (Popov et al.. 1979).

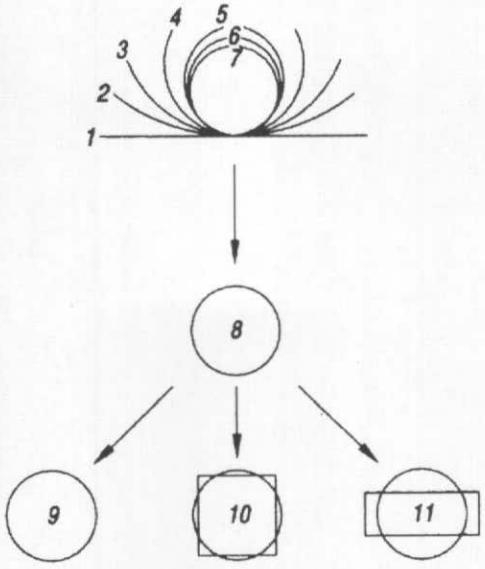

Figure 5-1: Formed-from-round process for HSS manufacturing

5.1.2 Specifications

The HSS chords used in the test specimens were manufactured under ASTM A53: *Standard Specification for Pipe, Steel, Black and Hot-Dipped, Zinc-Coated, Welded and Seamless*. This specification is intended for mechanical and pressure applications and is also acceptable for ordinary uses in steam, water, gas, and air lines. It is suitable for welding, and suitable for forming operations involving coiling, bending, and flanging. However, ASTM A53 is not necessarily meant for structural applications in buildings and bridges as is the more common ASTM A500 *Standard Specification for Cold-Formed Welded and Seamless Carbon Steel Structural Tubing in Rounds and Shapes*. ASTM A53 Grade B was selected since this is the

material specification used in Pennsylvania for fabrication of overhead sign trusses. The specification tensile requirements are as follows:

Min. Yield Strength = 35 ksi
Min. Tensile Strength = 60 ksi

5.1.3 Tolerances

Variations in geometric dimensions from the nominal values specified for the HSS members can have a significant affect on the behavior of the structure under investigation. The tolerances for fabrication of tubular members in general are not stringent as compared to similar open rolled structural shapes, and ASTM A53 is even more forgiving to manufacturers. The permissible variations as per ASTM A53 that should be noted are as follows:

HSS Outside Diameter: +/- 1%
HSS Wall Thickness: -12%
Straightness: No requirement
Mass (weight): +/- 10%

As a result of these generous tolerances, most HSS manufacturers tend to produce under-sized sections, but still within the specification limits (Packer and Henderson, 1997). Since connection capacity in tubular structures is typically a function of HSS wall thickness squared, the structural safety index can be very sensitive to this geometric property. As a result, the AISC HSS Specification (AISC, 2000) states that a design wall thickness of 0.93 times the nominal thickness should be used for design calculations.

5.1.4 Residual Stresses

Residual stresses in HSS members most commonly arise from the cooling effects after hot finishing, from the welding processes employed, or by the prevention of spring-back introduced during forming operations (Galambos, 1998). Recalling the numerous forming and welding operations that a steel plate must be subjected to for creation of a tubular section by the formed-

from-round method, it can be seen why significant residual stresses can develop. As a result of these operations, the exact shape of the stress-strain curve, the proportional limit, and the yield strength of tubular members are rather unpredictable (Galambos, 1998). Measurements on members fabricated for a column testing program (Chen and Ross, 1977) gave the longitudinal and through-thickness circumferential residual stress patterns shown in Figure 5-2. These patterns and general magnitudes have been confirmed by other researchers (Prion and Birkemoe, 1988). The distributions show that significant residual stresses develop in tubular members; approaching 35% of the yield stress σ_y in the circumferential direction and 100% of the yield stress in the longitudinal direction. It is noted that while the longitudinal residual stresses vary based on the distance from the seam weld, the circumferential residual stresses were found to be nearly the same in all locations around the perimeter (Toma and Chen, 1979).

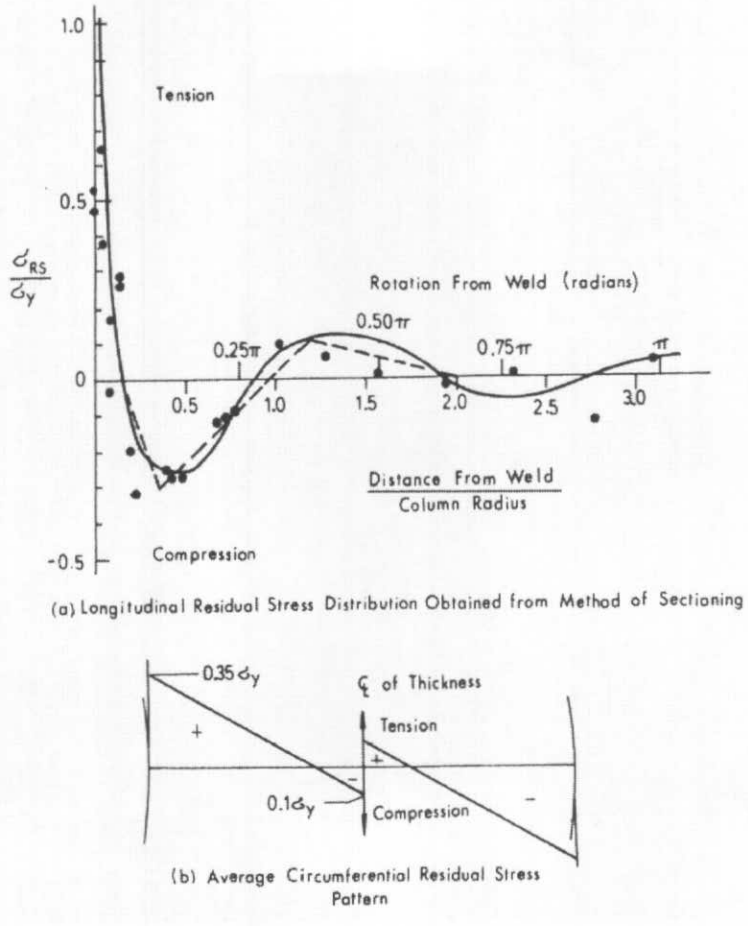

Figure 5-2: Residual stresses in fabricated round tubular members (Toma and Chen 1979)

5.1.5 Coupon Testing

Determining the mechanical properties of steel in HSS members can be problematic. Conventional coupon tests are possible for the longitudinal direction (with some machining of the coupon), but not for the transverse direction due to the circular cross-section. To conduct a transverse tensile test (as per ASTM A370 *Standard Test Methods and Definitions for Mechanical Testing of Steel Products*), a ring must be cut from the specimen and then flattened. However, these test specimens require normalization due to this additional treatment of the material being tested.

One of the unique features in the mechanical behavior of steels from tubular members is that the stress-strain response becomes nonlinear at low stresses and the yield point is typically not well defined as compared to conventional rolled steels. Toma and Chen attributed this to the residual stresses present in tubular members and subsequently they developed the concept of the *Effective Young's Modulus* for describing the material response, for which a variable modulus is used to describe the slope of the complete stress-strain curve (Toma and Chen, 1979). In this approach, the effective modulus is a function of the applied stress, the yield stress, and an *initial yield stress*, which results from the residual stresses present.

5.2 FINITE ELEMENT MODELING TECHNIQUES

The techniques employed for the finite element modeling are based on the techniques that were developed and validated by Li and Earls for earlier work on HSS connections (Li and Earls, 2002). Consistent with this earlier work, the current research employs dense meshes of nonlinear shell finite elements positioned at the mid-surface of the constituent plate components for each of the structural members comprising the connection under investigation. The application of shell elements in this fashion permits the actual three-dimensional geometry of the structure to be replicated in physically meaningful way.

Since the finite element models are to be used as the vehicle by which the response characteristics of multiple HSS truss connection geometries are to be quantified, it is important to ensure the robustness and viability of the modeling strategies adopted in the present work. As a means of validating the current modeling techniques, they are first applied to the case of two full-scale experimental specimens tested as part of the current research effort. Favorable agreement between the modeling results of these specimens and the laboratory results are obtained. A detailed discussion of this comparison follows in a subsequent section of the current paper.

Since the potential for steel yielding and localized buckling effects are present, the finite element modeling approach adopted considers both geometric and material non-linearities within the context of an incremental analysis. Thus, a Riks-based solution approach (ABAQUS 2003) is employed to capture both the intermediate loading steps leading up to the ultimate load as well as the response in the unstable (un-loading) region of the equilibrium path. The completed model of the experimental test in its deformed configuration at the ultimate load, and with the von Mises stress contours displayed, in a magnified state, is shown in Figure 5-3.

5.2.1 Boundary Conditions and Loading

For the boundary conditions and loading, there are a number of important features of the model that should be discussed. First, the interface between the saddles and the HSS is modeled as a fully pinned surface (i.e. every node at the interface between the HSS and the saddle is constrained against any translation). Thus, the HSS cannot separate from the saddle bearings or slide within the saddles. This is clearly an idealization of the true physical boundary condition, but was nonetheless found to be accurate (see discussion on contact below). At the opposite end of the specimen two (2) discrete pinned support conditions are imposed on the shell element mesh of the HSS to simulate a thru-bolt support condition that is consistent with that used in the experimental testing. Finally, the unconnected end of the ST member, at the point of load application, is prevented from any lateral translation; consistent with the physical boundary condition in the test specimens. In addition, loading is imposed on the model through the application of a concentrated force applied at the centroid of the ST cross-section.

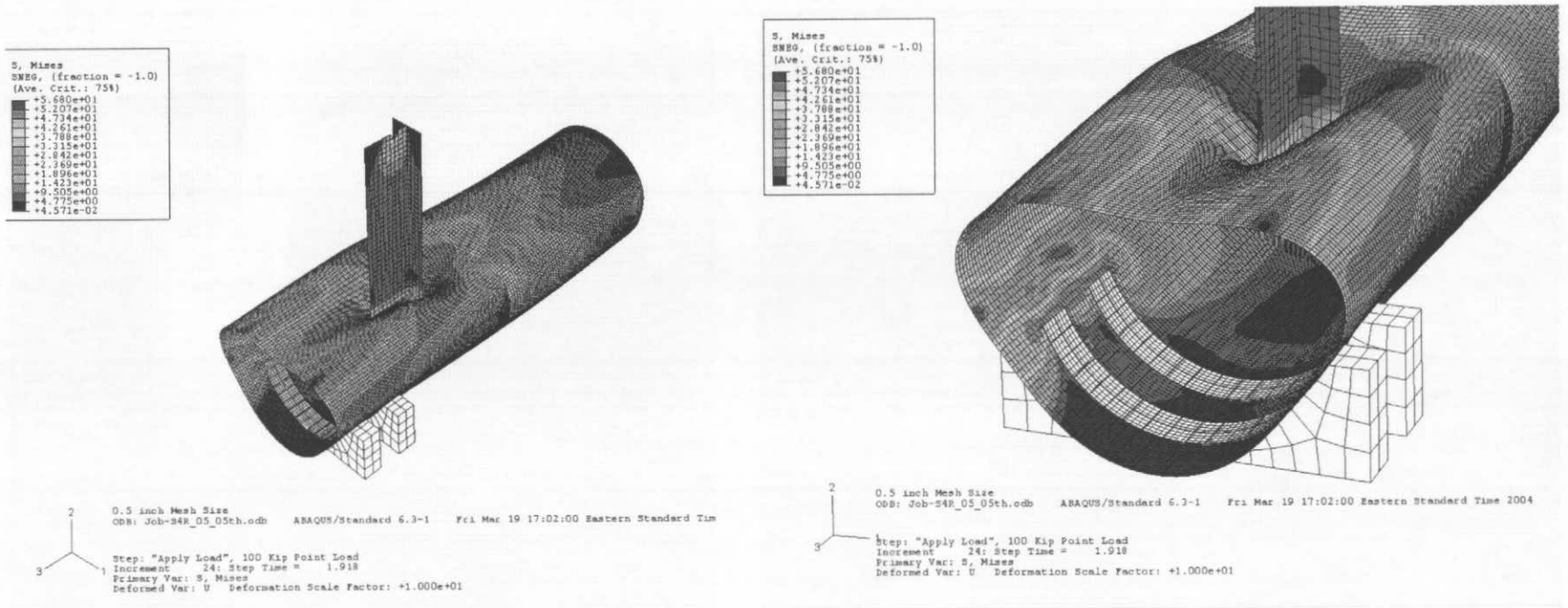

Figure 5-3: Finite element model with von Mises stress contours.

5.2.2 Element Type

Since this structure consists of relatively thin components (some with curvature) subjected to primarily flexural and membrane stresses, the shell element is deemed to be the most appropriate finite element for use in the modeling. In general, the failure mechanism involved in this type of connection is seen to involve a plastic collapse of the HSS chord wall as a result of the formation of a system of well-defined yield lines. While it is that the structural element formulation employed in shell element formulations is well suited to capturing this type of behavior, it should be noted that the regions of the HSS chord in the vicinity of the ST are also observed to be subjected to large local transverse shear stresses as the applied load is transferred from the ST to the chord; a condition where even the most robust shell formulation may experience difficulties.

In choosing the specific shell element to be used in the modeling, several different types from the ABAQUS library are considered initially: S4, S4R, S8R, and STRI3. All of these shell elements utilize 6 degrees of freedom (DOF) at each node (3 translational and 3 rotational), but each is somewhat different in terms of its *formulation, integration*, and/or *interpolation*.

The shell *formulation* refers to the mathematical theory used to define the element's behavior. Shell problems generally fall into one of two categories: thin shell problems and thick shell problems. For a detailed discussion on different shell formulations, as well as proper integration order for the integration of their stiffness matrices, the reader is referred to the book by Bathe (1996). What follows now is a very superficial discussion meant only as a summary of relevant concepts used in the present work. Thick shell problems assume that the effects of transverse shear deformation are important to the solution at hand. Thin shell problems, on the other hand, assume that transverse shear deformation is small enough to be neglected. Thin shell elements provide solutions to shell problems that are adequately described by classical (Kirchhoff) shell theory, thick shell elements yield solutions for structures that are best modeled by shear flexible (Mindlin) shell theory. The STRI3 shell in ABAQUS is a thin shell element, the S8R is a thick shell, and the S4 and S4R are general-purpose shell elements. In ABAQUS, so-called "general purpose" shell elements are considered valid for use in both thick and thin shell problems.

It should be noted that in the S4R shell, changes in the cross-section thickness, as a function of membrane strains and material definition are considered. This capability can be important in nonlinear analyses where large strains accompany large rotations. The membrane kinematics are based on an assumed-strain formulation that provides accurate solutions to many loading conditions, including in-plane bending behavior (ABAQUS, 2003).

The shell *integration* refers to the number of discrete points within each element that are utilized to calculate the internal strain energy in the deformed configuration. Shell elements can be either fully integrated (e.g. S4, STRI3) or use reduced integration (e.g. S4R, S8R). For full integration, the standard Gauss quadrature is employed which results in four (4) integration points for a quadrilateral and three (3) integration points for a triangular element. For reduced integration, only a single integration point is used for each of these elements. Reduced integration elements are attractive because they reduce computational expense while providing a means for mitigating shear locking effects which become pronounced when shear deformable shell formulations are used in situations where the through-thickness dimension is small. However, reduced integration elements often exhibit another numerical problem called hourglassing, in which the element can deform in certain ways with the internal strain energy remaining zero. Thus, fully integrated elements are recommended for conditions where greater solution accuracy is desired, or for problems where in-plane bending is expected (ABAQUS, 2003). In all cases, five (5) Simpson integration points through the element thickness are utilized.

The shell *interpolation* refers to the displacement functions that are assumed in the element formulation for describing the deformed shape between the element nodes. In the context of our present discussion, the interpolation order is either linear or quadratic. Quadratic elements are more accurate on a per element basis; however their use comes at an increased computational expense since additional nodes are required to adequately describe their shape.

A summary of the different shell elements considered and their respective features is shown in Table 5-1.

As part of the current research effort, an evaluation of element performance within the context of the current problem is undertaken. To complete this evaluative effort, analyses of the subject problem are conducted utilizing each of the four (4) elements identified in Table 5-1 and the model response characteristics are compared in the context of load-deflection response (see

Figure 5-4). For each of the finite element analyses, the geometry, boundary conditions, loading, and material model are identical. However, the finite element meshes vary slightly as a result of differences in elemental node layout. This is important to note since the solution is dependent upon the mesh density (# elements / unit area) as discussed below. To properly assess the relative performance of the four (4) shell elements, the mesh density is doubled for the STRI3 model and halved for the S8R model (as compared with the 4 node quadrilateral shell mesh). This results in the same number of nodes and DOFs for all four models.

Table 5-1: Summary of Shell Elements Considered

ABAQUS Name	#Nodes/El	Formulation	Integration	Interpolation
S4	4	Gen. Purpose	Full	Linear
S4R	4	Gen. Purpose	Reduced	Linear
S8R	8	Thick	Reduced	Quadratic
STRI3	3	Thin	Full	Linear

In general, it can be seen that the load-displacement response is very similar for all the element types. As expected theoretically, all models predict the same result in the elastic range. It is not until well into the plastic range where some subtle differences arise. It is observed that the general-purpose shell elements (S4, S4R) show a slightly higher peak load than the two special purpose elements (S8R, STRI3) by approximately 2%. This is likely due to the consideration of finite membrane strains (greater than 1%) in the S4 and S4R formulations. During the analyses, strains of greater than 1% were observable in regions of the mesh where yield lines formed. In addition, since the HSS chord is subjected to compressive hoop stress as the load travels from the ST to the saddles, the shell thickness will increase by the Poisson effect as inelastic deformation occurs. This increase in thickness will have a strengthening effect on

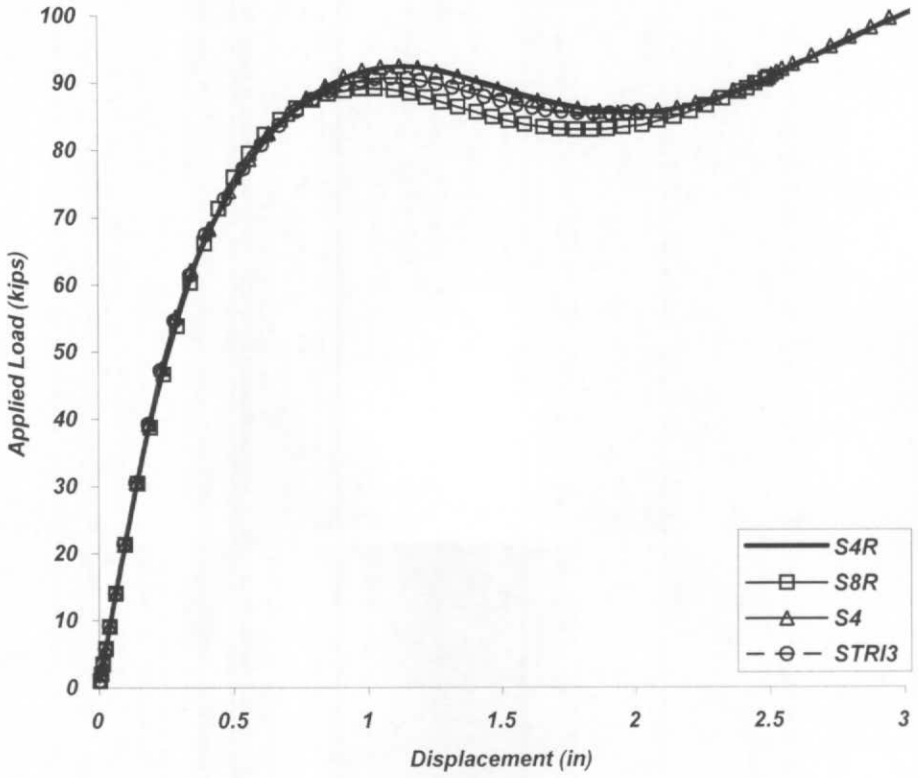

Figure 5-4: Effect of element formulation on predicted response

the yield line failure mechanism since the flexural strength (plastic moment capacity) is a function of the wall thickness. This strengthening effect was confirmed by performing a subsequent analysis with $\nu = 0$, for which the capacity was reduced to nearly the same value as that given by the STRI3.

The second observation to make is that the S4 and S4R models predict nearly the same response throughout. This indicates that the reduced integration does not have a significant impact on the solution, which is good news since the run time is less for the S4R model.

The last observation is that the two special purpose elements (S8R, STRI3) predict similar responses even though the S8R is based on a thick shell formulation and the STRI3 is based on a thin shell formulation. This indicates that the problem is truly a thin shell problem,

since reduced integrated thick shell elements like the S8R can have limited success solving a thin shell problem. The converse is not typically true for elements formulated for thin shell applications.

Based on this investigation, the S4R nonlinear, finite strain, general-purpose quadrilateral shell element from the ABAQUS element library is selected. A single integration point is used in this particular element, so computational expense is relatively low. Also, since consideration of finite membrane strains may be important to the behavior the structure under investigation, the S4R is the preferred choice. Furthermore, researchers have found the S4R element to produce reliable results for modeling of similar steel plate-type structures (Li and Earls, 2002), (Thomas and Earls, 2003), (Greco and Earls, 2003).

5.2.3 Contact

Frequently, stresses developing at contacting interfaces between structural components in a system may prove to dominate an analysis. Such intense stress states may admit the possibility for interfacial slip, separation, and/or sliding as a result of stress concentrations, load redistribution, or other local mechanism. Therefore, there may be a danger that using a simplified modeling approach in the treatment of interfacial behavior will lead to errors in the prediction of ultimate strength. Contact modeling is typically avoided in day-to-day structural engineering analysis due to the computational expense associated with such considerations. However, since the geometry of the structure under investigation involves a flexible shell structure bearing against a rigid curved surface, it is difficult to exercise engineering judgment regarding the potential effects of contact in this case. Therefore, an analysis is performed with a true contact interaction (separation and sliding allowed) at the interface between the HSS chord and the saddle bearings. For this analysis, the saddle bearings are modeled as analytical rigid bodies. That is, they are considered to be infinitely stiff. This approximation is acceptable since any deformation of the saddles is negligible and will have almost no affect on the capacity of the system.

The contact analysis results indicate that while some minor localized sliding may occur between the HSS and the saddles, uplift does not occur as a result of the compressive nature of the loading. More importantly, the ultimate load determined by contact analysis is within 1% of

the load when using the simplified boundary condition (but at significant increased cost in terms of analysis time). Thus, the simplified (fully pinned) boundary condition is deemed acceptable for the HSS/saddle interface.

5.2.4 Mesh Density

In development of the final modeling techniques (i.e. S4R element in a mesh pinned at the saddle), a mesh convergence study is performed employing S4R element sizes of 2 in., 1 in., ½ in., and ¼ in. It is determined that the accuracy of the solution is improved as the mesh size is refined, but the improvement between ½ in. and ¼ in. is insignificant in comparison to the increased run time. Thus, the recommended element size for the S4R element is ½ in., which is used throughout the model.

5.2.5 Material Model

Since the global failure mechanism observed involves plastification of the chord wall into well-defined yield lines exhibiting large strains (i.e. greater than 1%), the material model that is used to describe how the structural components will deform is vital to obtaining accurate overall results. Unfortunately, the material behavior, as opposed to geometry, loading and boundary conditions, is where the greatest uncertainties lie.

The basic form of the material definition utilized is consistent with that of a von Mises metal plasticity model and an associated plastic flow rule. In general, metals resist a portion of a large externally applied load through the development of an elastic strain potential. The remaining portion of the external work is then dissipated through the action of internal plastic work. For the case of mild steel, the primary mechanism for this plastic flow occurs along slip planes. This slipping coincides with atomic structural imperfections such as crystal dislocations and sites of non-metallic impurities in the metallic grains.

The foundation of the von Mises theory is the assumption that metallic materials resist all hydrostatic stress in an elastic fashion. Thus, only the deviatoric components of the stress state are associated with the initiation and propagation of plastic flow, which has been confirmed

experimentally for most common metals (ABAQUS, 2003). This assumption leads to the development of a *yield function* or *yield surface*, which defines the limit of purely elastic response as well as the direction of plastic flow for 3D stress states. The assumed direction of plastic flow is the same as the direction of the outward normal to the yield surface, which is often referred to as *associated flow*. Associated flow models are useful for materials in which dislocation motion provides the fundamental mechanisms of plastic flow (ABAQUS, 2003). To define the material for the finite element analysis model, only the uniaxial behavior need be employed; ABAQUS will use this data to generate the required von Mises yield surface in 3D stress space.

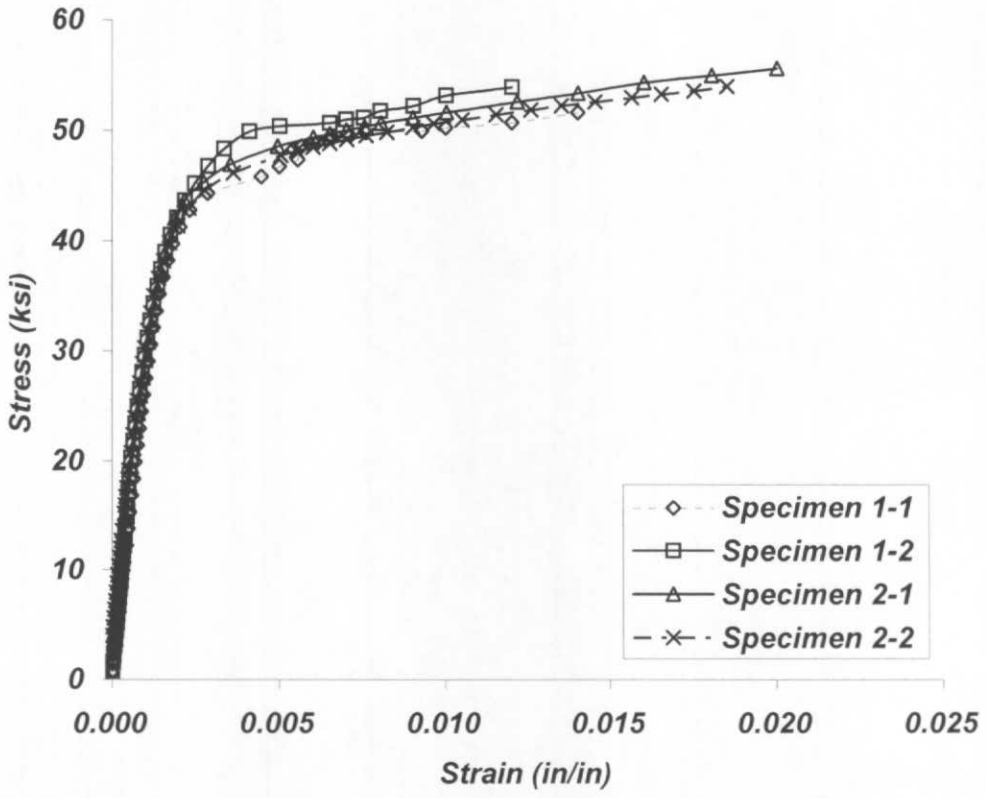

Figure 5-5: Coupon test results from HSS chord steel

For the uniaxial material definition, coupon test results from the actual test specimens are used. Two (2) coupons were cut and tested from each of the HSS chords in the test specimens, yielding a total of four (4) tests, which are all shown in Figure 5-5. Due to difficulties in machining coupons in the transverse direction of the HSS (see discussion above), only coupons from the longitudinal direction were taken. To utilize the coupon test data for the material model definition, it is assumed that the steel is isotropic, linear-elastic with isotropic plastic hardening and rate and temperature independence. That is, the response is assumed to be linear up to a discrete yield point, after which plastic (permanent) deformation occurs as described by a work hardening curve with no influence from temperature or strain rate. The elastic modulus is determined to be 21,000 ksi, and the yield point is established utilizing the standard 0.2% offset method to be 47 ksi. The work hardening curve is defined by using a piecewise linear function developed from the actual measured coupon test data. It should be noted that for large deformation finite element analysis, "engineering" stress and strain must be converted to "true" stress and strain using the following relationships:

$$\varepsilon_{true} = \ln (1 + \varepsilon_{eng}) \tag{5-1}$$

$$\sigma_{true} = \sigma_{eng} (1 + \varepsilon_{eng}) \tag{5-2}$$

The results from Equations (5-1) and (5-2) are then included in the ABAQUS input deck in order that a failure surface may be constructed in three dimensional stress space.

5.3 VERIFICATION OF FINITE ELEMENT ANALYSIS TECHNIQUES

To verify that the modeling techniques are producing accurate results, a full simulation of the experimental testing, carried out at as part of this research, is performed and the analytical results are compared to the experimental measurements. Specifically, the deflections recorded by the displacement transducers (DCDTs) and the strains measured by the rosette gauges installed on the surface of the HSS chord wall are compared to the finite element analysis results.

The DCDT measurements that are used for the verification are designated as DCDT 1 and DCDT 3 from the experimental test data (see Figure 3-1). The DCDT 1 measured the total

displacement at the point of load application (including both global and local deformation effects within the specimen) and the DCDT 3 measured the local deformation (ovalization) of the HSS cross section at the open end.

Strains measured with rosette gauges on the surface of the HSS chord wall are also used for verification of the finite element analysis modeling techniques. These gauges were positioned uniformly along the circumference of the HSS chord in three (3) sections between the ST and saddle bearings. The gauge locations and their respective numbers are shown in Figure 3-3.

5.3.1 Overall Agreement

First, the overall specimen behavior and response is discussed in the context of the observed evolution in the failure modes. As noted in the observations of the experimental results at failure, dimples form in the HSS wall around the ST flange tips and the open end of the HSS deforms into an oval shape (Boyle and Earls, 2004). A deformed shape consistent with this description is also predicted by the finite element analysis simulation (see Figure 5-6). In addition, a number of rosette gauges indicate yielding in the HSS chord wall during testing: 1, 3, 5, 8, 9, 13, and 14. In general, these locations of yielding are consistent with the yield line patterns as discernable in the exhibited von Mises stress contours presented in Figure 5-3. In general, these initial observations indicate that the same basic mechanisms of failure are being captured.

5.3.2 Agreement in Displacements

Next, the displacements from the finite element analysis and experimental results are compared. By studying the global deflection at the point of load application in Figure 5-7, it can be seen that the agreement between the experimental results and finite element modeling results appears to be favorable at this location. Recall that this is the DCDT 1 measurement discussed previously. The elastic stiffness (initial slope of the load-deflection curves) is consistent and the peak loads from the finite element analysis and experimental results of Specimen #2 are within 4% (92.4 kip

(a)

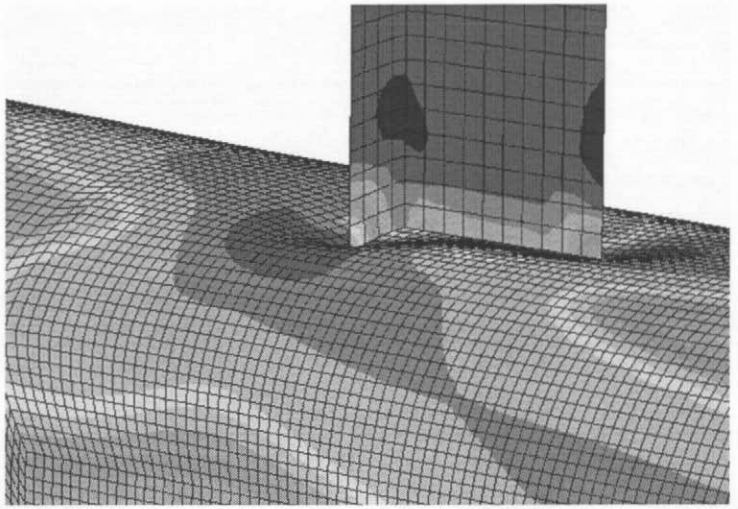

(b)

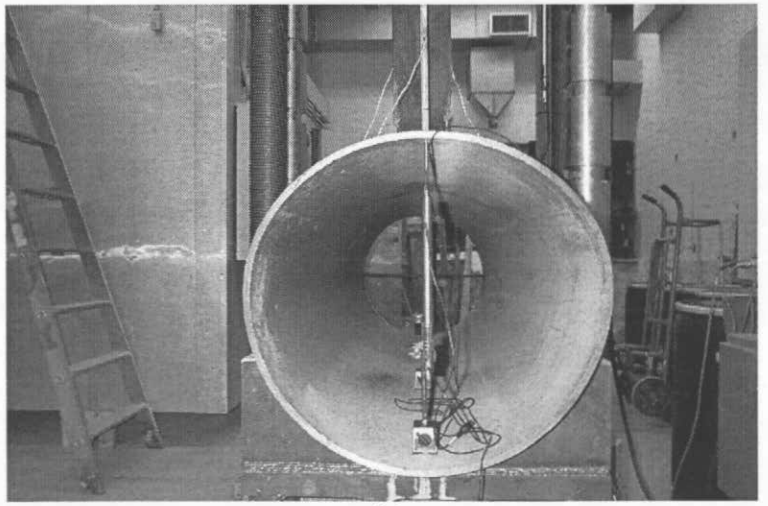

(c)

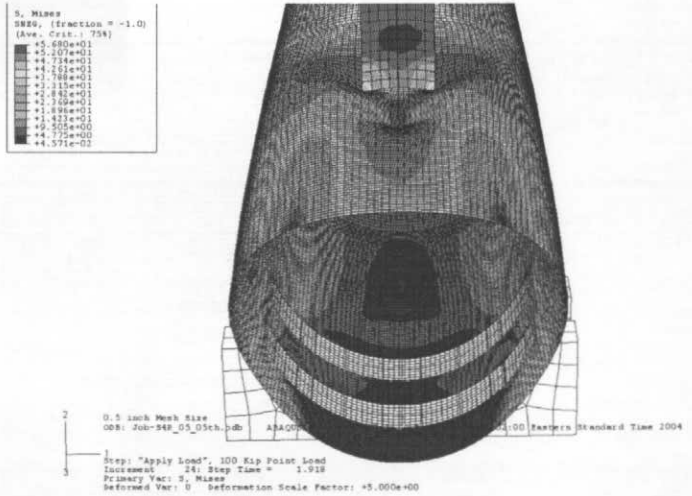

(d)

Figure 5-6: Deformed shape comparison: (a)(b) dimpling at ST and (c)(d) ovalization at end

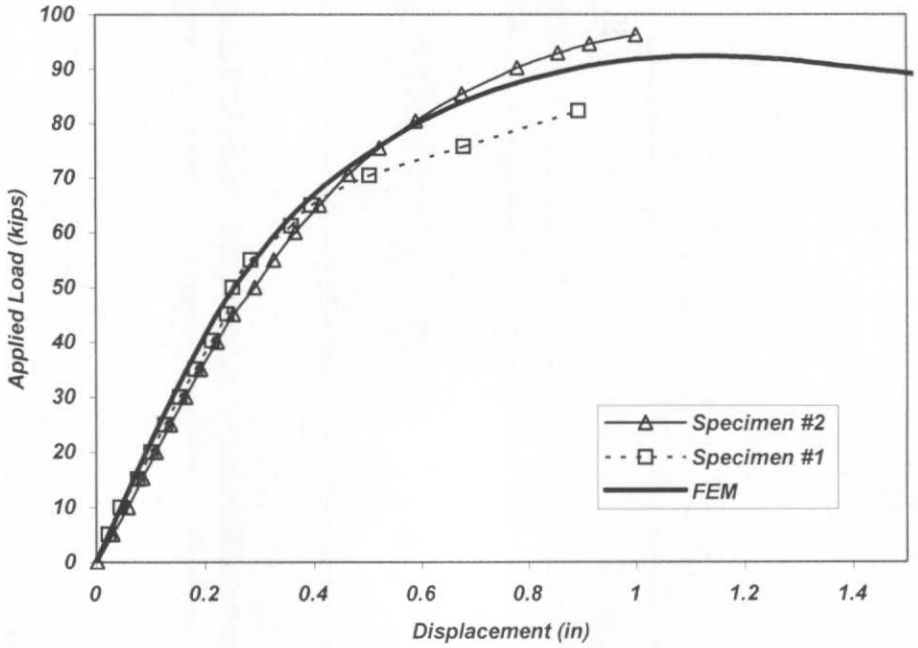

Figure 5-7: Load-deflection response comparison at applied load (DCDT 1)

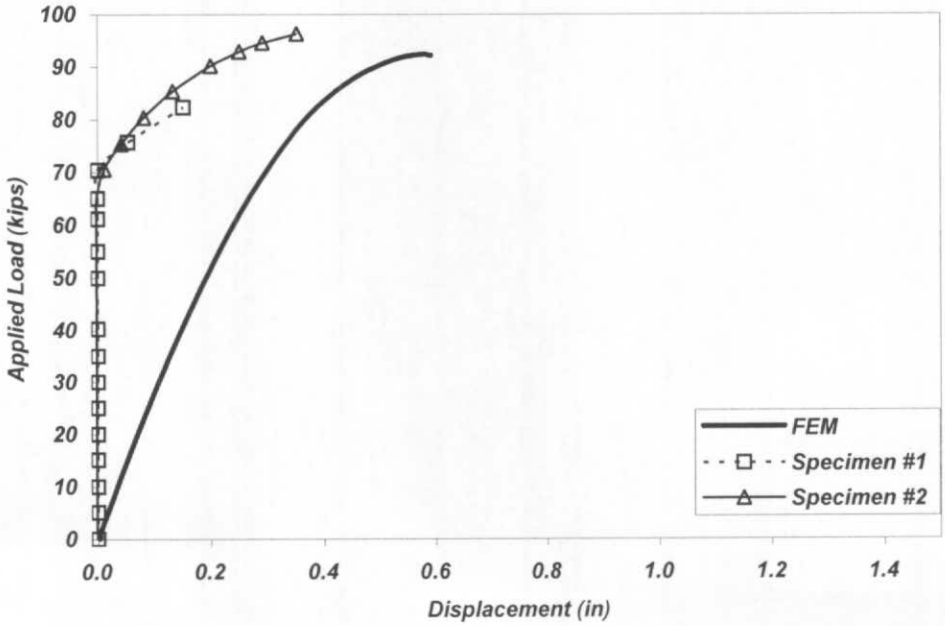

Figure 5-8: Load-deflection response comparison at HSS end (DCDT 3)

vs. 96.3 kips). For Specimen #1, the peak load was slightly less which is attributed to the problem in the testing noted earlier. It is also noted that these ultimate loads occur at nearly the same deflection; this may be important if one desired to use a deflection criterion for defining the nominal capacity in a design context. One minor difference to note is that the finite element analysis predicts a slightly softer response in the inelastic range; i.e. the load above 60 kips. This results in a slightly lower ultimate load predicted by finite element analysis as compared to the experiment, but still within a small percentage of the total load.

Additionally, the displacements at the open end of the HSS are compared (see Figure 5-8). Since this location is 33 in. away from the ST strut, the deflection here gives an indication as to what extent the applied load is dispersed longitudinally in the chord wall. Interestingly, both experiments showed no movement until a load of 70 kips, at which point the open end closed quickly. In contrast, this response is not predicted by the finite element analysis. The finite element analysis results indicate a gradual (smooth) increase in deflection from the beginning of load application up to a maximum of deflection of 0.6 in. Since similar responses were observed in both experimental tests, it cannot be attributed to the incident that occurred in testing of Specimen #1. This is discussed further below.

5.3.3 Agreement in Strains

Since strains are the actual measured data from the gauges (and thus do not require any additional assumptions regarding material mechanical behavior), comparisons based on these measures represent the most direct approach for determining agreement between the models and the physical tests (as opposed to stresses). However, strains are often difficult to correlate between experiments and analysis since strain is defined at an idealized point in space. This type of measurement is a simple matter for a computer model based on the finite element method, but in a real physical test, the strain rosettes tend to be quite large in size and thus the strain measurements are effectively being averaged over significant gauge lengths in the lab testing. Also, strain measurements tend to be very sensitive to the residual stresses and variations in the thickness in the base material.

The locations considered in this portion of the comparison in results are all the locations where yielding of the HSS wall occurs; these locations tend to exhibit large magnitudes of strain, which are more useful for comparison purposes. Since rosettes 1, 8, and 13 are mirror locations about the centerline of the HSS to rosettes 5, 9, and 14 respectively, symmetry is exploited and only one-half of the instrument readings are considered. It should be noted that the mirror locations all showed similar behavior to their associated rosette on the opposite side. This indicates that the experimental loading and response was symmetric; with no significant out-of-plane bending or twisting of the specimen.

The comparisons of the principal strains at the four (4) yielded locations are shown graphically in Figure 5-9 through Figure 5-12. By studying the figures, it can be seen that the finite element analysis and experimental strains agree very well at rosettes 3 and 14. The initial slope of the curves, the load at which the curves become nonlinear, and the strain magnitude at the peak load are all relatively consistent. Of all the rosettes, these two locations exhibited the largest magnitude of total strain: in the range of 3500-4500 microstrains (the uniaxial yield strain is approximately 2200 microstrains). Large strains are expected here since rosette 3 is located at the apex of the HSS adjacent to the ST web where a yield line is well defined. Large strains are also expected at rosette 14 since this is in close proximity to the ST flange tip where significant dimpling was observed to occur in the experimental specimens during testing. For rosettes 5 and 9, the comparisons are slightly less favorable, but are still very reasonable. The less favorable agreement observed between modeling results and physical testing results is likely due to the fact that the magnitudes of the strains are smaller than those observed at 3 and 14, and so any discrepancies are more pronounced in terms of gross percentages of measured response.

5.4 DISCUSSION OF RESULTS

Overall, the agreement between the finite element analysis results and the experimental tests is favorable. The finite element analysis simulation results support the general observations made during the testing. In addition, the displacement and strain measurements taken from the

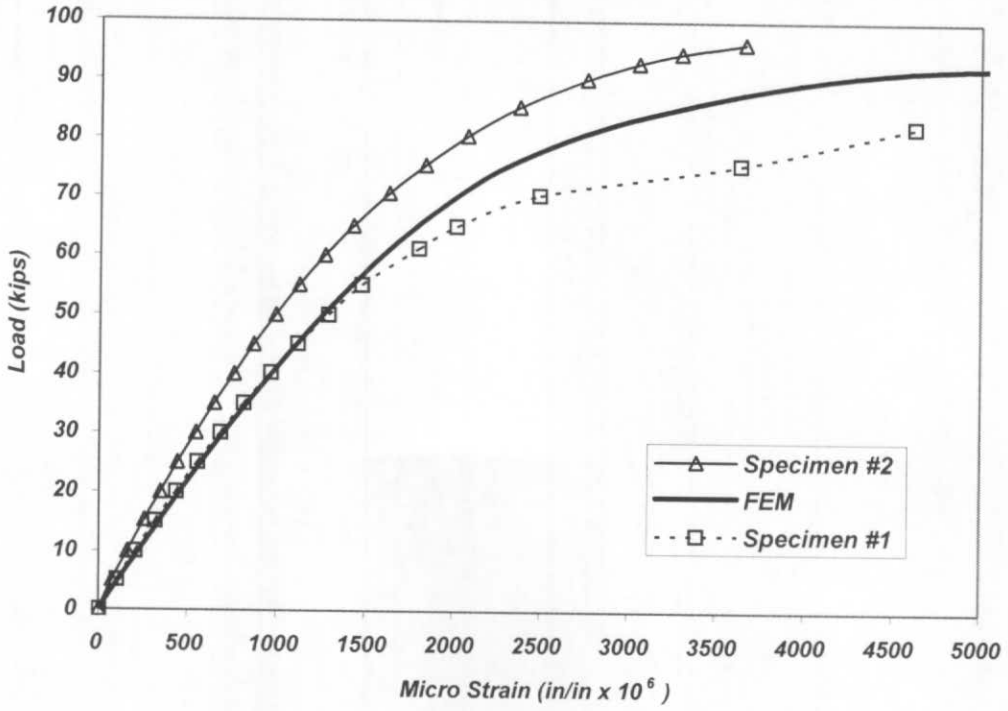

Figure 5-9: Maximum principal strain comparison at gauge location 3

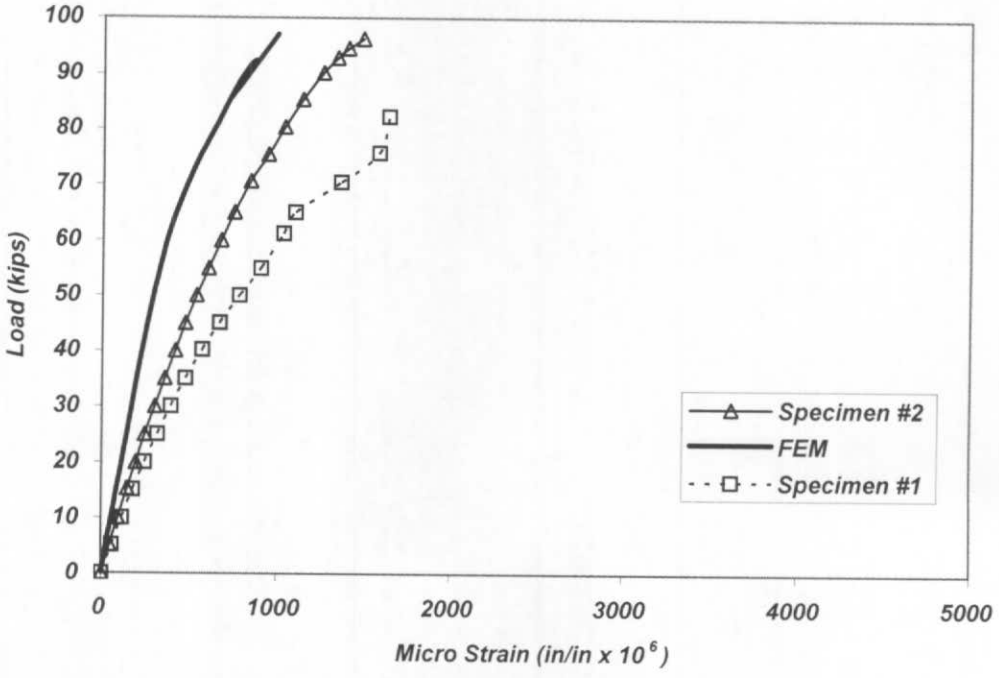

Figure 5-10: Maximum principal strain comparison at gauge location 5

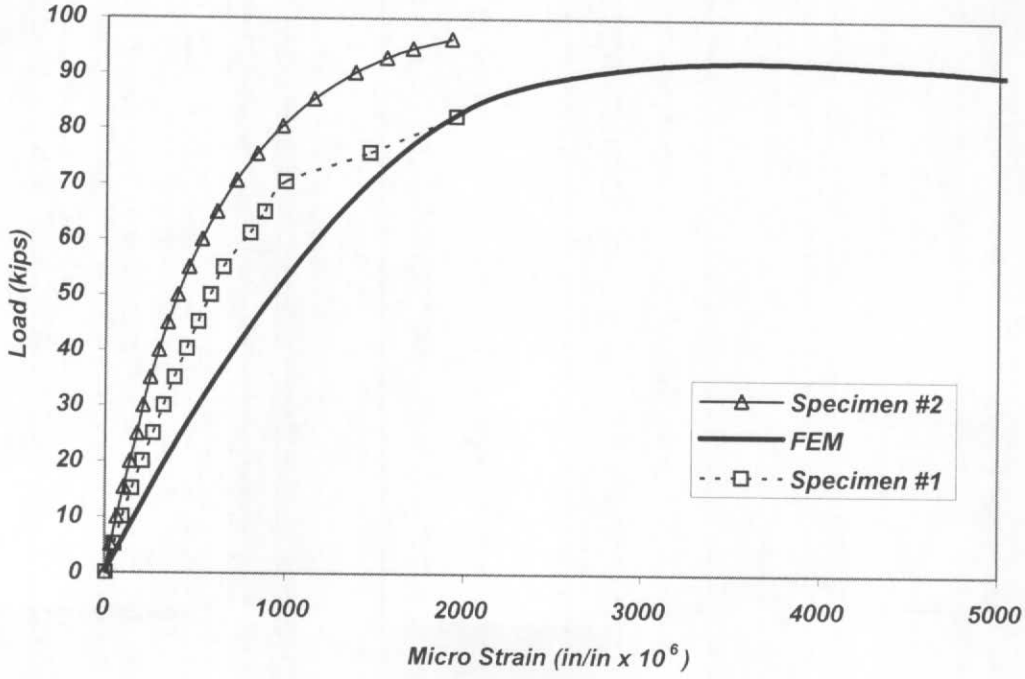

Figure 5-11: Maximum principal strain comparison at gauge location 9

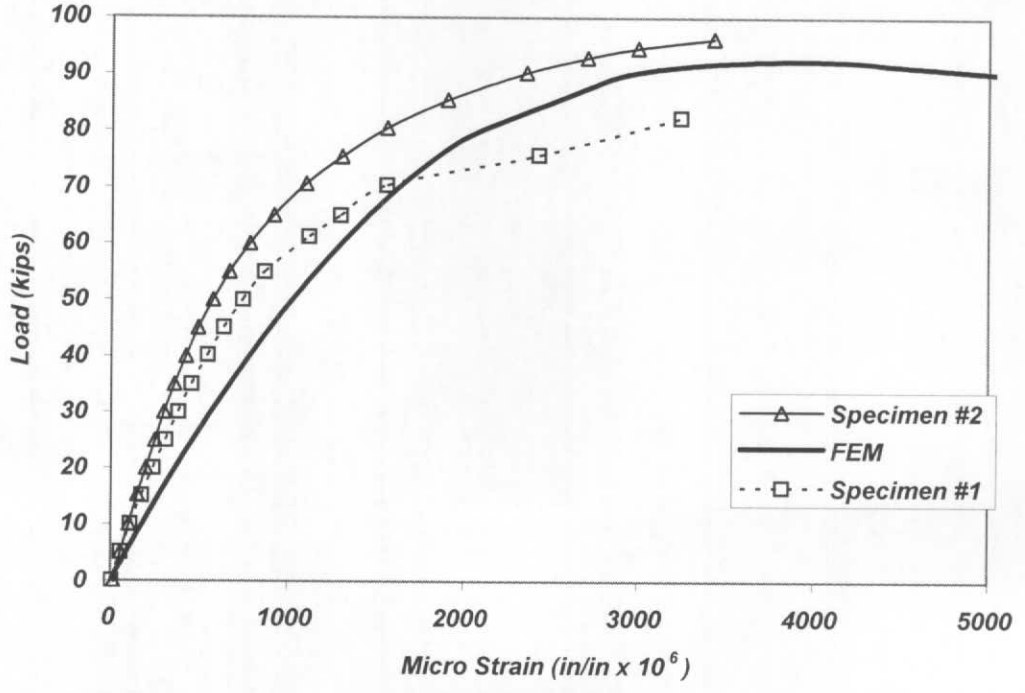

Figure 5-12: Maximum principal strain comparison at gauge location 14

specimens are mostly consistent with the analytical results. Thus, it is concluded that the finite element analysis techniques employed herein are valid for analysis of the structure under investigation. However, from this research, a number of issues with regard to finite element analysis of tubular steel structures have arisen which are discussed in more detail below.

5.4.1 Sources of Discrepancy

The potential sources of discrepancies between the finite element analysis and experimental results are: physical variations in HSS wall thickness, diameter, mass, and residual stresses as discussed previously. However, since actual measurements of these properties were not taken from of the specimens, it is difficult to ascertain their exact influence. These items will be discussed in a general sense by assuming that the magnitudes are consistent with other manufactured HSS members; in light of the tolerance values specified by ASTM A53. It is pointed out right away that, in general, the strains computed using the finite element method are less accurate than the nodal displacements in the context of a given mesh. This is due to the fact that the displacements are nodal quantities that are solved for directly in each equilibrium iteration. In contrast, the stresses are obtained from engineering theories applied at the mid-surface Gauss points and subsequently extrapolated out to the nodal locations. As a result of this extrapolation, the strains predicted with the finite element model are somewhat less accurate than the displacements predicted with the same model.

As discussed previously, the strain measurements on the chord wall surface are very sensitive to residual stresses and local variations in wall thickness. Residual stresses will result in a change in the localized yielding response and could cause a global redistribution of the applied loads in the form of shift in the trajectories of the yield line patterns. Note that in the present discussion, the strains are compared in terms of principal strain, which means that both longitudinal and transverse residual stresses will influence the onset of yielding. However, from the figures, it is observed that there are not significant differences in the yielding behavior. That is, the initiation of nonlinear behavior is relatively consistent between finite element analysis and the experiments. The differences that exist are more in terms of overall magnitude at a given load, which is more attributable to a yield line shift. If the actual yield lines deviate from the

theoretical patterns, this would have a more significant impact on the strain magnitude at discrete gauge locations.

Variations in wall thickness will also result in a change in the extreme fiber strain as compared to the idealized finite element analysis model, which uses the nominal thickness. By considering the linear strain distribution from fundamental flexural theory, the strain for a given elemental curvature is directly proportional to the distance from neutral axis. Thus, a 10% variation in wall thickness (as per ASTM) would result in a 10% variation in extreme fiber strain. This may partially explain the differences in strain magnitude between finite element analysis and the experiments, but some differences are much larger than this.

The most significant difference found in the comparison of finite element analysis versus the experimental results is in the displacement response at the open end of the HSS chord. As discussed previously, the open end in the physical test specimens showed no deformation until a load of 70 k was attained. In contrast a gradual distortion of the open end was observed in the finite element models. This difference in response is likely not the result of a modeling issue since the other displacements and strains compare so well. Also, it cannot be attributed to residual stresses and/or dimensional tolerances from the HSS chord manufacturing processes, since neither would have such a dramatic influence on how the applied load is dispersed longitudinally in the chord wall.

Since the experimental researchers noted that a moment was present in the ST strut and that shims for the load frame became loose and fell out during testing of both specimens (Boyle and Earls 2004), it is likely that there existed some unknown flexibility and/or restraint in the testing setup which would be a deviation from the ideal boundary conditions used in the analytical modeling.

5.4.2 Failure Mechanism

The mechanism of failure for this structure is an example of a yield line collapse mechanism in which well-defined plastic hinge lines develop in the HSS chord walls, causing instability at a critical load. This is defined as the point at which the tangent stiffness (slope of the load-deflection curve) equals zero. The yield lines exhibit a geometry that is somewhat complex due to the nature of the problem. However, based on the good agreement between finite element

analysis and the experiments in terms of global load-deflection response, the salient features of the governing failure mechanism appear to be captured sufficiently well in the analytical modeling.

The present discussion now shifts focus to two specific points: 1) the stiffness after yielding, and 2) the magnitude of the ultimate load; both of these are related to residual stresses in the HSS chord. The residual stresses present can affect both the mechanism geometry (i.e. shifting of the yield lines) and the onset of yielding. Based on Figure 5-2, the longitudinal residual stresses in an HSS member may approach the yield stress in the vicinity of the welded seam. Although this is significant in terms of magnitude, the yield line mechanism for this structure consists mostly of lines oriented longitudinally. Such yield line orientations are not significantly impacted by longitudinal residual stresses in terms of unit strength. However, the longitudinal weld seam might cause a shift in the yield line location. Since any deviation from the ideal (theoretical) mechanism will have a net strengthening effect and result in a higher capacity, this would explain the slightly larger experimental ultimate load.

In contrast, the transverse residual stresses directly influence the net unit capacity of the longitudinal yield lines. From Figure 5-2, the circumferential residual stress distribution is nearly linear, and resembles the stress distribution from simple flexural theory. Thus, the residual stress can be thought of as a residual moment of approximate magnitude $M_{residual} = \sigma S$, where $\sigma = 0.35\ \sigma_y$ and S is the section modulus per unit length of chord wall. For this structure, the residual moment is calculated:

$$M_{residual} = (0.35 \cdot 47ksi) \cdot (1" \cdot (0.5")^2 / 6) = 0.685k \cdot in / in$$

From simple plastic section analysis, the plastic moment resistance of the chord wall per unit length is $F_y t^2 / 4$ which yields:

$$M_p = (47ksi) \cdot (0.5")^2 / 4 = 2.94k \cdot in / in$$

Thus, there exists a residual moment that is 0.685 / 2.94 = 23% of the plastic moment resistance, which could have a stiffening or softening effect depending on the direction of the applied

flexure. It must be noted that this residual moment will affect the onset of yielding and the inelastic response for the collapse mechanism, but it will not affect the ultimate load since plastic moment resistance is independent of residual stress. Thus, the circumferential residual stress might explain the difference in tangent stiffness observed in the inelastic range.

5.4.3 HSS Material Modeling

As discussed previously, modeling of the HSS material is where the greatest uncertainties lie. It is likely that the steel in the test specimens contained residual stresses and was somewhat textured as a result of the manufacturing processes; but these internal properties are difficult to quantify for the purposes of analytical modeling. Thus, neither was utilized in the material definition for the finite element analysis model. However, it is believed that both may have contributed to observed differences in predicted versus observed responses throughout the verification study.

To transform a flat plate into a circular tube, significant circumferential strains will result. Based on the assumption of plane sections remaining plane from fundamental flexural theory, a plate of thickness "t" bent into a curve of radius "R" will have extreme fiber strains given by the relationship $\varepsilon = t / 2R$. For the test specimen chords, this results in maximum strains of ε = (0.5 in.) / 2(13 in.) = 0.0192 in/in, which is over ten times the yield strain ε_y. Thus, it is likely that some level of texturing has occurred and the properties of the steel are different in the longitudinal and transverse directions. However, coupon tests were conducted in the longitudinal direction only, and thus the significance of the texturing could not be quantified precisely, but it was clear that the longitudinal elastic modulus was somewhat less that the 29,000 ksi typically ascribed to steel.

In defining the material model, the von Mises metal plasticity model is utilized, which assumes that the stress-strain response is linear up to a discrete yield point. However, in studying the coupon test data closely it is observed that the material response is nonlinear throughout the elastic range, which is consistent with the findings of Toma and Chen (1979), but even more pronounced. To minimize the error from this linear approximation, an average elastic modulus of 21,000 ksi was specified for the model, as opposed to the initial tangent value of

29,000 ksi, as a means for considering the nonlinear elastic response exhibited by the A53 Grade B used in the HSS chord members being considered herein.

6.0 PARAMETRIC STUDIES

Now that the verification of the finite element modeling techniques is complete, parametric studies can be reliably conducted for formulation of generalized capacity equations for bearing connection regions in tubular trusses. The goal of this portion of the present work is to develop equations that predict the capacity of the bearing connection for the following:

1) the action of an axial load/reaction force (P)
2) the action of a locally applied moment (M)
3) combined axial load and moment

A number of parameters are identified as potentially influencing the strength of the bearing region in resisting axial forces and/or moments; these are studied individually to quantify their impact. The parameters identified are shown in Figure 6-1 and summarized below:

Chord Diameter (D)	Chord Wall Thickness (t)
ST Flange Width (b_f)	ST Depth (d)
Chord Yield Strength (F_y)	End Distance (h)
Saddle Width (A)	Saddle Length (B)

For each parameter study, a minimum of four (4) variations are analyzed using FEM analysis. For each variation, the ultimate capacity is determined by studying the load-deflection response. The range of values that is considered for each parameter study is arrived at based on practical limits from existing specifications and/or anticipated construction practice. Four (4) variations for each parameter are considered sufficient so long as the same failure mechanisms are being captured in each case.

In defining the parameter ranges for the study, it is determined that although variations in the saddle length or saddle position along the longitudinal axis of the HSS chord could have a small influence on the overall bearing capacity, it will not be considered in this study. BC-744 calls for two (2) - 4 in. thick saddles positioned precisely at 12 in. from the end of the HSS chord to their centerline (PennDOT, 2003b). However, for modeling purposes these have been simplified into one monolithic saddle of length "B". Since it is unknown at this time what saddle configurations with respect to the HSS end and/or the ST may be considered in the future, practical variations in this parameter cannot be developed. As long as the saddle is proportioned sufficiently long and positioned within reasonable proximity to the ST strut, the impact of Saddle Length (B) on the overall capacity will be minimal.

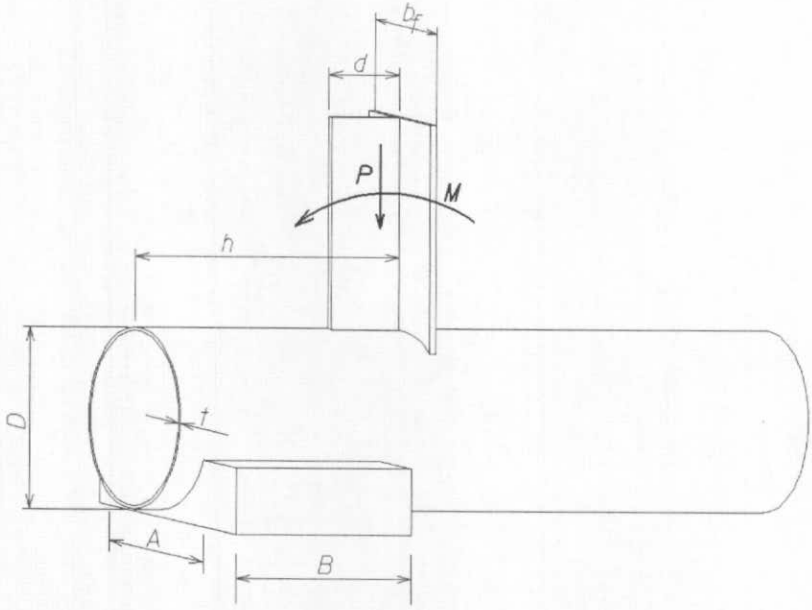

Figure 6-1: Parameters considered for study.

6.1 AXIAL LOAD STUDY

As discussed previously, the primary load path for the reaction force in the bearing connection under investigation extends from the saddle assembly, through the chord, and directly into the first intermediate member (in this case an upright ST member). This was the basis for the load in the experimental tests being applied axially through the ST strut and resisted at the saddles; in order to simulate the loading present in a real tubular truss bearing connection.

The applied load is compressive since overhead sign trusses are typically simple-span structures with the bearings in compression. Coincidentally, most existing provisions for other HSS connections are based on the compressive capacity, not tensile. Research has shown that HSS joints loaded in tension generally have a higher ultimate load capacity than those loaded in compression (Wardenier, 1982). For simplicity, researchers and code-writing bodies have typically based HSS capacity equations on the compressive resistance only, which is somewhat conservative for tensile loading. That same approach will be adopted for this research; and thus all axial loads will be applied in compression.

The next issue that must be addressed is the definition of capacity. Usually, capacity in tubular connections is defined using either a deflection criterion or a strength criterion depending on the application. In Chapter 4, the definition of "nominal capacity" was introduced due to the apparent unstable failure exhibited in the experimental test specimens. However, the finite element results of Chapter 5 showed that the connection contains significant reserve strength after the initial peak load. For the bearing region under investigation, as the applied load is increased from the start, the initial response is shown to be linear (see Figure 5-7). At some point, the structure begins to yield, as evident from the non-linear response. Load and deformation continue to increase until the load reaches a peak value, and then the load softens as deformation continues to increase. After more deformation, another resisting mechanism engages and the structure recovers; eventually resisting a much higher load than the initial peak load. Based on this behavior, either a deflection criterion or a strength criterion could be applied. But since it is difficult to develop a deflection criterion that is applicable to all HSS bearing configurations, the initial peak load is selected as the capacity of the system. At this load, the deflections are not considered excessive, as opposed to the 2nd peak in the load-history after

recovery. Thus, for all analyses performed in the parametric study for axial load, the first peak in load-deflection response is utilized as the capacity.

As the starting point for each study, the "benchmark case" is considered. The benchmark case is based primarily on the geometry of the experimental tests, thus being fully verified against physical testing. From this benchmark, different parameter variations are explored as needed, but these subsequent configurations still remain reasonably similar to the benchmark case. Except for the parameter "D" as will be shown below, the benchmark case is typically in the middle of all the parametric variations considered. This is not possible for the "D" study since HSS diameters greater than 26 in. are not of concern.

6.1.1 End Distance (h) Study:

Since the primary failure mechanism extends to the open end of the HSS chord, as indicated by strain and deflection measurements from the experimental tests and the stress contours from the FEM simulation, it is apparent that the open end will influence the strength of the bearing connection region. Therefore, its impact on the overall capacity must be assessed. To accomplish this, six (6) configurations are analyzed with the dimension "h" varied from 6 in. to 39 in. (0.25D to 1.5D) and the remaining parameters held constant. The study parameters are summarized as follows:

h values:	Constants:
6"	D = 26"
13"	b_f = 7.2"
26" *Benchmark case	d = 10.15"
33"	t = 0.5"
39"	F_y = 47ksi
	A = 24.1"
	B = h – 2"

As mentioned previously, the saddle length and longitudinal position are not considered as parameters for study and therefore were to remain constant throughout all studies. However, maintaining the same saddle length while varying the location of the ST (dimension "h") would be problematic for this study. If the ST is moved away from the saddle, then bending is

introduced into the HSS chord due to the eccentricity between the ST axial load and the reaction force at the saddle. This bending negatively affects the capacity of the system and it becomes more pronounced as the eccentricity increases. To prevent this, the saddle width (B) is specified as a constant 2 in. less than the ST flange position (h) for all variations. That is, the inside face of the saddle is always positioned at a dimension of h - 2 in. from the end. This ensures that the same eccentricity exists (although minimal) for all configurations.

The load-deflection results from each FEM analysis are shown in Figure 6-2. As expected, the axial capacity of the bearing region is increased as the end distance (h) of the ST is increased. However, note that the response for h = 33 in. is the same as the response for h = 39 in. This indicates that the open end no longer influences the failure mechanism once the ST is located at a distance 33 in. (1.27D) or more from the end.

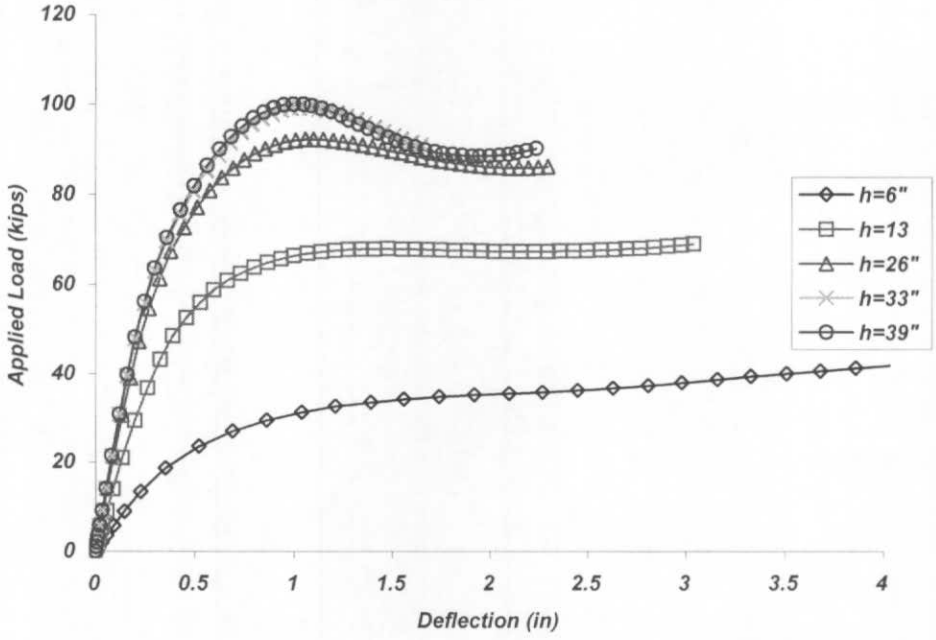

Figure 6-2: Axial load-deflection response for varying end distance (h)

6.1.2 ST Flange Width (b_f) Study:

By observing the yield line patterns indicated by the FEM stress contours in Figure 5-3, it is apparent that the ST flange width will also have an influence on the primary failure mechanism. For this study, five (5) configurations are analyzed with the dimension "b_f" varied from 0 in. (no flange) to 15.6 in. (0.6D) and the remaining parameters held constant. The case of $b_f/D = 0.6$ is a practical limit that is consistent with existing published specifications. The study parameters are summarized as follows:

b_f values:	Constants:
0"	D = 26"
3.9"	h = 26"
7.2" *Benchmark case	d = 10.15"
11.7"	t = 0.5"
15.6"	F_y = 47 ksi
	A = 24.1"

The load-deflection results from each FEM analysis is shown in Figure 6-3. As expected, the axial capacity of the bearing region is increased as the ST flange width (b_f) is increased. Note that significant capacity gain can be realized by increasing the flange width to 15.6 in.

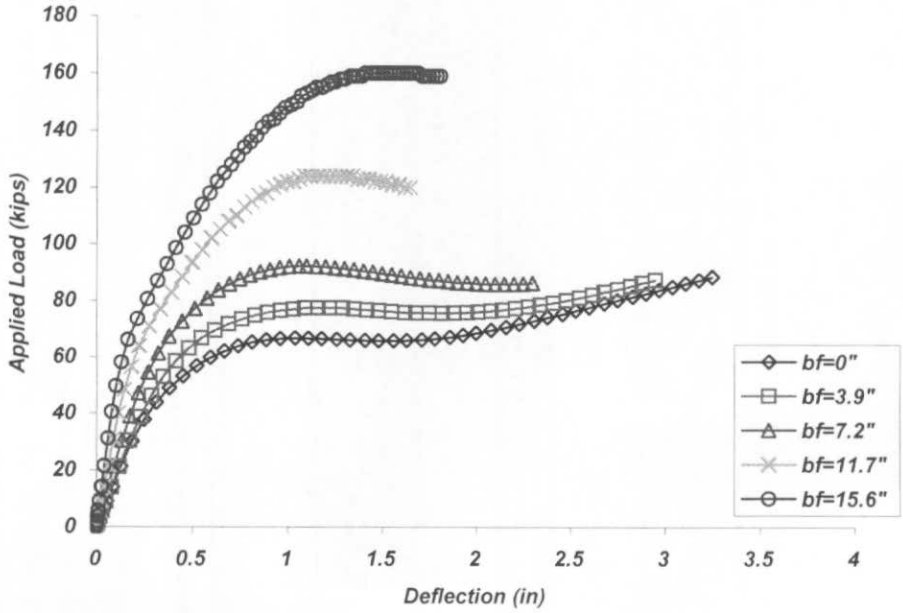

Figure 6-3: Axial load - deflection Response for varying ST flange width (bf)

6.1.3 HSS Chord Diameter (D) Study

For this study, four (4) configurations are analyzed with the chord diameter "D" varied from 10 in. to 26 in. while holding constant the ratios b_f /D, A/D, and h/D as well as the remaining parameters. The study is conducted in this way since "D" is a variable that is usually not used explicitly in HSS capacity equations. But rather, it is typically shown within a ratio to another variable (see Eqs. (4-1) to (4-4)). In these equations, "D" is combined with the branch member width to define a parameter ratio β, which equals D(branch)/D(chord) for a HSS-to-HSS connection or b_1/D for a Concentrated Force Distributed Transversely. Thus, the purpose of this portion of the investigation is to determine whether or not variations in "D", if the ratios of D to other variable remain constant, lead to the same overall connection capacity. The study parameters are summarized as follows:

D values:	Constants:
10"	b_f /D = 0.27
14"	h/D = 1.0
20"	d = 10.15"
26" *Benchmark case	t = 0.5"
	F_y = 47 ksi
	A/D = 0.927
	B = h – 2"

The load-deflection results from each FEM analysis is shown in Figure 6-4. As anticipated, the axial capacity of the bearing connection is not significantly affected by variations in D, as long as the ratios of b_f/D, h/D and A/D are held constant. There is a slight decrease in capacity as the diameter D is increased, but since the benchmark case utilizes a diameter D=26 in., then the final capacity equation will be formulated to be slightly conservative for smaller diameters.

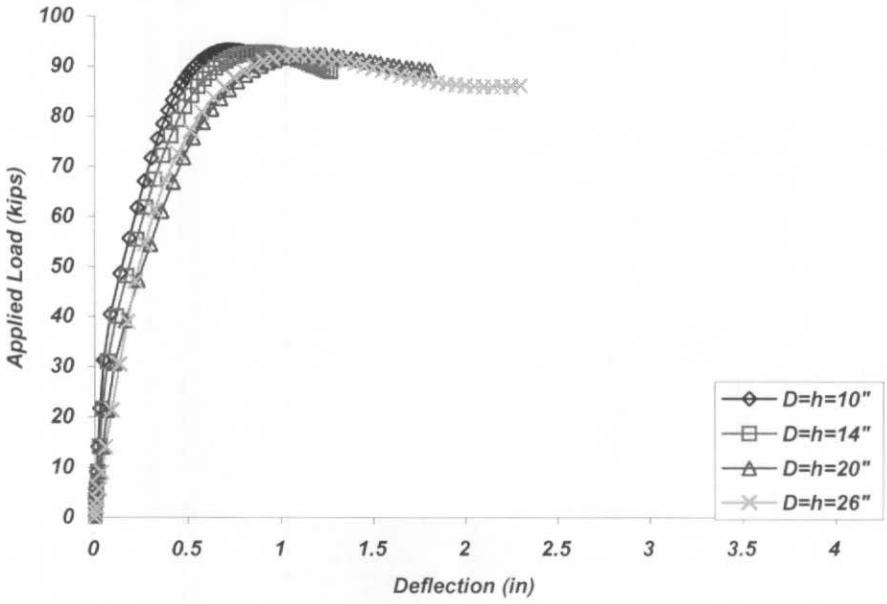

Figure 6-4: Axial load - deflection response for varying chord diameter (D)

6.1.4 Saddle Width (A) Study

For this study, five (5) configurations are analyzed with the dimension "A" varied from 0 in. to 26 in. and the remaining parameters held constant. Note that for A = 0 in., this is the case with no curved saddle bearing (i.e. a single line support) and for A = 26 in., this is the case in which the saddle covers the entire bottom half of the chord. The study parameters are summarized as follows:

A values:	Constants:
0"	D = 26"
7.6"	B = 24"
14.5"	h = 26"
24.1" *Benchmark case	d = 10.15"
26"	t = 0.5"
	F_y = 47 ksi
	b_f = 7.2"

The load-deflection results from each FEM analysis is shown in Figure 6-5. As expected, the capacity is increased as the saddle width (A) is increased. As mentioned, the case of A = 0 in. is

a configuration in which the chord is supported by a single line support rather than a curved bearing surface. Since many in-service bearing details consist of a simple flat plate bearing detail, this case is may be of particular interest to practicing engineers. To accurately model this condition of a round HSS chord bearing on a flat surface, the analysis is conducted with consideration of a true contact interaction between the chord wall and bearing surface. This more sophisticated boundary was not modeled for other parametric models due to its computational expense (see Section 5.2.3).

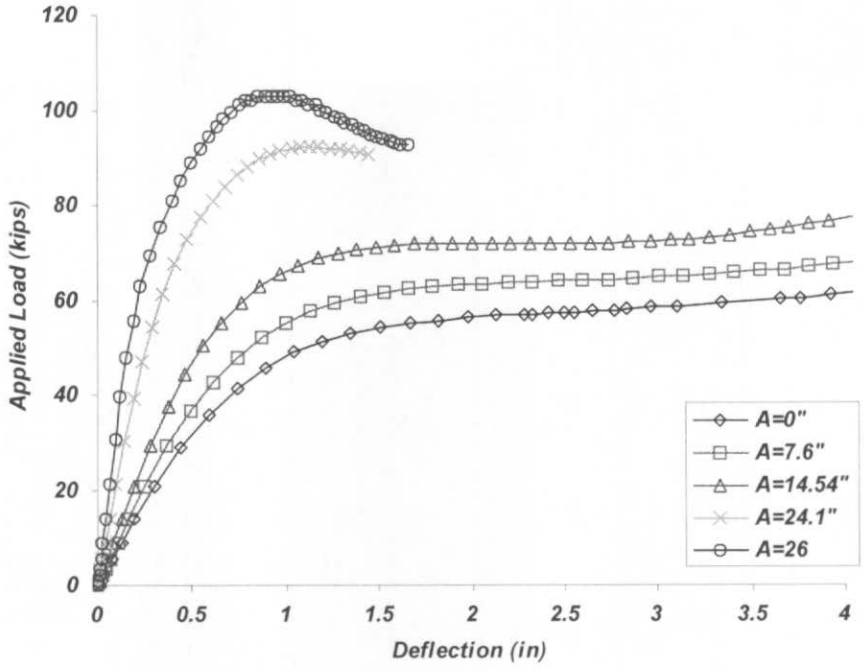

Figure 6-5: Axial load - deflection response for varying saddle width (A)

6.1.5 Chord Wall Thickness (t) Study

For this study, four (4) variations are analyzed with the chord wall thickness "t" varied from 3/8 in. to 1 in. (D/70 to D/26) and the remaining parameters held constant. These are selected based on practical limits on HSS members. The study parameters are summarized as follows:

t values:	Constants:
3/8"	D = 26"
1/2" *Benchmark case	h = 26"
3/4"	d = 10.15"
1"	F_y = 47 ksi
	A = 24.1"
	b_f = 7.2"
	B = 24"

The load-deflection results from each FEM analysis is shown in Figure 6-6. As expected, increasing the chord wall thickness results in significantly increased capacity.

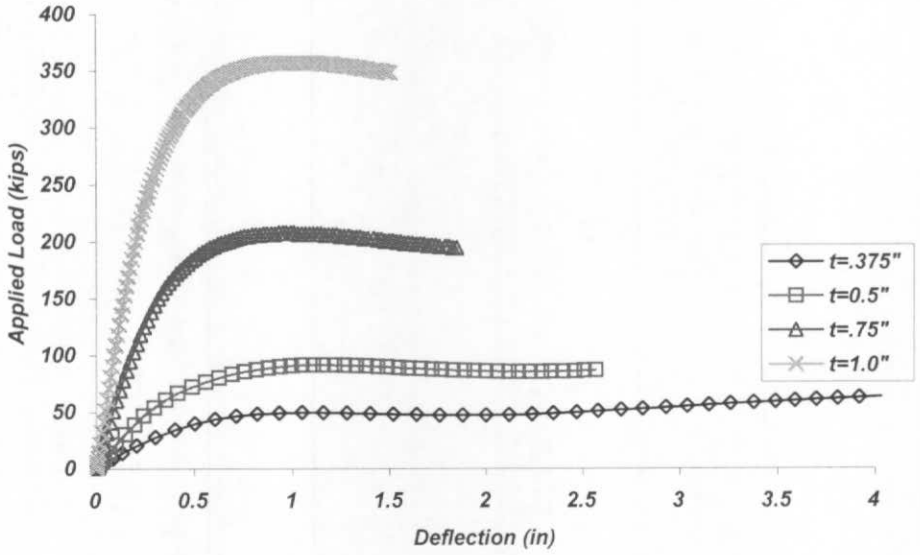

Figure 6-6: Axial load - deflection response for varying chord wall thickness (t)

6.1.6 Chord Yield Strength (Fy) Study

For this study, three (3) variations are analyzed with the chord yield strength Fy varied from 36 to 60 ksi and the remaining parameters held constant. To maintain consistency, the material models are simplified to a bi-linear response in which the ratio of σ_u/σ_y is held to a constant

value of 1.25 and the maximum tensile strain ε_u is specified as 0.0171 in/in for definition of the plastic hardening for all cases. For this study, only three (3) variations are considered since these steel strengths should envelope most applications in HSS construction. The study parameters are summarized as follows:

F_y values:	Constants:
36 ksi	D = 26"
47 ksi *Benchmark case	h = 26"
60 ksi	d = 10.15"
	t = 0.5"
	A = 24.1"
	b_f = 7.2"
	B = 24"

The load-deflection results from each FEM analysis is shown in Figure 6-7. As expected, increasing the chord yield strength results in increased capacity.

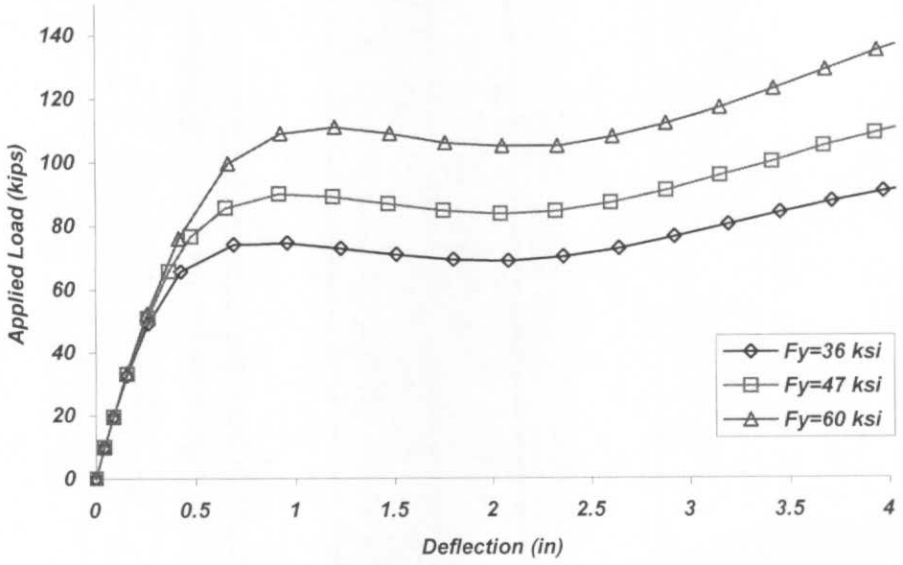

Figure 6-7: Axial load - deflection response for varying chord yield strength (Fy)

6.1.7 ST Depth (d) Study

For this study, three (3) configurations are analyzed with the dimension "d" varied from 0 in. (no stem) to 26 in. (end distance, h) and the remaining parameters held constant. The study parameters are summarized as follows:

d values:	Constants:
0"	D = 26"
10.15" *Benchmark case	h = 26"
26"	b_f = 7.2"
	t = 0.5"
	F_y = 47 ksi
	A = 24.1"
	B = 24"

The load-deflection results from each FEM analysis is shown in Figure 6-8. These responses show that the ST depth (d) does not have a significant impact on the overall capacity as seen by the similar response for the cases of d = 10.15 in. and d = 26 in. However, it is also observed that when there is no stem plate (d = 0), a different failure mechanism is

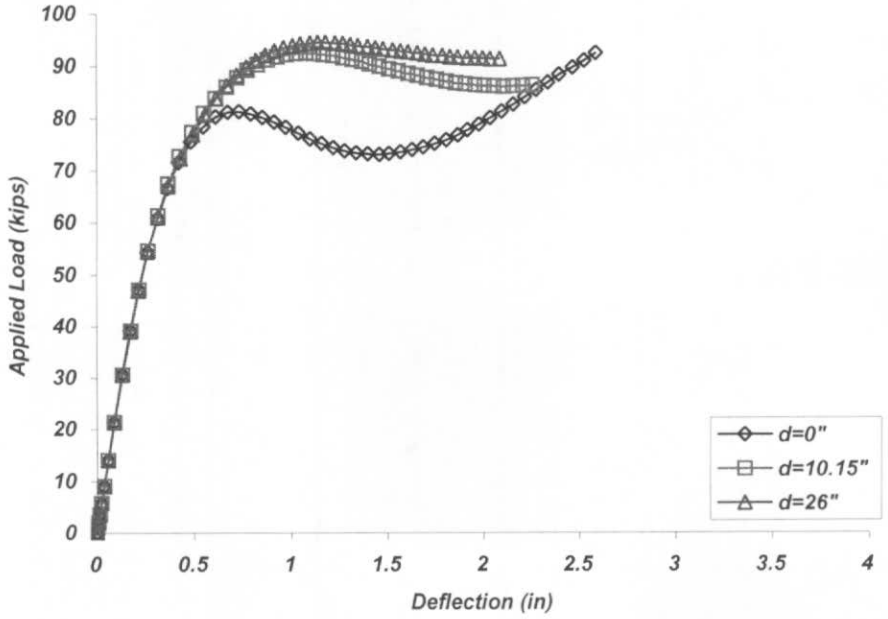

Figure 6-8: Axial Load - Deflection Response for varying ST depth (d)

manifested. Thus, if there is no stem plate (i.e. a single transverse gusset plate), then the final capacity equation will not apply. As long as the intermediate branch member is an ST shape with a typical stem plate, then the depth (d) will not have a significant influence on the overall capacity. It should be noted that if the ST was rotated by 180 degrees with the stem facing toward the interior of the HSS, then increasing (d) would likely result in an increase of the capacity.

A summary of all the parametric study results for axial load is shown in Table 6-1. Each row lists the parameter values used in the individual FEM analyses and the resulting axial load capacity. Note that the parameter variations for each study group are shown in boldface type. It should be noted that the bearing configuration under investigation includes a curved saddle bearing and a ST intermediate branch member, which may be considered to have limited applicability. Other bearing connection details may contain a flat bearing surface rather than a curved saddle bearing, an HSS intermediate branch member rather than an ST, or a branch member connected to the chord using a gusset plate. An attempt has been made to cover these related cases by selecting wide ranges in the parametric study (i.e. $A = 0$, $b_f = 0$, $d = 0$). For an HSS intermediate branch member, the branch diameter can be substituted for the ST flange width b_f, which will produce a conservative result.

Table 6-1: Summary of Parametric Study Results for Axial Load

F_y	t	d	D	h	h/D	A	A/D	b_f	b_f/D	P_u
ksi	in	in	in	in	-	in	-	in	-	kips
47	0.5	10.15	26	***6***	0.231	24.1	0.927	7.2	0.277	37
47	0.5	10.15	26	***13***	0.500	24.1	0.927	7.2	0.277	68
47	0.5	10.15	26	***26***	1.000	24.1	0.927	7.2	0.277	92.2
47	0.5	10.15	26	***33***	1.269	24.1	0.927	7.2	0.277	99.1
47	0.5	10.15	26	***39***	1.500	24.1	0.927	7.2	0.277	100
47	0.5	10.15	26	***52***	2.000	24.1	0.927	7.2	0.277	100
47	0.5	10.15	26	26	1.000	24.1	0.927	***0***	0.000	66.7
47	0.5	10.15	26	26	1.000	24.1	0.927	***3.9***	0.150	77.5
47	0.5	10.15	26	26	1.000	24.1	0.927	***7.2***	0.277	92.2
47	0.5	10.15	26	26	1.000	24.1	0.927	***11.7***	0.450	124
47	0.5	10.15	26	26	1.000	24.1	0.927	***15.6***	0.600	160
47	0.5	10.15	***10***	***10***	1.000	***9.27***	0.927	***2.7***	0.270	93.2
47	0.5	10.15	***14***	***14***	1.000	***12.98***	0.927	***3.78***	0.270	92.8
47	0.5	10.15	***20***	***20***	1.000	***18.54***	0.927	***5.4***	0.270	92.3
47	0.5	10.15	***26***	***26***	1.000	***24.1***	0.927	***7.2***	0.277	92.2
47	0.5	10.15	26	26	1.000	***0***	0.000	7.2	0.277	55
47	0.5	10.15	26	26	1.000	***7.6***	0.292	7.2	0.277	63
47	0.5	10.15	26	26	1.000	***14.54***	0.559	7.2	0.277	71.7
47	0.5	10.15	26	26	1.000	***24.1***	0.927	7.2	0.277	92.3
47	0.5	10.15	26	26	1.000	***26***	1.000	7.2	0.277	103
47	***0.375***	10.15	26	26	1.000	24.1	0.927	7.2	0.277	49.6
47	***0.5***	10.15	26	26	1.000	24.1	0.927	7.2	0.277	91.5
47	***0.75***	10.15	26	26	1.000	24.1	0.927	7.2	0.277	208
47	***1***	10.15	26	26	1.000	24.1	0.927	7.2	0.277	357
36	0.5	10.15	26	26	1.000	24.1	0.927	7.2	0.277	74.6
47	0.5	10.15	26	26	1.000	24.1	0.927	7.2	0.277	90
60	0.5	10.15	26	26	1.000	24.1	0.927	7.2	0.277	111
47	0.5	***0***	26	26	1.000	24.1	0.927	7.2	0.277	81.3
47	0.5	***10.15***	26	26	1.000	24.1	0.927	7.2	0.277	92.5
47	0.5	***26***	26	26	1.000	24.1	0.927	7.2	0.277	94.5

6.2 MOMENT STUDY

Since the intermediate members of in-service tubular trusses typically have fixed-end moments present, the current portion of the parametric study is conducted for determining the capacity of the bearing connection under the action of an applied moment. The moment is applied locally to the ST member and resisted by a force couple consisting of: 1) the reaction force at the saddle and 2) an internal "beam" shear force in the HSS chord.

This study is somewhat simplified as compared to the axial load investigation. For an applied moment in the direction of the HSS end, the stress contours at failure are as shown in Figure 6-9. It can be seen that the yield zones are much more concentrated than those observed

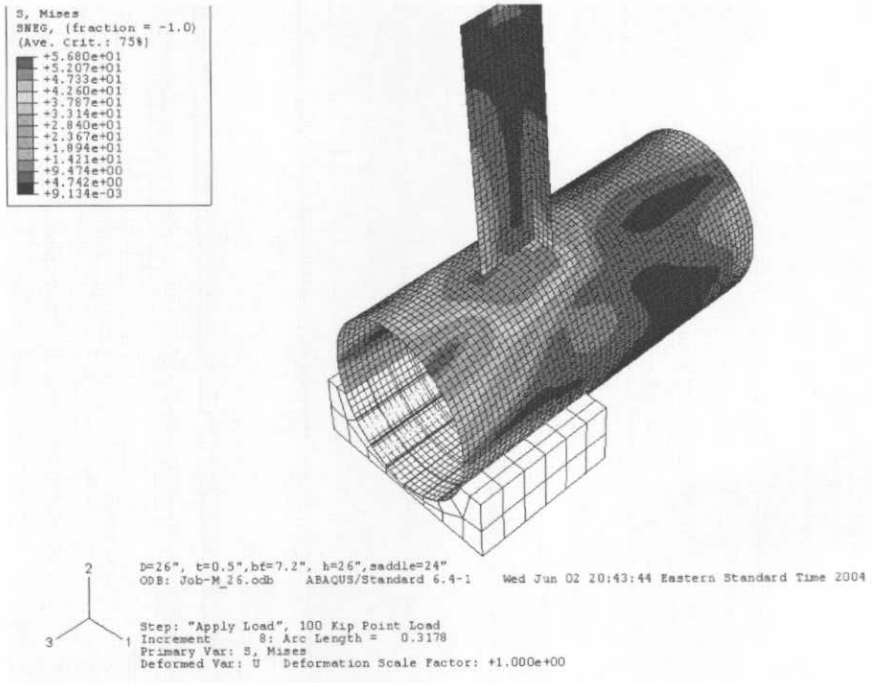

Figure 6-9: Von Mises Stress Contours for applied moment.

for axial loading. Based on this and by analyzing a number of related configurations, it is determined that the moment capacity of the system is not significantly impacted by the parameters A, h, or b_f. The failure mechanism occurs in the HSS chord wall locally around the tip of the ST stem and therefore the ST depth "d" essentially controls the capacity. As the depth "d" is increased, the chord wall stresses are reduced; thus increasing capacity.

The second difference from the axial load investigation is in the definition of capacity. Recall that for axial loading, the first peak in the load-deflection response was used as the nominal capacity of the system. For an applied moment, the moment-rotation response is somewhat different. In this case a subtle plateau is observed, but no distinctive peak is present. Therefore, a deformation limit state must be applied. *It is decided that a limit will be placed on the rotation of 0.05 radians for determining the capacity.* This is approximately the start of the plateau region, after a moderate amount of plastic deformation has occurred in the HSS chord wall.

As with axial loading, the compression case controls over the tension condition. That is, if the moment is applied toward the ST flange with the stem in tension, then a higher capacity will be observed. As before, this will be neglected and all capacities will be based on the ST stem in compression (i.e. moment applied toward the open end). This is reasonable since the fixed-end moments in HSS structures could be in either direction.

Since it is found that A, h, and b_f all have a negligible impact on the moment capacity of the system, these components are removed from the study and a simplified structure is used for the analyses (see Figure 6-10). A series of models are constructed with the dimension "d" varied from 5 in. to 30 in. and the remaining parameters held constant. They are summarized as follows:

d values:	Constants:
5"	D = 26"
10"	t = 0.5"
20"	F_y = 47ksi
30"	

The moment-rotation results from each FEM analysis is shown in Figure 6-11. As expected, the capacity is increased as the plate depth (d) increases.

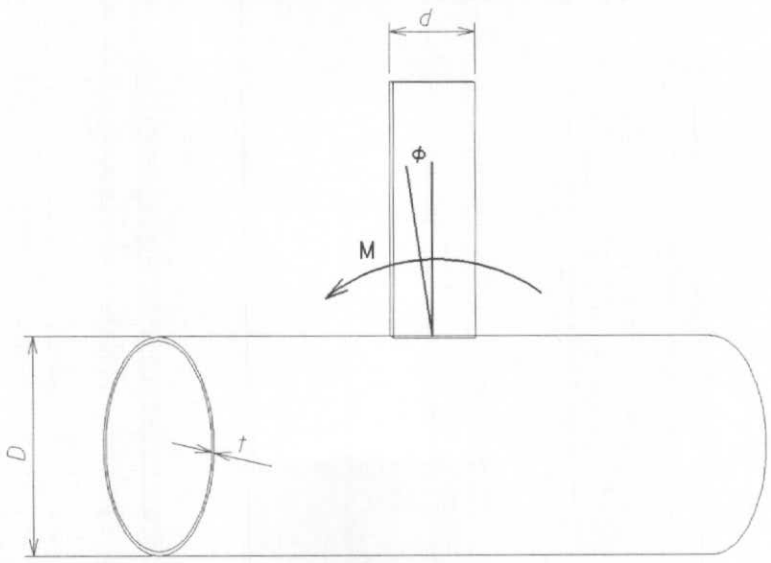

Figure 6-10: Parameters considered for Moment Study.

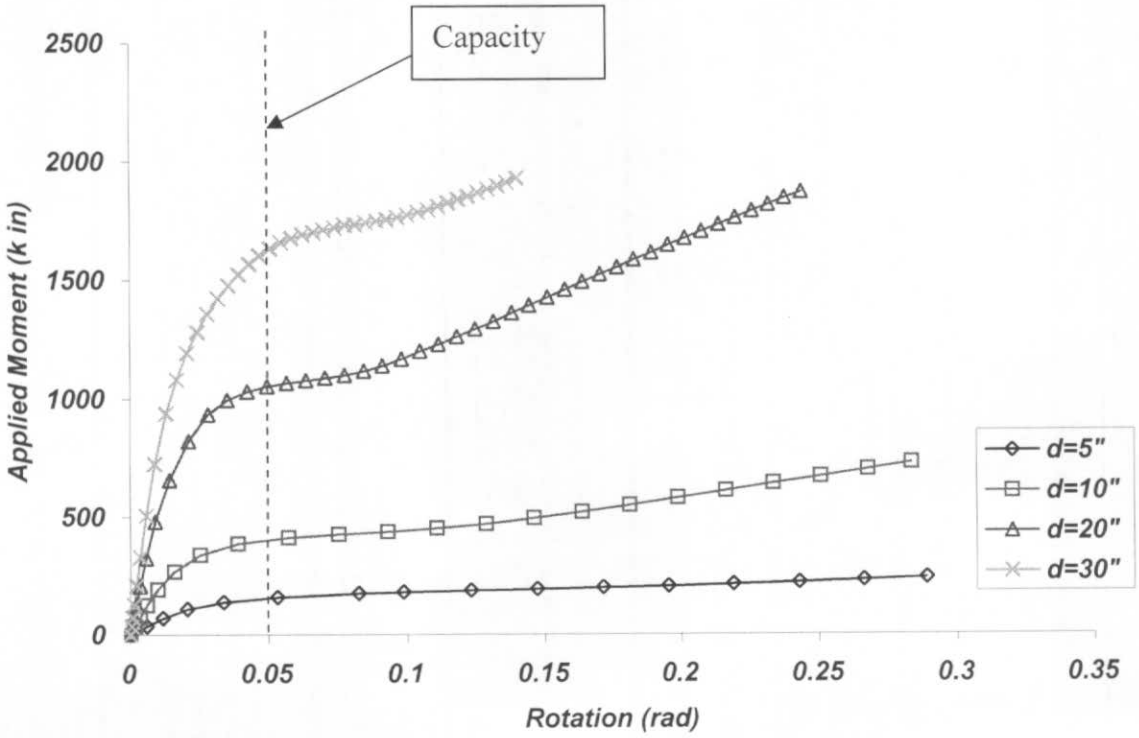

Figure 6-11: Moment-Rotation Response for Applied Moment

To determine whether the HSS chord diameter influences the moment capacity, three (3) additional configurations are analyzed with D = 10 in. They are:

d values:	Constants:
5"	D = 10"
10"	t = 0.5"
20"	F_y = 47ksi

For efficiency, it is decided that it is unnecessary to carry out another study on the influence of the parameters t and F_y, which was done for the axial load study. Since it is known that the failure mechanism is a classic case of a yield line mechanism based on the stress contours observed in Figure 6-9, then the capacity will be directly proportional to F_y and t^2. This will be confirmed in the formulation of the capacity equations in the next chapter.

The results of all analyses are summarized in Table 6-2. Each row lists the parameter values used in the individual FEM analyses and the resulting moment capacity based on the 0.05 radian rotation limit. Note that the parameter variations for each study group are shown in boldface type.

Table 6-2: Summary of Parametric Study results for applied moment

F_y	t	d	D	M_u*
ksi	in	In	in	k in
47	0.5	***5***	26	154
47	0.5	***10***	26	400
47	0.5	***20***	26	1051
47	0.5	***30***	26	1624
47	0.5	***5***	10	198
47	0.5	***10***	10	554
47	0.5	***20***	10	1498

*Using a 0.05 radian rotation limit.

6.3 AXIAL LOAD – MOMENT INTERACTION STUDY

This study is conducted for quantifying the capacity of the bearing region when subjected to a combined axial load and moment. To begin, it is assumed that the primary demand likely to cause failure of an in-service bearing connection is the axial load. Thus, the general approach is to first apply a constant moment (within the moment capacity) to the joint and then apply the axial load to failure. This will reveal to what extent the axial capacity is reduced by the addition of a fixed-end moment and will be the basis of an interaction capacity equation. Only the benchmark case is considered, and it is assumed that the same capacity interaction applies to other bearing configurations.

For the benchmark case, the moment capacity is found to be 400 kip in (see Table 6-2). To explore the moment interaction range between 0 and 1.0, moment values of 0, 100, 200, 300, and 400 kip in are considered. As described, the loading is applied in a two-step process: the constant moment is first applied and then the structure is loaded with an axial load to failure with the moment remaining constant. The resulting load-deflection response for each analysis is shown in Figure 6-12.

From the figure, first note that the case of M = 0 is the same case considered previously in the Axial Load Study, for which the capacity was determined to be P_u = 92.2 kips. As the moments are introduced for the subsequent cases, the distinct peak in the load-deflection response curve disappears; a behavior consistent with the application of a simple moment observed previously. As before, a deflection limit must be utilized for establishing the capacity. It is decided that the deflection value corresponding to failure of the benchmark case (M = 0) will be used as the limit criterion for the subsequent cases. This deflection limit is determined to be 1.3 in. and is identified with a dotted line in Figure 6-12. From the load-deflection data, the remaining axial load capacities are determined to be as follows:

M (k in)	*P_u (kips)*
100	87.2
200	78.4
300	67.9
400	56.7

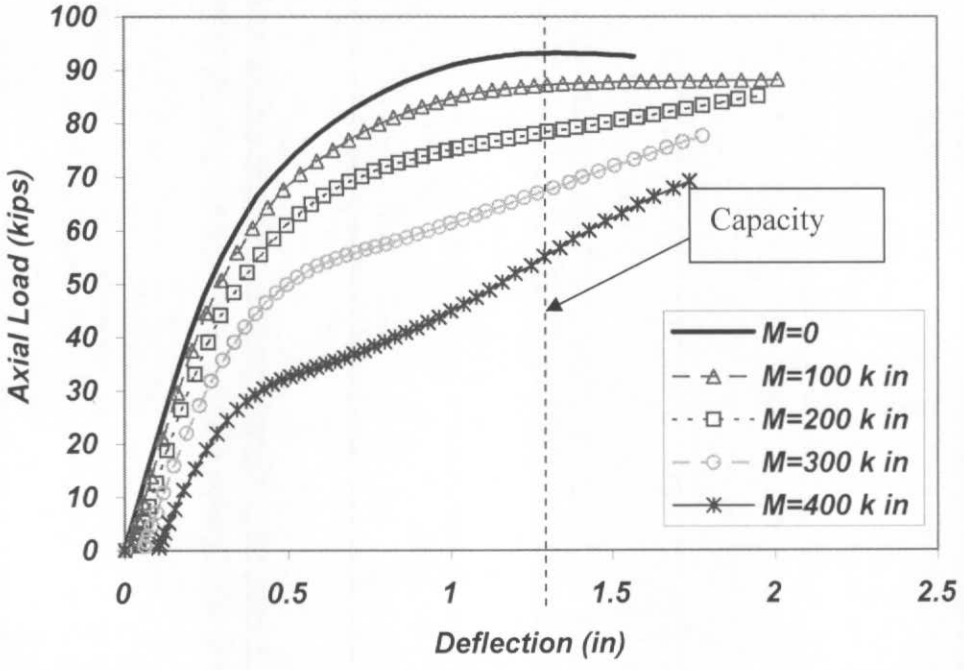

Figure 6-12: Axial load-deflection response with corresponding applied moment

6.4 INTERIOR ST-TO-HSS JOINT STUDY

Since no research has been found in the literature for the case of a simple interior ST-to-HSS joint, this case is considered so that recommendations can be made for these types of joints when located at the interior of a primary chord member. Also, the capacity will be compared to that provided by the bearing assembly at the chord end. A full parametric study for this related joint configuration is beyond the scope of this research, but a single case is carried out for the purposes mentioned. To this end, a simple interior ST joint is analyzed in two configurations: 1) T-connection and 2) Cross-connection. In both cases, the branch member is an ST10x48 and the chord member is a 0.5 in. x 26 in. diameter HSS. The resulting von Mises stress contours for each analysis are shown in Figure 6-13 and Figure 6-14 and the load-deflection response for each is shown in Figure 6-15. The results indicate the capacity is 95.4 kips for the T-Connection and 86.2 kips for the Cross-Connection.

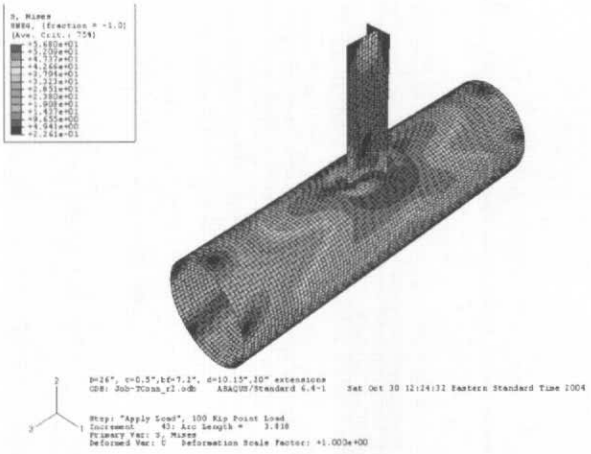

Figure 6-13: Interior ST-to-HSS T-Connection

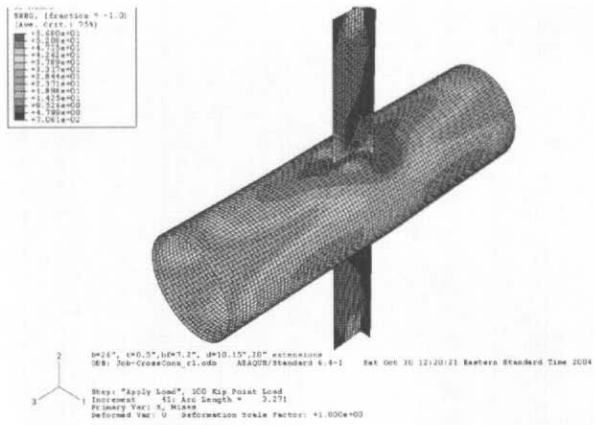

Figure 6-14: Interior ST-to-HSS Cross-Connection

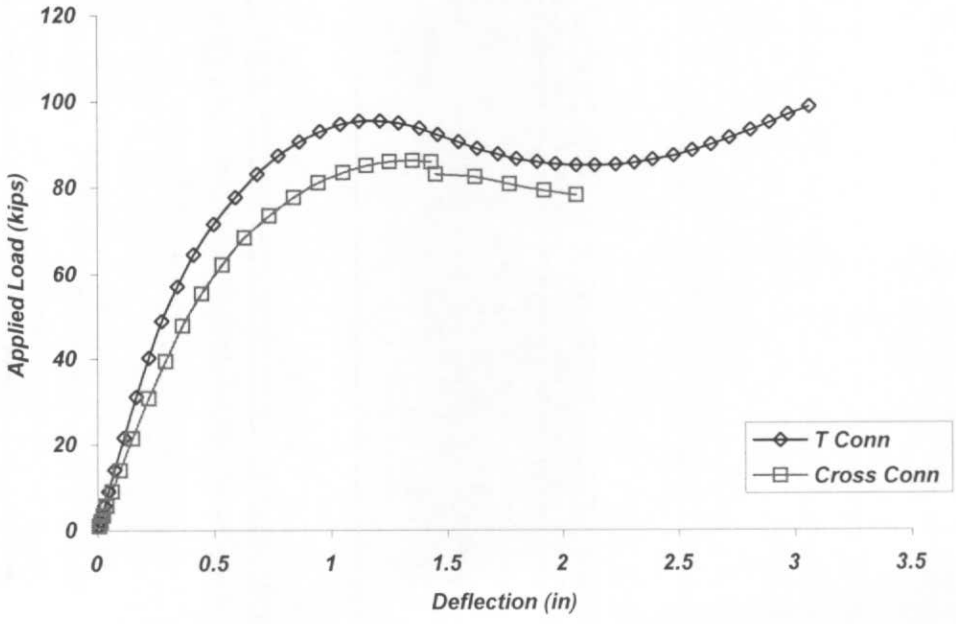

Figure 6-15: Axial load-deflection response for interior ST joints

7.0 DEVELOPMENT OF NEW BEARING CAPACITY EQUATIONS

This chapter describes the development of new capacity equations for predicting the strength of the bearing connection region under the actions of axial force and moment. These equations are developed based on the results from the parametric studies reported on in Chapter 6.

7.1 AXIAL LOAD CAPACITY EQUATION

As discussed in Chapter 2, a common approach to developing a theoretical solution to the capacity of a tubular connection is the method of cutting sections, or the "ring model." The limitation of the ring model is that it generally works well only for symmetric connection geometries. For the bearing connection under investigation, there is very little symmetry due to the ST shape and vicinity to the open end of the HSS chord. Li and Earls (2002) applied a form of the ring model to this type of structure, but stopped short of calculating the effective width, which is where symmetry and empirical data is needed for completion of the analysis. For developing a capacity equation, the ring model philosophy will be used in a slightly modified form.

For development of an axial load capacity equation, we begin by studying the stress patterns in the HSS wall at failure (see Figure 7-1). It can be seen that there are yield lines present as indicated by the areas colored red. Based on these yield lines, two (2) distinct regions are identified and their rings are shown; one for the end region and one for the interior region. In the end region, the ring consists of five (5) yield lines: two at the tops of the saddle, one at the

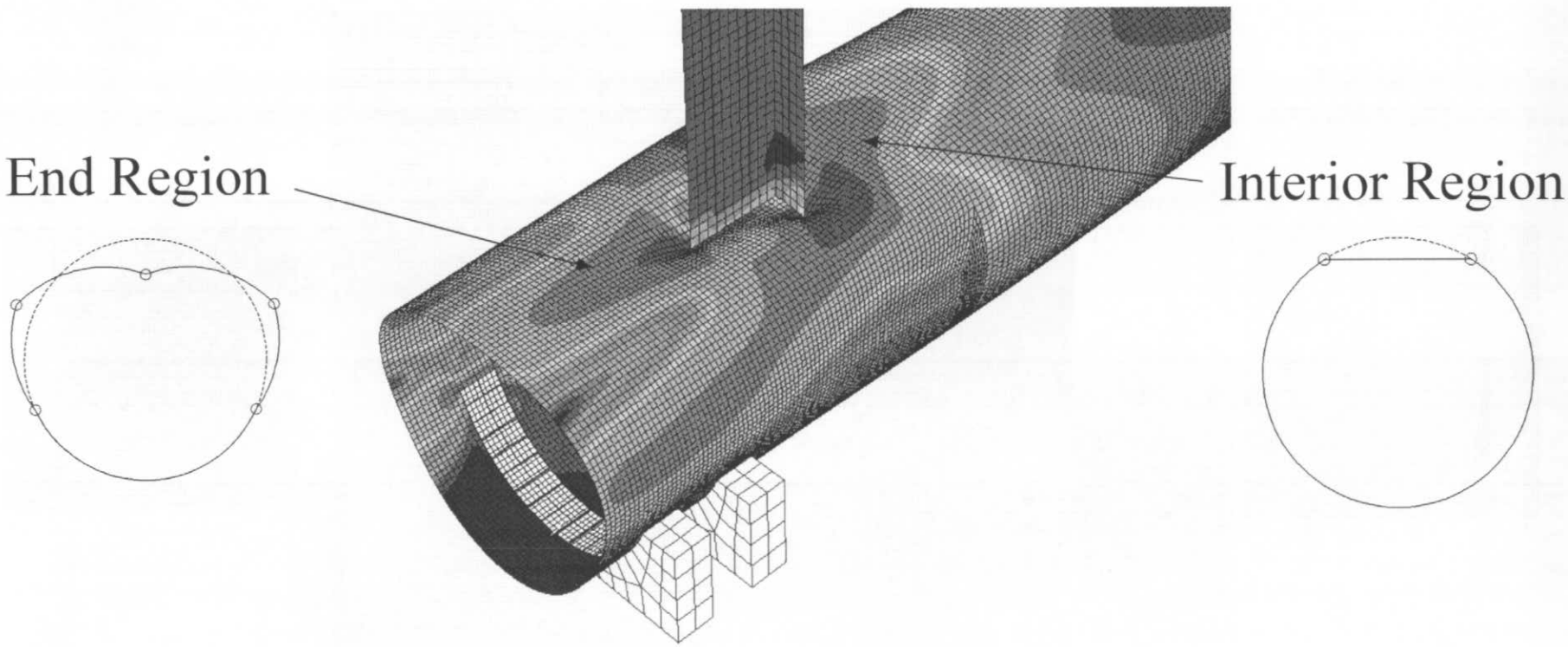

Figure 7-1: Yield Line Failure Mechanism for Bearing Connection Region

apex of the HSS, and two at approximately midway between. This same ring is present in the entire region between the open end and the stem of the ST. That is, the yield line geometry is uniform throughout this region. This is the mechanism that Li and Earls (2002) proposed as the basis for an earlier version of a capacity equation. There is also a second zone where the ring mechanism is quite different; at the interior region. In this region, there exists essentially only one primary yield line that wraps around the flange of the ST and connects with the yield lines from the end region. These observations are used as the basis for the generalized capacity equation.

Since the observed mechanism of failure involves a distinct pattern of yield lines, it is surmised that the overall capacity will be some function of the unit flexural yield line capacity of the HSS chord wall. Based on simple plastic section analysis, the plastic moment resistance of the chord wall per unit length is equal to $F_y t^2/4$. Thus, the final capacity will be directly proportional to F_y and t^2. Based on the two distinct regions observed, it is also theorized that the total capacity will be the capacity of the end region *plus* the capacity of the interior region. It is further assumed that the end region capacity is influenced only by the parameters A and h, and the interior region capacity is influenced only by the parameters b_f and h. By normalizing these parameters to the HSS chord diameter "D", the basic form of the capacity equation is stated:

$$P_n = F_y t^2 \cdot \left[f(A/D) + f(b_f/D) \right] \cdot f(h/D) \qquad (7\text{-}1)$$

End Region Interior Region

where $f(\alpha)$ are a series of functions to describe the geometry of the yield line mechanism. Assuming that quadratic functions are sufficient for this purpose yields functions of the form:

$$f(\alpha) = C1\ [1 + C2(\alpha) + C3(\alpha)^2] \qquad (7\text{-}2)$$

where C1, C2, and C3 are constants that are to be determined using regression-type analysis on the parametric study data.

With the basic form of the equation in place and the unknown function constants established, a curve-fit analysis of the parametric study data is performed using a method of least squares. The results are summarized in Table 7-1. Using the quadratic form of the parameter functions yields a total of nine (9) constants that must be determined. However, C1 is unnecessary for both f (A/D) and f (b_f/D) since these constants can be combined with C1 of f (h/D). This reduces the total number of unknown constants to seven (7). While these constants are easily determined, this yields a capacity equation that is somewhat cumbersome for use in an engineering design application. Since combining the three equations from (7-2) into Eq (7-1) is impractical, the designer must calculate the three (3) functional values and then manually plug these into Eq (7-1).

Table 7-1: Quadratic Function Constants for Axial Load Capacity Equation

Function	C1	C2	C3
f (A/D)	-	1.01	2.28
f (b_f/D)	-	4.17	13.0
f (h/D)	0.161	9.48	-3.48

In an attempt to simplify the capacity equation, reduced linear functions are also considered for f(α). Functions of the same form as Eq (7-2) are once again utilized, but with the quadratic term eliminated:

$$f(\alpha) = C1\ [1 + C2(\alpha)] \qquad (7\text{-}3)$$

As before, C1 is unnecessary for both f (A/D) and f (b_f/D) since these constants can be combined with C1 of f (h/D). This reduces the total number of unknown constants to four (4). In this case, the same curve-fit solution approach applied previously is not used, since it is desired that the capacity equation predict a *conservative* value for all parameter ranges, not the mean. The approach taken is to minimize the errors by the method of least squares, while simultaneously

applying a constraint that the capacity equation cannot produce an unconservative result. This is accomplished by using an optimization tool in Microsoft Excel called Solver®. Solver explores all of the possible options for the trial function constants that satisfy the constraints and minimize the residual errors. The resulting function constants are summarized in Table 7-2.

Table 7-2: Linear Function Constants for Axial Load Capacity Equation

Function	C1	C2	C3
f (A/D)	-	7.23	-
f (b_f/D)	-	37.3	-
f (h/D)	0.104	2.58	-

In this case, the functions of Eq (7-3) can be combined reasonably with Eq (7-1). By substitution, a stand-alone capacity equation for axial load is formulated:

$$P_n = 0.104 \cdot F_y t^2 \cdot \left[2 + 7.23 \cdot (A/D) + 37.3 \cdot (b_f/D)\right] \cdot \left[1 + 2.58 \cdot (h/D)\right] \qquad (7\text{-}4)$$

The nominal axial load capacities predicted by Eq (7-1) and Eq (7-4) along with the capacities obtained from the FEM analyses in the parametric studies are shown graphically in Figure 7-2 through Figure 7-6. It can be seen that Eq (7-1) correlates very well to the FEM results throughout. The simplified Eq (7-4) agrees reasonably well and produces a conservative prediction for capacity in all ranges.

Based on the parametric study results on the parameter "h" (see Table 6-1), it can be seen that the capacity of the bearing region is essentially the same for h = 33 in., 39 in., and 52 in. This indicates that if the ST is located at a distance of 33 in. (1.27D) or more, then the open end of the HSS chord no longer influences the capacity of the structure. To account for this, only the

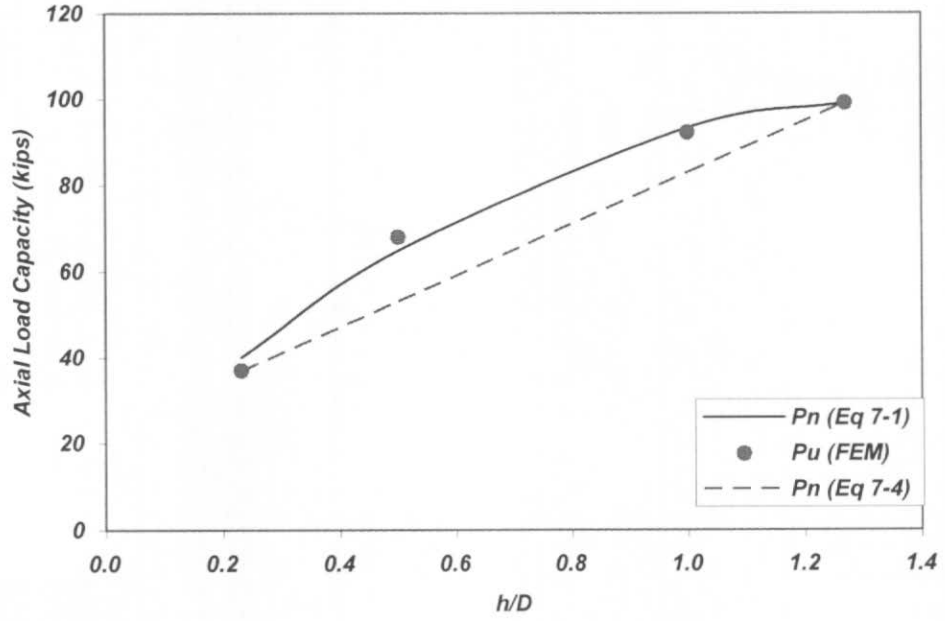

Figure 7-2: Axial load capacity vs. h/D

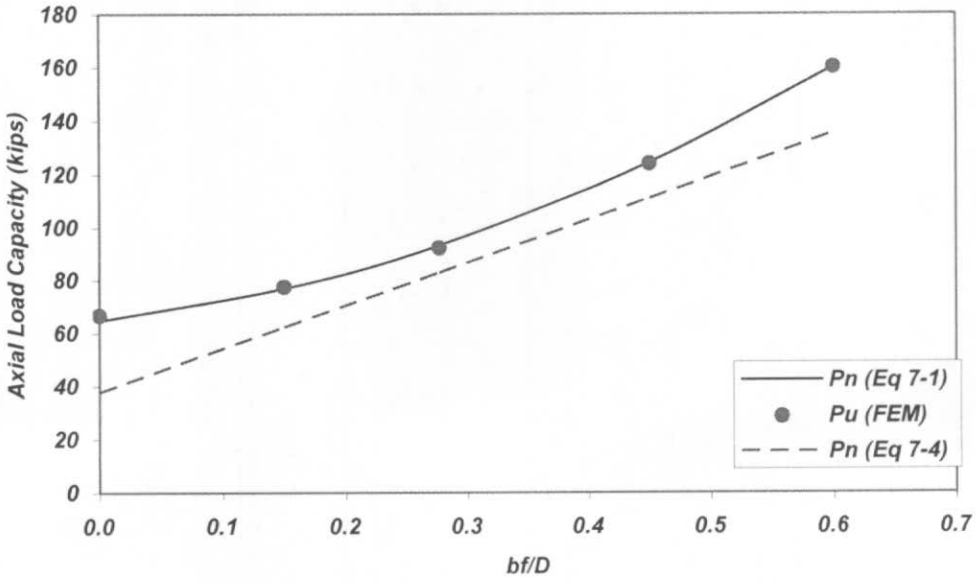

Figure 7-3: Axial load capacity vs. bf/D

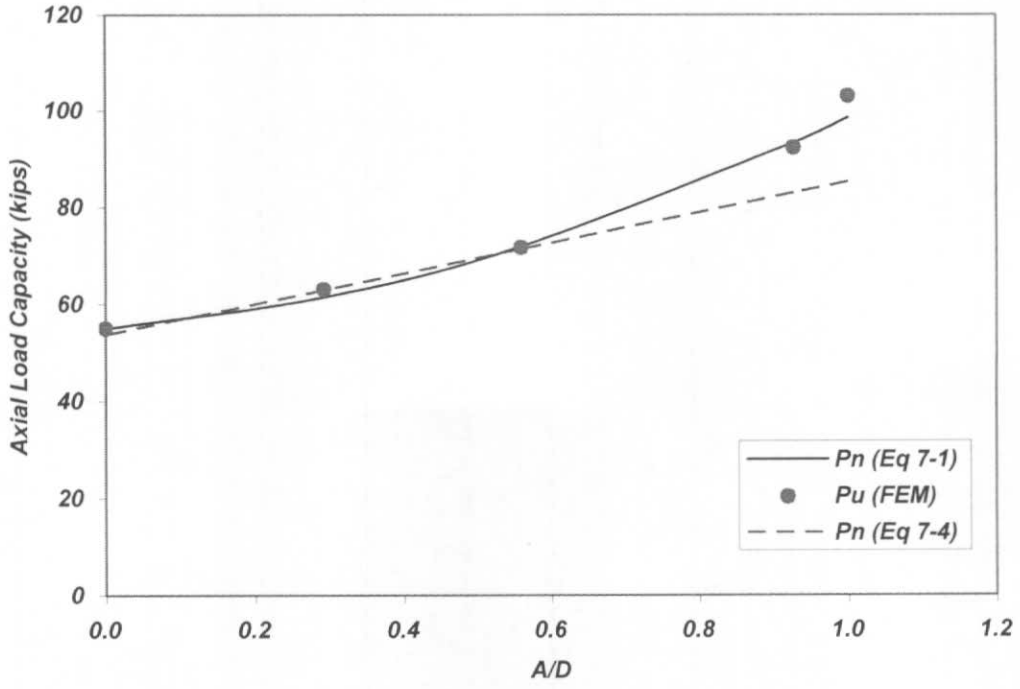

Figure 7-4: Axial load capacity vs. A/D

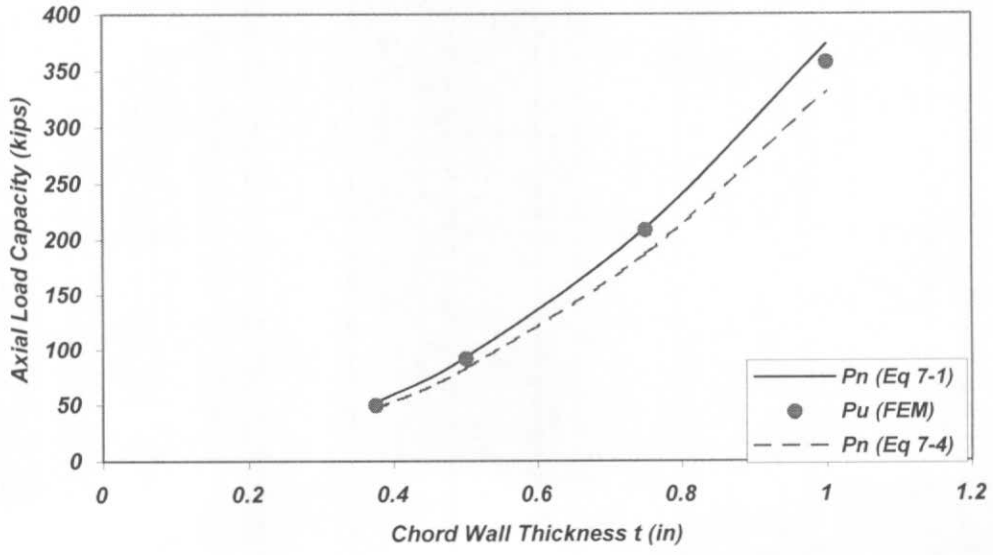

Figure 7-5: Axial load capacity vs. chord wall thickness (t)

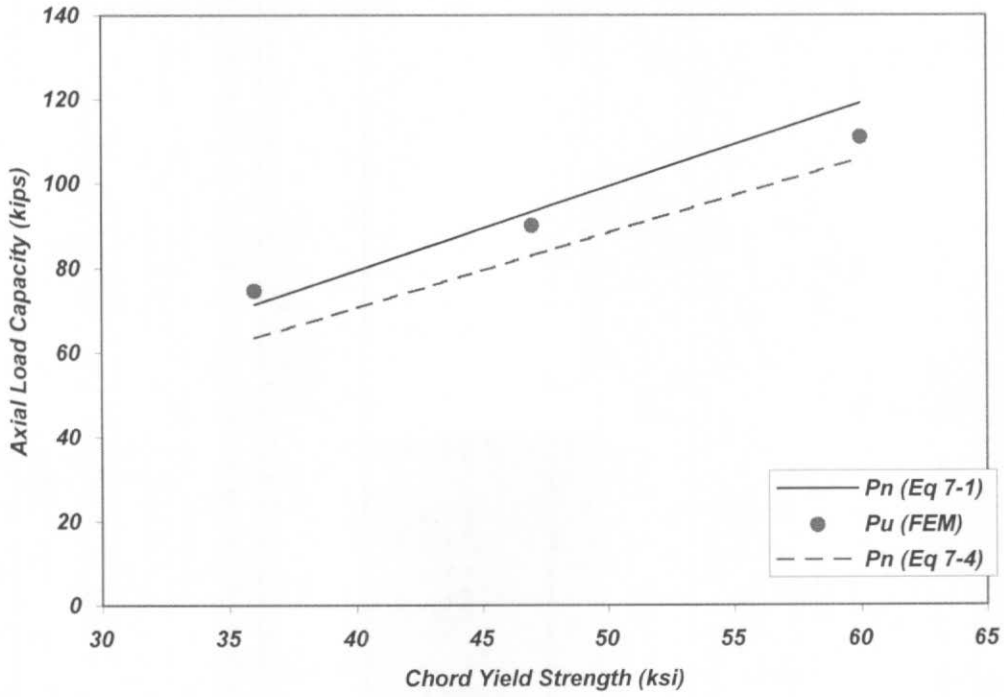

Figure 7-6: Axial load capacity vs. chord yield strength (F_y)

values of h less than 33 in. (1.25D) were included in the curve-fit analysis, and subsequent development of the capacity equation. For the case of h greater than 1.25D, then f (h/D) is a constant of 1.19 for the quadratic Eq (7-1) and 0.44 for the linear equation (7-4).

The parameter ranges that were studied should be noted, since these are typically used as limits of applicability in specifications. A full range of possible h and A values were studied; no limit exists for these parameters. For the ST flange width b_f, the range of $0 < b_f/D < 0.6$ was studied, which is consistent with limits in the existing specifications. For the HSS chord diameter "D", values of 10 in. to 26 in. were considered, which should envelope most practical applications. Practical limits were also utilized for t, yielding a range for the wall stiffness ratio of $26 < D/t < 69$.

Another notable observation is that the overall capacity is most sensitive to the ST flange width bf, which is apparent by observing the relative magnitudes of the C2 constants in Table 7-1. Thus, an effective way to increase the bearing capacity is to utilize a larger width flange.

7.2 MOMENT CAPACITY EQUATION

In developing a moment capacity equation for the bearing region, the solution is much simpler than the one required for axial loading. As discussed previously, the moment capacity of the system is not significantly impacted by the parameters A, h, or b_f; the stem plate depth of the ST essentially controls the capacity. Based on this finding, existing provisions that address the case of a moment applied to a single longitudinal plate are used and modified as needed. The simple case of a moment applied to a longitudinal plate is addressed in the Canadian HSS Design Guide (Packer and Henderson, 1997) with the following capacity equation (recast into a form that is consistent with the current nomenclature):

$$M_n = 5.0 \cdot F_y t^2 \left(1 + 0.25 \cdot d / D\right) \cdot d \qquad (7\text{-}5)$$

The capacity predicted by Eq (7-5) is compared to the results from the analyses performed in the parametric studies (see Figure 7-7). It can be seen that Eq (7-5) predicts a consistently higher capacity than that observed from the FEM analyses, although the general trend of the curve follows the data. Recall that the nominal capacity determined from the analysis results was based on a limit on the rotation of 0.05 radians, which was somewhat subjective. This is likely not the same limit criterion that was used in the formulation of Eq (7-5). To develop an equation that agrees with the limit criterion of 0.05 radians, the constant term in Eq (7-5) is reduced from 5.0 to 3.5, yielding:

$$M_n = 3.5 \cdot F_y t^2 \left(1 + 0.25 \cdot d / D\right) \cdot d \qquad (7\text{-}6)$$

This equation is also compared to the FEM results in Figure 7-7. As shown, by simply adjusting the constant term, Eq (7-6) can be made to agree very well with the capacities indicated by the FEM analyses. It appears that the general form of this equation works for determining moment capacity, but the constant term may need adjustment based on the deformation limit specified by the designer.

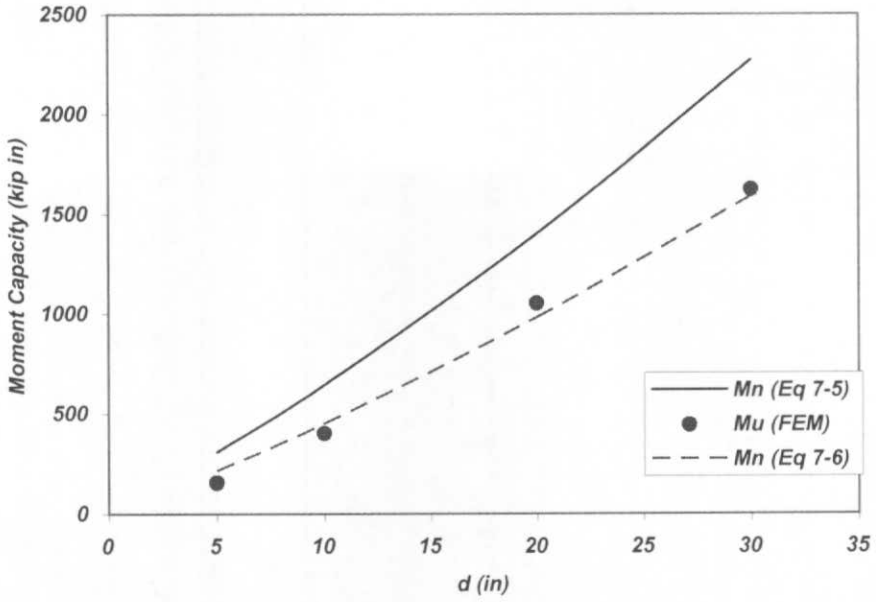

Figure 7-7: Moment capacity vs. plate depth (d)

7.3 AXIAL LOAD - MOMENT INTERACTION EQUATION

This section discusses the development of an interaction equation for the combined actions of axial load and moment, which may be present at an in-service bearing connection. The typical forms of interaction equations that are used are either linear or quadratic. Stamenkovic and Sparrow (1983) found that a linear interaction exists for simple HSS-to-HSS T-Connections. However, since a deformation limit has been placed on the moment capacity as described earlier,

it is determined that a quadratic equation fits the data more reasonably. Thus, the following quadratic interaction equation is proposed:

$$(P/P_n)^2 + (M/M_n)^2 \leq 1.0 \qquad (7\text{-}7)$$

where P and M are the applied axial force and moment and P_n and M_n are the respective capacities. The results from the FEM analyses along with Eq (7-7) are shown in Figure 7-8. It is once again noted that the loading is applied in a non-proportional fashion in that a given moment of imposed and held constant while the axial force is permitted to grow until failure is achieved.

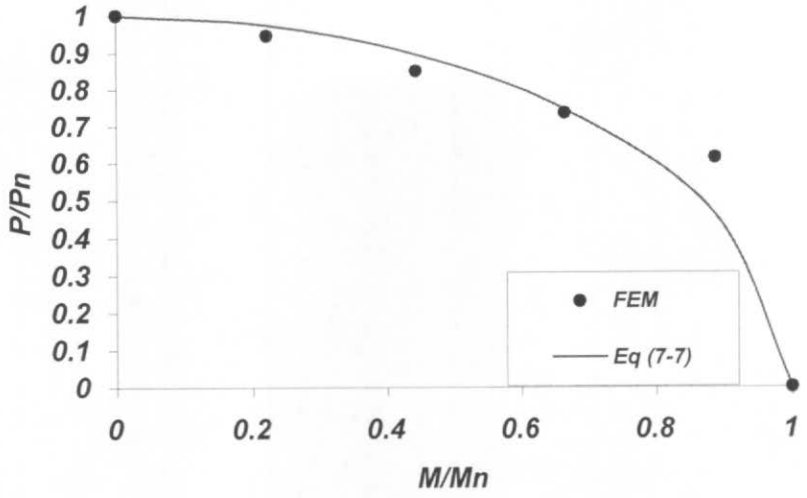

Figure 7-8: Axial load – moment interaction

7.4 INTERIOR ST-TO-HSS JOINT CAPACITY

Since a full parametric study has not been conducted for the interior ST-to-HSS joint, a new capacity equation is not developed. However, some general guidance can be offered for addressing these types of joints, if they are located sufficiently far from any chord end region.

First, it is noted that the capacity of the T-Connection is shown to be 95.4 kips from Figure 6-15, which is within 3% of the capacity for the benchmark case considered in the parametric study. Therefore, the notion that the ST-to-HSS joint is the "weak link" in the bearing connection region appears to be supported. Recall that this assumption was the basis of the development of the approximate methods in Chapter 4. Thus, to predict the capacity of an interior ST-to-HSS T-Connection, the methods described in Chapter 4 are applicable. However, these should be used with caution since they have not been fully verified for other geometric configurations.

For the ST-to-HSS Cross-Connection, a different failure mechanism is engaged as evident from the stress contours in Figure 6-14 and the different load-deflection response shown in Figure 6-15. This appears to be the limit state of general collapse that is found throughout the literature, in which the chord cross-section fails by excessive ovalization. Since this limit state is more global in nature, it should be less sensitive to the cross section geometry of the branch member. Thus, it is recommended that the equations as presented in the literature can be applied to this case. In calculating the β ratio, the ST flange width b_f should be used.

8.0 STRUCTURAL RELIABILITY CONSIDERATIONS

Up to this point, the term "capacity" has been referring to the nominal strength of the connection, with no consideration of variability in geometric properties or material strength. However, in real structures variability in these properties do exist. Therefore, safety must added to the design process using a factor of safety (SF) in the context of an allowable stress design approach (ASD) or load/resistance factors in the context of the load and resistance factor design (LRFD) approach. In tubular connection design, since the capacity equations are typically formulated empirically, safety factors are typically based on statistical analysis of experimental test data.

This research uses experimental testing only to validate finite element modeling techniques, which are subsequently used for a parametric study. Statistical methods are utilized in the formulation of the capacity equations, but this is merely to obtain an accurate curve-fit to the analytical results. A conventional statistical analysis (linear regression, confidence limits, etc.) does not apply in this case since there is no scatter with analytical data other than minor errors introduced from any approximations in the capacity formulation. (Recall from Chapter 7 that the quadratic form of the capacity equations contain minimal errors with respect to the parametric study results and the linear form of the capacity equations contain only minor errors, which always add conservatism) Therefore, we look to related research for making recommendations with regard to safety in the proposed capacity equations.

The literature that addresses structural safety in tubular joint connections most thoroughly is *AWS D1.1 Structural Welding Code – Steel* (AWS 2004). In the commentary, the database of testing results used for development of the capacity equations of Section 2.24.1.1 for the limit state of ultimate plastic collapse is summarized in Figure C2.9. From the figure, it is observed that the mean SF of 2.44 is provided by the capacity equation. However, it is noted that this is the raw ratio of $P_{test}/P_{allowable}$, which includes the material strength bias. In the context of the ASD method, the nominal SF that results is 1.8. When used in the context of LRFD, with a

resistance factor or 0.8, this is nominally equivalent to the ASD method for structures having 40% dead load and 60% service loads (AWS 2004).

For the bearing connection under investigation, the failure mechanism is also a form of plastic collapse, which is consistent with the limit state used as the basis of the safety recommendations in AWS. For this limit state, variations in the material yield strength (F_y) and chord wall thickness (t) will dominate the uncertainty in the overall bearing capacity. That is, small variations (within the fabrication tolerances) in the other variables (D, A, b_f, h) will not have a significant impact on the capacity, and can be considered negligible. Thus, it is recommended that the same SF=1.8 also be used for the capacity equations developed herein until further experimental testing is conducted.

9.0 SUMMARY AND CONCLUSIONS

Existing design specifications used in North America and Europe do not directly treat the general limit state of local collapse of tubular truss chords at bearing supports, while a number of overhead highway sign structures in Pennsylvania have been shown to be inadequate for this limit state. There are published capacity equations provided for the connection type that is related to the deficient details in question in which a concentrated force is applied to an unstiffened HSS wall through a single gusset plate. Unfortunately, the specification guidance on this related case is based on very limited experimental testing. This research is aimed at quantifying the bearing strength of circular chords in long, simple-span tubular trusses. The following is a summary of the research findings:

1) Two identical full-scale experimental tests are conducted on the bearing connection region of a long-span tubular highway sign truss proportioned in a fashion that is consistent with PennDOT design practice (as a matter of course, this leads to a connection detail which has been observed to be susceptible to bearing failure in field installations). The test specimen consists of a circular HSS chord of 26 in. outer diameter with a 1/2 in. wall thickness and 7 ft-6 in. length. The chord is loaded to failure with an axial load applied through an ST10x48 strut connected at 90 degrees and bearing directly on the HSS side wall through a full penetration weld made at a location 33 in. from the open end of the HSS section. The applied load is resisted by two curved steel "saddle" bearings. The objective of the experimental testing is to simulate the loading conditions present at the bearing region of an in-service long-span tubular truss. The results from these tests indicate that the ultimate bearing capacity is 96 kips for this configuration, but the load cuasing first yield is identified to be 40 kips.

2) Four (4) approximate methods are proposed for predicting the bearing capacity for the detail under investigation based on modified application of existing U.S. and international specifications. All of the proposed approximate methods provide a safe estimate of the bearing

capacity as compared to the experimental results. However, the safety margins may be considered too low, depending on the application.

3) Finite element modeling techniques are developed and validated using the experimental test results including deflection measurements and strain gauge data. Agreement between the experimentally measured response and the response of the finite element analogs is deemed reasonable to enable a parametric study to proceed. As part of these verified modeling techniques, linearly interpolated, quadrilateral shell elements based on a general-purpose formulation and reduced integration are employed as the primary finite element type for modeling of the structure under investigation. Since the demands on the shell are mostly flexural, this problem could be solved adequately using a simplified thin shell element. However, a general-purpose element that is able to consider finite membrane strains displays a slightly better agreement with experimental results. A simplified boundary condition at the saddle bearings, as opposed to a true contact interaction, is sufficiently accurate for modeling of this structure. Tubular (HSS) members have somewhat loose dimensional tolerances governing their manufacturing and also contain significant residual stresses as a result of the manufacturing processes; both require that analytical modeling of the steel material properties be done with great care. Useful approaches to treating these unique challenges are proven to be successful in the work reported herein.

4) The experimentally verified nonlinear finite element modeling techniques are used to perform a parametric study on all parameters relevant to the overall bearing capacity: h, b_f, A, D, t, F_y. Analyses are conducted to observe the following: 1) the bearing capacity of the HSS chord under the action of an axial load/reaction force (P), 2) the flexural capacity of the HSS chord wall under the action of a locally applied moment (M) and 3) the capacity of a combined axial load and moment. The results indicate that the open end of the chord no longer influences the failure mechanism once the intermediate branch member is located at a distance 33 in. (1.27*D) or more from the end. It is determined that the moment capacity of the connection is not significantly impacted by the parameters A, h, or b_f.

5) Capacity equations are developed for axial loading (P), moment (M), and interaction of both (P+M). For axial loading, the global failure mechanism observed in both the experimental tests and the finite element analysis involves a flexural collapse of the HSS chord through plastification of the chord wall into a well-defined yield line mechanism. However, the yield line patterns in this case cannot be described with simple geometry. Thus, quadratic functions are used for formulating the capacity equations, which are solved for by a regression-type curve-fit procedure. Due to the complexity of the final axial load capacity equations, two (2) equations are developed: one complex version yielding the more accurate capacity prediction and one simplified version for easy design office use. The moment capacity equation is a modified version of an existing published equation based on the deformation limit selected. The interaction behavior can be described in this case by a classic quadratic interaction equation.

6) The bearing configuration considered in this research includes a curved saddle bearing and a ST intermediate branch member, which may be considered to have limited applicability. Other bearing connection details may contain a flat bearing surface rather than a curved saddle bearing, a HSS intermediate branch member rather than an ST, or a branch member connected to the chord using a gusset plate. An attempt has been made to address these related cases by selecting wide ranges in the parametric study (i.e. A=0, b_f=0, d=0). For an HSS intermediate branch member, the branch diameter can be substituted for the ST flange width b_f, which will produce a conservative result.

7) The parameter ranges that are considered herein are consistent with geometric limits of applicability currently indentified by the dominant design specifications. A full range of possible h and A values are studied; no limit is needed for these parameters. For the ST flange width b_f, the range of $0 < b_f/D < 0.6$ is studied. For the HSS chord diameter "D", values of 10 in. to 26 in. are considered, which should envelope most practical applications. Practical limits are also utilized for t, yielding a range for the wall stiffness ratio of $26 < D/t < 69$.

APPENDIX A

LOAD DEFLECTION DATA

The load-deflection data is presented in this appendix. Table A- 1 contains the results gathered from Specimen 1, while Table A- 2 reports the results of test Specimen 2.

Table A- 1: Specimen 1 DCDT Full Results

ID	Seconds Elapsed	Load (kips)	[1] (in)	[2] (in)	[3] (in)
1	26.8	0	-0.000397931	0.000234149	-0.000116985
2	56.7	5.1	0.022284133	0.020253876	-0.000233969
3	107.2	10	0.044170336	0.039805306	-0.000233969
4	142.8	15.1	0.076402742	0.061229927	-0.000116985
5	229.7	20	0.101074461	0.082537473	-0.000116985
6	274.3	25	0.126939973	0.105132838	-0.000116985
7	320.2	30	0.153999278	0.128898947	-0.000233969
8	365.8	35	0.182252375	0.153133354	-0.000116985
9	417.3	40.2	0.213290989	0.17970925	-0.000233969
10	659.8	45.1	0.240748225	0.206168071	-0.000350954
11	694.5	50	0.250696499	0.235787902	0
12	734.4	55	0.284122699	0.267515073	-0.000233969
13	826.9	61.2	0.358933717	0.315983887	-0.000233969
14	909	65	0.395941296	0.349818397	-0.000116985
15	956.7	70.4	0.503780583	0.403672635	-0.000233969
16	1114.1	75.7	0.678870201	0.55657184	0.053929939
17	1161.3	82.3	0.894150846	0.678095099	0.152080088

Table A- 2: Specimen 2 DCDT Full Results

ID	Seconds Elapsed	Load (kips)	[1] (in)	[2] (in)	[3] (in)
1	334.2	0	0.001591724	0.000702447	-0.001403816
2	382.8	5.1	0.030640683	0.021073397	-0.00175477
3	418.1	10	0.05849585	0.040741902	-0.00175477
4	440.7	15.3	0.085555154	0.062283597	-0.00175477
5	466.7	20	0.110226873	0.08218625	-0.001871755
6	500.1	25	0.136490316	0.103727945	-0.001871755
7	527.4	30	0.164743413	0.127845278	-0.00175477
8	560.7	35	0.192200649	0.150440643	-0.00198874
9	594.1	40	0.222443401	0.174557975	-0.002105724
10	619.7	45	0.252686154	0.198792382	-0.00198874
11	646	50	0.291285456	0.225836575	-0.002105724
12	670.9	55	0.32670131	0.254871034	-0.00198874
13	701.9	60	0.366096474	0.288705544	-0.002105724
14	729.2	65	0.411858534	0.324881543	-0.00198874
15	762.5	70.6	0.465181281	0.36972105	0.011815453
16	786.5	75.4	0.522085407	0.415263003	0.04246544
17	812.7	80.4	0.5901316	0.469819688	0.082123248
18	845.2	85.4	0.676084685	0.536903336	0.133596508
19	876.4	90.2	0.779944663	0.619089586	0.200160793
20	896.3	92.9	0.855949474	0.678680471	0.251049131
21	908	94.6	0.915241186	0.725041945	0.291876785
22	921.7	96.3	1.001194271	0.791540221	0.352240882

APPENDIX B

FULL-REDUCED DATA SET

This Appendix contains all of the information captured by the strain rosettes during the experimental testing of Specimens 1 and 2. The data was retrieved from Strain Smart and was reduced into Excel files. Columns 4, 5, and 6 represent the strains of the corresponding rosette assignment. The next two columns are the maximum and minimum principle strains respectively, followed by the shear strain. Columns 10 and 11 are the maximum and minimum principle stresses followed by the shear stress. Table A- 3 contains the results from the first experimental test and Table A- 4 includes the results from test specimen #2.

Table A- 3: Reduced Data Specimen 1

Specimen 1

ID	Seconds Elapsed	Load (kips)	[1] e(1)	[1] e(2)	[1] e(3)	[1] e(max)	[1] e(min)	[1] Shear Strain	[1] s(max)	[1] s(min)	[1] Shear Stress
1	26.8	0	3.415714078	0.977641568	1.966242856	4.551291622	0.830665312	3.72062631	0.15562032	0.071190723	0.042214799
2	56.7	5.1	59.0462925	32.75201719	30.96920814	63.64329863	26.37220201	37.27109662	2.319638788	1.473871596	0.422883596
3	107.2	10	109.3142502	60.12845828	57.02412979	118.0179991	48.32038096	69.6976181	4.295787191	2.714187396	0.790799898
4	142.8	15.1	162.0277456	87.99528008	85.04695058	175.9277031	71.1469931	104.78071	6.395074867	4.017358757	1.188858055
5	229.7	20	216.2112078	115.3746995	114.546325	236.6833511	94.07418168	142.6091694	8.587599303	5.351468151	1.618065576
6	274.3	25	271.8651067	144.7114299	145.0308097	298.3594689	118.5364474	179.8230215	10.82489219	6.744292856	2.040299667
7	320.2	30	330.4547481	176.0058102	180.43444	364.7013722	146.1878158	218.5135564	13.24445346	8.285876605	2.479288429
8	365.8	35	390.5161463	211.2142931	218.7911541	431.5523566	177.7549438	253.7974128	15.71859975	9.959350768	2.879624491
9	417.3	40.2	458.8873577	248.8705107	266.4952062	511.7176318	213.6649321	298.0526997	18.66659867	11.9030951	3.381751785
10	659.8	45.1	521.8946936	285.5513287	318.1386563	588.7177716	251.3155784	337.4021932	21.52891992	13.87248554	3.828217192
11	694.5	50	593.7032796	324.6804546	378.1500132	679.8754463	291.9778464	387.8975999	24.87948308	16.0771914	4.401145845
12	734.4	55	670.4080152	367.2368007	448.992201	781.7324602	337.667756	444.0647042	28.62578815	18.54893525	5.038426451
13	826.9	61.2	830.2060241	448.9354103	633.031201	1031.000092	432.2371326	598.7629598	37.62615533	24.03884201	6.79365666
14	909	65	901.0805555	495.9058284	721.1375981	1138.901625	483.3165285	655.5850965	41.62082331	26.74408459	7.438369364
15	956.7	70.4	894.2370661	438.1719677	819.5985479	1277.323331	436.5122826	840.8110487	45.65293624	26.57299321	9.539971514
16	1114.1	75.7	1002.277191	549.2420891	903.7977693	1359.823993	546.2509675	813.5730257	49.3946471	30.93279767	9.230924714
17	1161.3	82.3	1044.815126	609.4356035	922.0181476	1362.404219	604.4290543	757.9751651	50.04408967	32.84388401	8.600102834

ID	Seconds Elapsed	Load (kips)	[2] e(1)	[2] e(2)	[2] e(3)	[2] e(max)	[2] e(min)	[2] Shear Strain	[2] s(max)	[2] s(min)	[2] Shear Stress
1	26.8	0	1.467458314	1.96324239	0.579529599	2.0628358	-0.015847887	2.078683687	0.066718025	0.019547895	0.023585065
2	56.7	5.1	11.73978529	5.398934831	1.73859081	11.91627714	1.562098961	10.35417818	0.401488738	0.166528541	0.117480099
3	107.2	10	21.03397454	11.77956816	0.289764716	21.09402234	0.229716912	20.86430543	0.686051268	0.212592029	0.236729619
4	142.8	15.1	30.32833394	16.19697665	0	30.36346484	-0.035130896	30.39859573	0.983968466	0.294154178	0.344907144
5	229.7	20	39.13367351	21.59608365	1.73859081	39.16961928	1.702645036	37.46697425	1.286343052	0.436130944	0.425106054
6	274.3	25	50.385163	26.01357751	2.897654706	50.39346209	2.889355617	47.50410647	1.661733988	0.583756187	0.5389889
7	320.2	30	60.16926961	30.43110979	2.897654706	60.1904796	2.876444715	57.31403489	1.979204048	0.678616334	0.650293857
8	365.8	35	70.93200468	35.33952406	2.318122422	70.9560819	2.294045203	68.6620367	2.322534853	0.764434789	0.779050032
9	417.3	40.2	81.69496793	38.28459538	4.056721286	81.96553512	3.786154098	78.17938102	2.693945879	0.91987531	0.887035285
10	659.8	45.1	89.52272089	42.21138371	0.579529599	89.61329474	0.488955748	89.12433899	2.909801597	0.887364674	1.011218462
11	694.5	50	97.83984065	45.64734839	1.448825255	98.00529703	1.283368875	96.72192816	3.189575909	0.994732154	1.097421877
12	734.4	55	105.6678426	49.57419364	2.897654706	105.8831204	2.682376865	103.2007435	3.458561634	1.116698608	1.170931513
13	826.9	61.2	103.221579	65.2818782	2.318122422	104.7499211	0.78978032	103.9601408	3.403420031	1.044324529	1.179547751
14	909	65	106.6463513	68.71799895	3.47718766	108.4233819	1.700157026	106.7232249	3.531358413	1.109562156	1.210898128
15	956.7	70.4	110.560405	75.09942771	5.215790551	113.3011091	2.475086448	110.8260227	3.697018939	1.182120732	1.257449104
16	1114.1	75.7	128.6632962	72.15414294	11.01117714	128.708905	10.96556834	117.7433366	4.2790747	1.607206676	1.335934012
17	1161.3	82.3	144.3203712	55.95538191	12.74980621	148.0875621	8.982615349	139.1049467	4.887999151	1.731386898	1.578306127

ID	Seconds Elapsed	Load (kips)	[3] e(1)	[3] e(2)	[3] e(3)	[3] e(max)	[3] e(min)	[3] Shear Strain	[3] s(max)	[3] s(min)	[3] Shear Stress
1	26.8	0	-1.47411195	0.490274604	-0.489499192	0.570414005	-2.534025147	3.104439152	-0.006152648	-0.076599536	0.035223444
2	56.7	5.1	-58.9611372	-13.7274965	-60.20486047	-13.72328007	-105.4427176	91.71943753	-1.470334959	-3.551660657	1.040662849
3	107.2	10	-118.4066792	-29.90585465	-118.4450462	-29.90585259	-206.9458728	177.0400202	-2.982080908	-6.999527521	2.008723306
4	142.8	15.1	-182.2660284	-45.59346666	-183.529114	-45.59201428	-320.2031281	274.6111138	-4.592046269	-10.82360616	3.115779946
5	229.7	20	-247.0996039	-59.31972909	-249.0940992	-59.3170951	-436.876608	377.5595129	-6.171661853	-14.73935849	4.283848319
6	274.3	25	-314.3802334	-74.02602658	-316.1182043	-74.02446143	-556.4739763	482.4495148	-7.811556376	-18.75944921	5.473946418
7	320.2	30	-385.0889393	-86.77113945	-387.0464877	-86.76953911	-685.3658879	598.5963488	-9.478230233	-23.06176276	6.791766265
8	365.8	35	-455.2968574	-98.53557471	-459.4320337	-98.52961809	-816.1992731	717.669655	-11.13185418	-27.41743481	8.142790316
9	417.3	40.2	-536.7847687	-111.2800716	-542.0758797	-111.2718983	-967.5887501	856.3168518	-13.01723235	-32.44903783	9.715902741
10	659.8	45.1	-615.8057165	-124.0242482	-627.1507518	-123.9919073	-1118.964561	994.9726538	-14.90175564	-37.47998124	11.2891128
11	694.5	50	-703.1561583	-135.2976759	-723.4539417	-135.2085837	-1291.401516	1156.192933	-16.94236993	-43.17905571	13.11834289
12	734.4	55	-799.8129807	-153.4326642	-831.9564502	-153.2377351	-1478.531696	1325.293961	-19.34672384	-49.42070218	15.03698917
13	826.9	61.2	-965.1172114	-191.6610554	-1028.374934	-191.0400037	-1802.452142	1611.412138	-23.72239732	-60.28905737	18.28333003
14	909	65	-1082.318109	-224.0059046	-1156.836433	-223.2311788	-2015.923363	1792.692184	-26.84202367	-67.52234631	20.34016132
15	956.7	70.4	-1347.513783	-272.029299	-1414.150003	-271.5288288	-2490.134957	2218.606128	-33.01955474	-83.36484765	25.17264645
16	1114.1	75.7	-1968.537984	-318.0882812	-1984.949087	-318.0679849	-3635.419086	3317.351101	-45.66644446	-120.9447964	37.63917595
17	1161.3	82.3	-2464.124947	-299.9591812	-2459.637286	-299.9580173	-4623.804215	4323.846198	-54.69168002	-152.8097284	49.05902417

ID	Seconds Elapsed	Load (kips)	[4] e(1)	[4] e(2)	[4] e(3)	[4] e(max)	[4] e(min)	[4] gamma	[4] s(max)	[4] s(min)	[4] tau
1	26.8	0	1.473042879		0	0	0	0	0	0	0
2	56.7	5.1	36.82735239		13.3703682	0	0	0	0	0	0
3	107.2	10	72.1841205		22.77935643	0	0	0	0	0	0
4	142.8	15.1	111.9634237		34.6646429	0	0	0	0	0	0
5	229.7	20	154.201646		45.0644963	0	0	0	0	0	0
6	274.3	25	195.4609714		58.43604872	0	0	0	0	0	0
7	320.2	30	238.1973737		71.31269058	0	0	0	0	0	0
8	365.8	35	282.4112247		85.18020776	0	0	0	0	0	0
9	417.3	40.2	332.5249033		96.07637925	0	0	0	0	0	0
10	659.8	45.1	378.7124701		105.4868969	0	0	0	0	0	0
11	694.5	50	430.3099248		116.3835033	0	0	0	0	0	0
12	734.4	55	484.3700158		126.2897115	0	0	0	0	0	0
13	826.9	61.2	583.6589667		134.7101401	0	0	0	0	0	0
14	909	65	629.3777224		141.1493855	0	0	0	0	0	0
15	956.7	70.4	704.6013905		139.1680705	0	0	0	0	0	0
16	1114.1	75.7	850.1637274		172.3561132	0	0	0	0	0	0
17	1161.3	82.3	926.4038639		201.0878085	0	0	0	0	0	0

ID	Seconds Elapsed	Load (kips)	[5] e(1)	[5] e(2)	[5] e(3)	[5] e(max)	[5] e(min)	[5] gamma	[5] s(max)	[5] s(min)	[5] tau
1	26.8	0	1.469433914	2.449583134	1.470489763	2.449583276	0.490340402	1.959242874	0.084178263	0.039718521	0.022229871
2	56.7	5.1	36.73712489	37.23493751	57.35225391	61.27413486	32.81524394	28.45889092	2.30549658	1.65969867	0.322898955
3	107.2	10	68.57811865	69.08277156	110.2985412	118.5844647	60.29219518	58.2922695	4.430579819	3.107793704	0.661393058
4	142.8	15.1	103.8504756	98.4825431	164.2309858	180.6865902	87.39487122	93.29171899	6.707361562	4.59035717	1.058502196
5	229.7	20	141.0850687	129.8441734	223.0729075	248.4791183	115.6788579	132.8002604	9.18010097	6.166556599	1.506772185
6	274.3	25	183.7122342	163.6580983	284.3738201	320.5717907	147.5142636	173.0575271	11.82677919	7.899704532	1.963537327
7	320.2	30	230.2632299	199.924807	349.11561	397.3423707	182.0364692	215.3059014	14.65123372	9.765445959	2.442893881
8	365.8	35	282.6994663	237.664534	415.3373336	478.6250526	219.4117473	259.2133053	17.64970661	11.76755853	2.941074041
9	417.3	40.2	345.4340459	280.3088949	490.8896854	574.0232698	262.3004615	311.7228083	21.15939071	14.08568083	3.53685494
10	659.8	45.1	411.1176197	324.4275147	567.9253953	672.2869202	306.7560948	365.5308253	24.77720394	16.48246598	4.14736898
11	694.5	50	486.6152132	373.452693	652.8253964	782.8574242	356.5831854	426.2742389	28.84621451	19.17306832	4.836573095
12	734.4	55	565.0661692	421.011632	743.1392216	903.6201233	404.5852676	499.0348557	33.2278827	21.9036302	5.662126247
13	826.9	61.2	647.9431621	401.3991595	779.9565238	1033.394379	394.505307	638.8890719	37.33681994	22.83895254	7.248933701
14	909	65	689.6319719	441.1152012	842.7975428	1100.212728	432.2167868	667.9959412	39.86966378	24.71129434	7.579184717
15	956.7	70.4	861.8185019	534.7788892	1024.491034	1359.55175	526.7577862	832.793964	49.19624509	30.29822822	9.449008437
16	1114.1	75.7	994.8002003	694.1939285	1260.298254	1580.781087	674.3173671	906.4637203	57.80302283	37.23326918	10.28487683
17	1161.3	82.3	1017.866991	779.0721587	1362.515333	1635.965157	744.417167	891.5479901	60.27369677	40.04241546	10.11564066

ID	Seconds Elapsed	Load (kips)	[6] e(1)	[6] e(2)	[6] e(3)	[6] e(max)	[6] e(min)	[6] gamma	[6] s(max)	[6] s(min)	[6] tau
1	26.8	0	0	0.98061756	0.984727237	1.185771034	-0.201043797	1.386814831	0.036484624	0.005014595	0.015735014
2	56.7	5.1	-24.90389729	-8.825472674	-3.938889858	-2.538750147	-26.304037	23.76528686	-0.338114128	-0.87740333	0.269644601
3	107.2	10	-49.31829474	-20.59253055	-8.862459226	-7.149956511	-51.03079746	43.88084094	-0.728072829	-1.723830374	0.497878772
4	142.8	15.1	-73.7315159	-30.88848212	-15.75537616	-12.61451484	-76.87237722	64.25786238	-1.156537062	-2.614696247	0.729079592
5	229.7	20	-95.21417757	-41.18422455	-21.66351623	-17.81684624	-99.06084756	81.24400132	-1.540973038	-3.384586915	0.921806938
6	274.3	25	-119.6251876	-52.95053126	-26.58691379	-22.40817046	-123.8039309	101.3957604	-1.930445953	-4.231349747	1.150451897
7	320.2	30	-144.0350215	-66.18729984	-34.46425062	-29.80798561	-148.6912865	118.8833009	-2.412366441	-5.110102884	1.348868222
8	365.8	35	-167.4673557	-78.93349102	-41.35682012	-36.40381126	-172.4203646	136.0165534	-2.856958966	-5.943488446	1.54326474
9	417.3	40.2	-193.3392992	-95.60110354	-53.17243596	-47.91349332	-198.5982419	150.6847486	-3.484662081	-6.90404676	1.70969234
10	659.8	45.1	-217.2574679	-109.8171635	-68.43386627	-61.4331487	-224.2581855	162.8250368	-4.172486625	-7.86736246	1.847437917
11	694.5	50	-242.1506892	-123.5426361	-83.69483801	-74.44757707	-251.3979501	176.9503731	-4.858324596	-8.873736908	2.007706156
12	734.4	55	-267.5307535	-139.2284354	-101.908946	-90.23644083	-279.2032586	188.9668178	-5.640575652	-9.928668826	2.144046587
13	826.9	61.2	-317.3110329	-203.4371151	-175.2510398	-163.3300749	-329.2319977	165.9019228	-8.496637791	-12.26133527	1.882348739
14	909	65	-341.2233493	-213.2392512	-195.4305632	-176.9566144	-359.6972981	182.7406837	-9.234660674	-13.3814685	2.073403911
15	956.7	70.4	-326.5832896	-180.8914825	-241.6927855	-172.5071702	-395.7689048	223.2617346	-9.441226735	-14.50755071	2.533161989
16	1114.1	75.7	-416.368996	-224.021382	-290.9032894	-209.6382362	-497.6340492	287.995813	-11.63559264	-18.17088224	3.267644801
17	1161.3	82.3	-475.8920498	-247.5452347	-312.0623399	-226.1905374	-561.7638522	335.5733148	-12.79585818	-20.4107911	3.807466456

ID	Seconds Elapsed	Load (kips)	[7] e(1)	[7] e(2)	[7] e(3)	[7] e(max)	[7] e(min)	[7] gamma	[7] s(max)	[7] s(min)	[7] tau
1	26.8	0	1.960935216	1.958911406	2.446777706	2.548832999	1.858879924	0.689953074	0.100705122	0.085048494	0.007828314
2	56.7	5.1	30.88560878	23.99718565	37.68168273	45.11683165	23.45045986	21.66637179	1.690640773	1.198980798	0.245829988
3	107.2	10	57.85077055	46.03641674	68.02480827	80.58811969	45.28745914	35.30066055	3.052904994	2.251851543	0.400526725
4	142.8	15.1	86.28830965	64.6480682	100.8169965	123.3561044	63.74920173	59.6069027	4.618885183	3.266267006	0.676309088
5	229.7	20	115.2177842	84.72982589	134.1007836	165.6898034	83.62876437	82.06103901	6.184575565	4.322421219	0.931077173
6	274.3	25	144.1489058	104.812378	167.3867501	208.0311729	103.504483	104.5266899	7.750477225	5.378525416	1.185975905
7	320.2	30	173.0816747	123.9160308	200.6748962	251.3344099	122.422161	128.9122489	9.338243095	6.412926678	1.462658209
8	365.8	35	202.016091	141.5508098	232.0069073	293.9476928	140.0753055	153.8723873	10.89134439	7.399624828	1.745859779
9	417.3	40.2	234.3853565	159.6760822	263.8304577	339.7434674	158.4723468	181.2711206	12.55484897	8.441388921	2.056730022
10	659.8	45.1	262.3422905	171.4333617	290.2699992	382.1044902	170.5077996	211.5966906	14.045139	9.243521786	2.400808605
11	694.5	50	293.2438491	182.70101	316.2212566	427.3037066	182.1613991	245.1423076	15.62372278	10.06087811	2.781422336
12	734.4	55	326.1094732	193.9689085	342.1738386	474.5443449	193.7389669	280.8053779	17.26774509	10.89562305	3.186061019
13	826.9	61.2	368.2983145	174.8626195	389.1856622	582.8886693	174.5953074	408.2933619	20.59382881	11.32871021	4.632559298
14	909	65	398.7156983	172.9030408	388.6959333	614.565419	172.8462126	441.7192064	21.60370202	11.58007388	5.011814073
15	956.7	70.4	416.8688752	76.89294789	311.3246915	656.1086611	72.08490561	584.0237555	21.97050211	8.717655348	6.62642338
16	1114.1	75.7	516.4775731	91.58719339	257.9551908	709.8695589	64.56320498	645.306354	23.64014984	8.996659498	7.32174517
17	1161.3	82.3	578.3134802	101.3835934	196.268987	731.1410225	43.44144462	687.6995779	24.12430434	8.518813918	7.802745211

ID	Seconds Elapsed	Load (kips)	[8] e(1)	[8] e(2)	[8] e(3)	[8] e(max)	[8] e(min)	[8] gamma	[8] s(max)	[8] s(min)	[8] tau
1	26.8	0	1.954380987	1.469806549	2.458535391	2.985045726	1.427870651	1.557175075	0.1106544	0.075318504	0.017667948
2	56.7	5.1	17.10108868	9.798790724	31.47015008	40.45613841	8.115100346	32.34103807	1.390411782	0.656518995	0.366946393
3	107.2	10	31.75962307	18.12791158	60.97518345	78.16136702	14.57343949	63.58792753	2.67553326	1.232576443	0.721478409
4	142.8	15.1	48.37314024	27.43709075	95.39988463	122.171995	21.60102985	100.5709652	4.170596667	1.888409381	1.141093643
5	229.7	20	64.49854434	35.27653196	132.2860773	170.0330042	26.75161746	143.2813867	5.772225757	2.520840442	1.625692657
6	274.3	25	81.11313261	45.07600374	171.142425	218.8408232	33.41473437	185.4260889	7.419257895	3.211512033	2.103872931
7	320.2	30	99.19433161	54.87566472	210.0017395	268.6774888	40.51858233	228.1589064	9.10392898	3.926476873	2.588726054
8	365.8	35	116.7874675	65.16551237	252.3076575	321.8192069	47.27591808	274.5432888	10.89237196	4.66235117	3.115010393
9	417.3	40.2	136.336111	76.92559369	300.0290179	381.4381117	54.92701718	326.5110945	12.89948176	5.490191534	3.704645111
10	659.8	45.1	152.9530497	89.66598926	347.262811	437.673085	62.54277559	375.1303095	14.79654898	6.283976574	4.256286203
11	694.5	50	174.9468927	106.326989	402.866538	504.1326376	73.6807931	430.4518445	17.05932728	7.291381582	4.883972851
12	734.4	55	199.3856132	124.4586984	456.0156001	568.0586953	87.34251803	480.7161773	19.26451956	8.355960149	5.454279704
13	826.9	61.2	241.4229633	172.9764572	522.9519428	634.3459	130.0290062	504.3168938	21.8285283	10.38441417	5.722057064
14	909	65	270.2645531	195.0315169	571.6831983	692.5677809	149.3799705	543.1878105	23.90413437	11.57794944	6.163092465
15	956.7	70.4	327.952646	236.2035256	696.7322022	844.3850139	180.2998343	664.0851796	29.1263862	14.05676097	7.534812615
16	1114.1	75.7	473.1796451	299.9286936	866.6314246	1088.932907	250.8781626	838.0547445	37.74043132	18.72303519	9.508698062
17	1161.3	82.3	600.8376521	338.6578956	981.4070316	1281.970932	300.273752	981.6971798	44.47864307	22.2016686	11.13848723

ID	Seconds Elapsed	Load (kips)	[9] e(1)	[9] e(2)	[9] e(3)	[9] e(max)	[9] e(min)	[9] gamma	[9] s(max)	[9] s(min)	[9] tau
1	26.8	0	3.423521748	0	0.987414342	4.724941029	-0.314004939	5.038945968	0.150117381	0.035772069	0.057172656
2	56.7	5.1	40.59467283	15.74952025	25.67339659	52.05181641	14.21625302	37.83556339	1.825651015	0.967074768	0.429288123
3	107.2	10	76.79025149	30.02294468	48.8793136	98.49108377	27.17848132	71.31260245	3.457161023	1.838913506	0.809123759
4	142.8	15.1	117.8802525	46.26560508	75.04895965	151.0408794	41.88833273	109.1525467	5.303755701	2.826832526	1.238461588
5	229.7	20	163.3766337	63.0010104	102.2075647	208.9905888	56.59360957	152.3969792	7.325358038	3.867118894	1.729119572
6	274.3	25	209.3663671	81.70593927	132.3306246	267.9567951	73.74019654	194.2165986	9.403655159	4.996432346	2.203611407
7	320.2	30	255.360267	101.396082	162.4554703	326.0257989	91.78993845	234.2358604	11.46165057	6.146298357	2.657676109
8	365.8	35	302.3370616	122.0715531	195.0515774	386.2111139	111.1775251	275.0335889	13.60126259	7.360115767	3.120573412
9	417.3	40.2	356.6593993	144.2247771	228.1437036	453.9113885	130.8917144	323.019674	15.98766773	8.657605895	3.665030917
10	659.8	45.1	405.6034191	164.4096665	261.237985	517.2006649	149.6407392	367.5599257	18.22169248	9.88090955	4.170391465
11	694.5	50	460.4263228	193.4576219	300.7563679	584.0431924	177.1394983	406.9036941	20.65599861	11.42241478	4.616791914
12	734.4	55	517.2134277	224.4767633	345.2182222	655.1279221	207.3037278	447.8241943	23.25374911	13.0915847	5.081082204
13	826.9	61.2	624.4408793	261.8991999	418.8358434	800.9818589	242.2948638	558.6869951	28.32227954	15.64438234	6.338948598
14	909	65	682.2257879	299.3243924	481.0979927	881.3743528	281.9494278	599.424925	31.31406137	17.71172653	6.801167418
15	956.7	70.4	785.5694305	402.750439	600.7022451	997.8777759	388.3938997	609.4838762	36.12602242	22.29542677	6.915297826
16	1114.1	75.7	1085.924069	566.7977557	941.382581	1466.315407	560.9912434	905.3241636	52.99019452	32.44630003	10.27194724
17	1161.3	82.3	1372.725072	682.5987536	1255.069585	1947.93092	679.863738	1268.067182	69.75907276	40.9837021	14.38768533

ID	Seconds Elapsed	Load (kips)	[10] e(1)	[10] e(2)	[10] e(3)	[10] e(max)	[10] e(min)	[10] gamma	[10] s(max)	[10] s(min)	[10] tau
1	26.8	0	0	2.434773463	1.47437108	2.587927898	-1.113556818	3.701484716	0.07306472	-0.01093051	0.041997615
2	56.7	5.1	34.86596933	23.86128335	27.52229853	39.39493101	22.99333685	16.40159416	1.500704941	1.128514919	0.186095011
3	107.2	10	65.80538486	41.87973012	52.58854535	77.73227839	40.66165181	37.07062658	2.915338276	2.074120211	0.420609032
4	142.8	15.1	94.78210371	58.43778546	77.65602804	115.2901023	57.14802946	58.14207283	4.293206679	2.973828873	0.659688903
5	229.7	20	124.2516504	77.91854181	103.7078589	151.4753933	76.48411606	74.99127721	5.654295086	3.95256995	0.850862568
6	274.3	25	155.1965164	94.96481666	132.2189394	193.7863027	93.62915308	100.1571497	7.192652677	4.919855819	1.136398429
7	320.2	30	185.6520364	111.524603	160.2400073	235.6678959	110.2241477	125.4437482	8.711743558	5.865135424	1.423304067
8	365.8	35	215.1268605	128.572006	191.2124579	278.7195402	127.6197781	151.0997621	10.27655107	6.847748776	1.714401147
9	417.3	40.2	243.1295291	145.6199812	225.6285046	323.5683541	145.1896796	178.3786744	11.90131331	7.853489541	2.023911883
10	659.8	45.1	265.7293005	160.7200943	257.5883481	362.6795944	160.6380542	202.0415402	13.31944485	8.734656055	2.292394398
11	694.5	50	291.7694153	172.4108128	293.9758459	413.3395001	172.4057612	240.9337389	15.0761607	9.608818165	2.733671268
12	734.4	55	313.8799955	181.1790283	332.8248322	465.8410038	180.8638239	284.9771798	16.86038951	10.39359966	3.233394925
13	826.9	61.2	284.8907646	128.572006	361.348762	521.3879811	124.8515455	396.5364357	18.11635343	9.118026619	4.499163405
14	909	65	288.3300783	131.4944754	390.3661252	553.3713918	125.3248117	428.0465802	19.15778093	9.444416222	4.856682352
15	956.7	70.4	328.1295465	104.7058021	442.5031746	671.6948115	98.93790955	572.7569019	22.73692026	9.73974441	6.498587926
16	1114.1	75.7	279.9774997	105.6799109	566.473091	771.5857438	74.86484682	696.720897	25.74102565	9.930820675	7.905102485
17	1161.3	82.3	212.1793011	104.2187483	641.2632067	814.0662107	39.37629714	774.6899135	26.77300378	9.193501901	8.789750942

ID	Seconds Elapsed	Load (kips)	[11] e(1)	[11] e(2)	[11] e(3)	[11] e(max)	[11] e(min)	[11] gamma	[11] s(max)	[11] s(min)	[11] tau
1	26.8	0	0.980326651	0	0	1.183358948	-0.203032297	1.386391245	0.036387091	0.004926675	0.015730208
2	56.7	5.1	-5.881920159	-13.27109548	-17.627057	-5.689246926	-17.81973023	12.13048331	-0.357733403	-0.633002063	0.13763433
3	107.2	10	-14.70467264	-27.52484841	-35.25350142	-14.39397995	-35.56419412	21.17021417	-0.812489589	-1.292890603	0.240200507
4	142.8	15.1	-24.01741172	-39.32075488	-46.51452023	-23.30890589	-47.22302606	23.91412016	-1.21487528	-1.757541853	0.271333286
5	229.7	20	-31.85958583	-50.6249079	-57.77528901	-30.6176969	-59.01717795	28.39948106	-1.566509982	-2.210959744	0.322224881
6	274.3	25	-40.19176311	-60.94587112	-71.48371357	-39.37901539	-72.2964613	32.9174459	-1.979675425	-2.726648236	0.373486405
7	320.2	30	-49.99414956	-72.2495423	-86.17090017	-49.52037641	-86.64467332	37.12429691	-2.447974135	-3.290410103	0.421217984
8	365.8	35	-60.28645165	-81.58716765	-100.8576614	-60.26106897	-100.8830441	40.62197515	-2.934633489	-3.856439848	0.46090318
9	417.3	40.2	-73.51910492	-91.4160613	-117.0126076	-73.18097195	-117.3507406	44.16976866	-3.513618381	-4.515932362	0.501156991
10	659.8	45.1	-89.20180295	-103.2104823	-131.2089537	-88.06765602	-132.3431007	44.27544464	-4.142013509	-5.146725522	0.502356007
11	694.5	50	-106.8442592	-114.021794	-146.8734262	-103.0812614	-150.636424	47.55516254	-4.806625895	-5.885762276	0.53956819
12	734.4	55	-124.9761449	-122.3758316	-161.5584297	-115.5000618	-171.0345128	55.53445095	-5.407590397	-6.667795246	0.630102424
13	826.9	61.2	-160.7479661	-94.85612909	-142.4678422	-94.12482227	-209.090986	114.9661638	-5.084766465	-7.693614028	1.304423781
14	909	65	-181.8178593	-109.5990125	-157.6424704	-108.3960974	-231.0642323	122.6681349	-5.761102558	-8.54472562	1.391811531
15	956.7	70.4	-267.5584041	-169.5489915	-177.2219648	-152.8750081	-291.9053608	139.0303526	-7.794698003	-10.94961754	1.57745977
16	1114.1	75.7	-328.792785	-209.3479332	-254.5535783	-201.3664184	-381.9799449	180.6135265	-10.24267237	-14.34121009	2.049268858
17	1161.3	82.3	-355.2437528	-230.9658026	-312.7892238	-228.802228	-439.2307487	210.4285207	-11.68885478	-16.46396352	2.387554369

ID	Seconds Elapsed	Load (kips)	[12] e(1)	[12] e(2)	[12] e(3)	[12] e(max)	[12] e(min)	[12] gamma	[12] s(max)	[12] s(min)	[12] tau
1	26.8	0	2.937428995		0.98303964	0	0	0	0	0	0
2	56.7	5.1	29.37505474		25.55964804	0	0	0	0	0	0
3	107.2	10	53.85556534		48.66274258	0	0	0	0	0	0
4	142.8	15.1	80.29584259		70.29212241	0	0	0	0	0	0
5	229.7	20	105.7581517		92.90563915	0	0	0	0	0	0
6	274.3	25	131.7114345		116.0117923	0	0	0	0	0	0
7	320.2	30	157.6660439		138.6273413	0	0	0	0	0	0
8	365.8	35	183.1322331		161.7355711	0	0	0	0	0	0
9	417.3	40.2	209.5792429		185.3365486	0	0	0	0	0	0
10	659.8	45.1	232.1092636		204.0214322	0	0	0	0	0	0
11	694.5	50	255.6199162		221.7235339	0	0	0	0	0	0
12	734.4	55	280.1113368		240.4097538	0	0	0	0	0	0
13	826.9	61.2	303.6242118		260.0802004	0	0	0	0	0	0
14	909	65	322.7292243		266.4732592	0	0	0	0	0	0
15	956.7	70.4	336.9359816		216.8062216	0	0	0	0	0	0
16	1114.1	75.7	410.9155194		223.1987368	0	0	0	0	0	0
17	1161.3	82.3	459.9145224		213.3641314	0	0	0	0	0	0

ID	Seconds Elapsed	Load (kips)	[13] e(1)	[13] e(2)	[13] e(3)	[13] e(max)	[13] e(min)	[13] gamma	[13] s(max)	[13] s(min)	[13] tau
1	26.8	0	2.447498184	0.983839564	1.965864754	3.453010083	0.960352855	2.492657227	0.121277934	0.06471379	0.028282072
2	56.7	5.1	35.2451143	18.2013404	37.84423108	54.93398184	18.15536354	36.7786183	1.957392782	1.122801059	0.417295862
3	107.2	10	67.06572563	32.46771178	72.25052079	106.9387781	32.37746835	74.56130972	3.781576426	2.089608244	0.845984091
4	142.8	15.1	105.7426969	49.19431262	108.1338447	164.6946047	49.18193694	115.5126678	5.81730877	3.196059771	1.3106245
5	229.7	20	149.3190232	67.88940065	147.4609422	228.8959255	67.88403992	161.0118856	8.080443468	4.426712218	1.826865625
6	274.3	25	198.2856576	86.58517672	190.2326117	302.0083532	86.5099161	215.4984371	10.63171338	5.741556539	2.44507842
7	320.2	30	252.1544195	106.7577068	234.9746425	380.6407628	106.4882992	274.1524636	13.37508126	7.153929206	3.110576029
8	365.8	35	311.9064697	130.8673911	284.1462472	465.7606061	130.2921108	335.4684953	16.36595941	8.753405091	3.806277159
9	417.3	40.2	381.9526758	159.4068636	346.6010355	569.907953	158.6457582	411.2621949	20.01791162	10.68542335	4.666244134
10	659.8	45.1	452.4984965	188.932143	410.0472122	674.5413237	188.0043849	486.5369389	23.69539325	12.65474733	5.52032296
11	694.5	50	540.2045574	226.8254324	488.2591988	802.8095021	225.6542541	577.155248	28.21969281	15.12270834	6.548492237
12	734.4	55	635.2774222	270.1355097	576.3235561	942.7572638	268.8437145	673.9135493	33.17649028	17.88383666	7.646326809
13	826.9	61.2	768.6054814	352.3363766	700.3282589	1118.119263	350.8144769	767.3047865	39.65849054	22.24657423	8.705958154
14	909	65	875.9796534	414.3649949	803.1963508	1266.365412	412.8105917	853.5548208	45.06720154	25.69807292	9.684564313
15	956.7	70.4	1063.816533	489.203247	1010.964678	1586.214539	488.5666724	1097.647866	56.17268565	31.26452253	12.45408156
16	1114.1	75.7	1585.514338	791.6226119	1555.897495	2349.929944	791.4818893	1558.448055	83.87642645	48.51164367	17.68239139
17	1161.3	82.3	2033.53233	1031.124526	2045.158188	3047.58275	1031.107769	2016.474981	108.8230713	63.06460056	22.87923536

ID	Seconds Elapsed	Load (kips)	[14] e(1)	[14] e(2)	[14] e(3)	[14] e(max)	[14] e(min)	[14] gamma	[14] s(max)	[14] s(min)	[14] tau
1	26.8	0	-5.861788688	1.469208716	1.952370911	3.240335318	-7.149753096	10.39008841	0.035510524	-0.200264559	0.117887542
2	56.7	5.1	34.19511859	23.01809159	43.93016025	55.82928112	22.29599772	33.5332834	2.026685025	1.26573744	0.380473792
3	107.2	10	70.34675267	43.0985555	82.00603846	109.7640159	42.58877524	67.17524065	3.972471571	2.448110341	0.762180615
4	142.8	15.1	115.7842199	64.64920497	123.9904425	175.2776382	64.49702419	110.780614	6.309328561	3.795460782	1.25693389
5	229.7	20	156.828014	86.69058789	170.8608519	241.3166598	86.37220606	154.9444538	8.662896141	5.146848921	1.75802361
6	274.3	25	199.8298392	110.6922929	221.1537034	310.8591598	110.1243827	200.7347771	11.14829231	6.593156984	2.277567663
7	320.2	30	245.2789148	136.1647306	271.9398856	381.7775735	135.4412268	246.3363467	13.6935091	8.10356892	2.794970088
8	365.8	35	292.6871309	161.1485549	324.1963513	456.5750948	160.3083875	296.2667072	16.36010387	9.637128594	3.36148764
9	417.3	40.2	351.8314299	189.073107	383.296586	546.7469194	188.3810966	358.3658228	19.55627124	11.42412372	4.066073759
10	659.8	45.1	413.915926	215.0394189	437.5185483	636.7253271	214.7091472	422.0161798	22.72920121	13.15268021	4.788260502
11	694.5	50	492.1434371	252.7664262	505.9148583	745.3881153	252.67018	492.7179353	26.62096758	15.44006058	5.590453497
12	734.4	55	581.6309505	294.9063966	580.6727803	867.397735	294.9059958	572.4917393	30.98697939	17.99582069	6.495579349
13	826.9	61.2	741.0849963	328.7189007	702.8499106	1115.680426	328.2544811	787.4259447	39.36002716	21.49151534	8.934255911
14	909	65	870.2501716	388.0187264	811.36782	1294.555413	387.062579	907.4928336	45.7306467	25.13754009	10.2965533
15	956.7	70.4	1071.402344	495.8543287	979.5674589	1557.102203	493.8676002	1063.234603	55.28048709	31.15324033	12.06362338
16	1114.1	75.7	1672.39714	773.8816357	1526.600757	2428.3283	770.6695975	1657.658702	86.21550636	48.59940503	18.80805066
17	1161.3	82.3	2196.58282	1000.044221	2043.838343	3242.977429	997.4437345	2245.533694	114.8299024	63.87356089	25.47817076

ID	Seconds Elapsed	Load (kips)	[15] e(1)	[15] e(2)	[15] e(3)	[15] e(max)	[15] e(min)	[15] gamma	[15] s(max)	[15] s(min)	[15] tau
1	26.8	0	-20.86044638	-27.4464126	36.5107141	53.2887952	-37.63852748	90.92732268	1.36144889	-0.701901894	1.031675392
2	56.7	5.1	-11.53993261	-24.79037623	81.49130791	110.709995	-40.75861975	151.4686148	3.192561614	-0.244610798	1.718586206
3	107.2	10	-8.876895677	-34.0864397	139.1781649	188.9572263	-58.6559571	247.6131834	5.555091161	-0.063823386	2.809457274
4	142.8	15.1	-11.09609414	-14.60876835	173.0524158	213.6979011	-51.74157941	265.4394805	6.424368247	0.400933881	3.011717183
5	229.7	20	-4.438468206	-52.67803057	250.8659343	340.54527	-94.11780394	434.663074	10.12433286	0.260824641	4.931754109
6	274.3	25	27.96328642	10.62483598	304.3365891	374.1970668	-41.89719121	416.094258	11.72310256	2.280963627	4.721069465
7	320.2	30	23.96843223	-37.18508781	385.3474672	506.5465989	-97.23069943	603.7772983	15.47542085	1.774320623	6.850550115
8	365.8	35	65.25018356	25.23436659	436.7140312	543.3147773	-41.35056262	584.66534	17.21080599	3.9434002	6.633702896
9	417.3	40.2	161.5879748	65.96629747	462.6640739	600.6677292	23.58431948	577.0834097	19.7015596	6.606205306	6.547677149
10	659.8	45.1	51.93310458	-72.59679909	489.674717	678.0243391	-136.4165176	814.4408567	20.65322178	2.171679267	9.240771258
11	694.5	50	89.66578074	-55.77655956	517.7461303	722.0848209	-114.6729098	836.7577308	22.29301864	3.305054752	9.493981945
12	734.4	55	193.5568275	27.44797034	532.5769403	739.0638444	-12.93007657	751.993921	23.83291454	6.768437103	8.532238719
13	826.9	61.2	388.9679578	48.69908181	612.5648809	966.4527662	35.08007259	931.3726936	31.67122554	10.5362298	10.56749787
14	909	65	428.5038994	4.426986625	605.1482481	1036.781486	-3.129338596	1039.910825	33.5795156	9.981539191	11.7989882
15	956.7	70.4	617.7881008	-237.6696788	600.3804702	1455.882982	-237.7144108	1693.597393	44.8843686	6.452735463	19.21581657
16	1114.1	75.7	1181.190983	-634.8527072	708.4611451	2542.090411	-652.4382828	3194.528693	76.06328386	3.572055813	36.24561402
17	1161.3	82.3	1170.957618	-1031.709592	762.5101479	2975.58521	-1042.117444	4017.702654	86.32640036	-4.844544492	45.58547242

Table A- 4: Reduced data Specimen 2

Specimen 2

ID	Seconds Elapsed	Load	[1] e(1)	[1] e(2)	[1] e(3)	[1] e(max)	[1] e(min)	[1] Shear Strain	[1] s(max)	[1] s(min)	[1] Shear Stress
1	334.2	0.000000	-0.435965547	0.445549091	0.427490538	0.619218255	-0.627693264	1.246911519	0.01	-0.01	0.01
2	382.8	5.1	57.11471581	40.54656481	31.63526761	57.67752615	31.07245727	26.60506888	2.17	1.57	0.3
3	418.1	10	106.3867574	73.07526547	59.42462139	108.3614901	57.4498887	50.91160135	4.07	2.92	0.58
4	440.7	15.3	159.588476	106.497329	87.64305283	163.4538971	83.77763181	79.67626524	6.11	4.31	0.9
5	466.7	20	208.8704386	135.9105607	114.5802846	215.4753591	107.9753641	107.499995	8.04	5.6	1.22
6	500.1	25	260.774301	167.9996613	144.5122105	270.3144982	134.9720133	135.3424849	10.08	7	1.54
7	527.4	30	317.4820484	182.707842	177.0117186	342.631716	151.8620511	190.7696649	12.58	8.26	2.16
8	560.7	35	369.3969861	213.0169486	208.230301	399.4428172	178.18447	221.2583472	14.68	9.66	2.51
9	594.1	40	423.9351851	245.556675	241.5892538	458.9260678	206.598371	252.3276968	16.89	11.16	2.86
10	619.7	45	480.2247325	280.7732434	276.233552	519.2991696	237.1591148	282.1400548	19.14	12.74	3.2
11	646	50	538.2662081	315.9922485	313.8744683	583.248896	268.8917803	314.3571157	21.52	14.39	3.57
12	670.9	55	602.8614929	357.4557193	357.9349774	653.9266527	306.8698176	347.056835	24.18	16.31	3.94
13	701.9	60	672.7034516	404.719278	408.8445751	730.2898904	351.2581363	379.0317541	27.09	18.49	4.3
14	729.2	65	750.4138873	455.5547957	464.0380284	815.8090937	398.642822	417.1662716	30.32	20.86	4.73
15	762.5	70.6	848.6603401	521.1133518	532.5033197	922.3325158	458.831144	463.5013718	34.36	23.84	5.26
16	786.5	75.4	953.0406648	595.1556132	599.6938166	1029.450533	523.2839487	506.1665841	38.46	26.98	5.74
17	812.7	80.4	1069.238063	674.1161524	674.1700535	1151.097443	592.3106733	558.7867701	43.08	30.4	6.34
18	845.2	85.4	1202.067549	766.92159	757.2195923	1287.414698	671.8724428	615.5422554	48.27	34.3	6.98
19	876.4	90.2	1346.733777	867.7774427	842.4236247	1433.726151	755.4312505	678.2949008	53.82	38.43	7.7
20	896.3	92.9	1447.281326	938.7455221	898.0922311	1533.423077	811.9504802	721.4725972	57.61	41.23	8.19
21	908	94.6	1522.923644	990.5272157	939.2052528	1609.270676	852.8582212	756.4124544	60.46	43.3	8.58
22	921.7	96.3	1628.754279	1059.280012	994.0277657	1716.704972	906.0770724	810.6278995	64.46	46.07	9.2

ID	Seconds Elapsed	Load	[2] e(1)	[2] e(2)	[2] e(3)	[2] e(max)	[2] e(min)	[2] Shear Strain	[2] s(max)	[2] s(min)	[2] Shear Stress
1	334.2	0.00	3.540291	9.638807271	2.389068534	9.663583132	-3.734223457	13.39780659	0.28	-0.03	0.15
2	382.8	5.1	16.8166	18.40151767	22.09931263	22.30274607	16.61316891	5.68957716	0.88	0.76	0.06
3	418.1	10	27.4379	26.28808596	41.51166411	45.27013806	23.67942684	21.59071122	1.7	1.21	0.24
4	440.7	15.3	39.38713	34.61292946	63.3141124	71.92427816	30.77696086	41.1473173	2.63	1.7	0.47
5	466.7	20	51.77921	45.12871578	83.32540212	94.96777715	40.13683777	54.83093939	3.47	2.22	0.62
6	500.1	25	63.72901	55.64471927	106.324425	121.3157541	48.73768124	72.57807286	4.41	2.76	0.82
7	527.4	30	79.21991	68.35184658	134.4025655	154.1441642	59.47830774	94.66585644	5.58	3.43	1.07
8	560.7	35	93.38342	81.49748438	158.3000775	180.7958858	70.88761603	109.9082697	6.55	4.06	1.25
9	594.1	40	107.99	107.3515621	183.9911566	200.1848179	91.79630367	108.3885143	7.38	4.92	1.23
10	619.7	45	122.5969	111.7337392	210.8785608	237.2632859	96.21219987	141.051086	8.63	5.43	1.6
11	646	50	137.647	122.6893471	238.3649333	270.4819165	105.5299757	164.9519408	9.79	6.05	1.87
12	670.9	55	153.1401	136.2746282	269.4382754	306.202312	116.3760692	189.8262429	11.06	6.75	2.15
13	701.9	60	169.9618	155.1193279	302.9039996	341.4581377	131.4076328	210.0505049	12.35	7.58	2.38
14	729.2	65	185.8986	166.9524026	337.2684205	382.7579792	140.4090396	242.3489396	13.77	8.27	2.75
15	762.5	70.6	203.1641	173.0881793	377.313373	436.205301	144.27213	291.9331711	15.54	8.92	3.31
16	786.5	75.4	216.0029	180.100586	413.4760786	481.7021783	147.7767568	333.9254215	17.05	9.48	3.79
17	812.7	80.4	235.483	189.7428028	458.6083538	539.8938881	154.1974972	385.6963909	19	10.25	4.38
18	845.2	85.4	256.2922	197.1937318	509.4243208	607.5587091	158.1578359	449.4008733	21.23	11.04	5.1
19	876.4	90.2	278.8734	200.7000891	566.8225816	687.5711751	158.1247811	529.446394	23.83	11.81	6.01
20	896.3	92.9	295.6992	205.5213697	604.7927013	739.6847483	160.8071502	578.8775981	25.54	12.41	6.57
21	908	94.6	307.6547	206.397971	630.8053653	777.7544092	160.7056811	617.0487281	26.78	12.77	7
22	921.7	96.3	322.2674	201.5766821	665.191964	832.4813575	154.9780245	677.5033331	28.49	13.12	7.69

ID	Seconds Elapsed	Load	[3] e(1)	[3] e(2)	[3] e(3)	[3] e(max)	[3] e(min)	[3] Shear Strain	[3] s(max)	[3] s(min)	[3] Shear Stress
1	334.2	0.00	6.96716082	2.726942	3.632237073	8.3655605	2.233837393	6.131723108	0.29	0.15	0.07
2	382.8	5.1	-47.46124363	-9.3494	-39.54935168	-9.121078661	-77.88951665	68.76843799	-1.05	-2.61	0.78
3	418.1	10	-99.70703281	-20.6464	-83.93782836	-20.21099291	-163.4338683	143.2228753	-2.24	-5.49	1.63
4	440.7	15.3	-158.4771311	-33.5012	-131.9537395	-32.7168406	-257.71403	224.9971894	-3.57	-8.67	2.55
5	466.7	20	-212.8878339	-44.4081	-178.3513753	-43.42533151	-347.8138778	304.3885463	-4.79	-11.7	3.45
6	500.1	25	-272.0800667	-58.0415	-229.1822001	-56.8507355	-444.4115313	387.5607958	-6.16	-14.96	4.4
7	527.4	30	-331.2654101	-68.5583	-283.2348196	-67.35324867	-547.1469811	479.7937324	-7.5	-18.39	5.44
8	560.7	35	-393.0545209	-82.97	-338.4916494	-81.65713352	-649.8890368	568.2319032	-8.97	-21.86	6.45
9	594.1	40	-460.4918108	-98.9392	-396.9686331	-97.4132549	-760.047189	662.6339341	-10.55	-25.59	7.52
10	619.7	45	-527.0501706	-114.908	-456.6485696	-113.267822	-870.4309182	757.1630962	-12.14	-29.32	8.59
11	646	50	-604.9080419	-139.055	-525.1912281	-137.1940876	-992.9051825	855.7110949	-14.1	-33.52	9.71
12	670.9	55	-686.6677177	-162.032	-598.1588716	-159.9979573	-1124.828632	964.8306747	-16.13	-38.02	10.95
13	701.9	60	-774.501226	-188.124	-679.1770001	-186.019477	-1267.658749	1081.639272	-18.36	-42.9	12.27
14	729.2	65	-878.40345	-221.613	-770.2566329	-219.191905	-1429.468178	1210.276273	-21.01	-48.47	13.73
15	762.5	70.6	-1004.448759	-258.993	-882.6732035	-256.2905607	-1630.831402	1374.540841	-24.17	-55.36	15.6
16	786.5	75.4	-1133.938617	-292.477	-991.0370304	-289.1693102	-1835.806337	1546.637027	-27.23	-62.32	17.55
17	812.7	80.4	-1280.76973	-327.906	-1120.721055	-324.2450738	-2077.245711	1753.000638	-30.71	-70.49	19.89
18	845.2	85.4	-1462.295094	-368.003	-1276.539867	-363.7055303	-2375.12943	2011.4239	-34.89	-80.53	22.82
19	876.4	90.2	-1686.289596	-399.145	-1467.725218	-394.0861283	-2759.928686	2365.842557	-39.62	-93.3	26.84
20	896.3	92.9	-1851.183638	-406.151	-1605.736558	-400.4686741	-3056.451521	2655.982847	-42.71	-102.98	30.14
21	908	94.6	-1982.626575	-404.984	-1714.348919	-398.7646106	-3298.210883	2899.446273	-45	-110.8	32.9
22	921.7	96.3	-2173.006646	-391.36	-1871.192551	-384.392158	-3659.807039	3275.414881	-48.05	-122.38	37.16

ID	Seconds Elapsed	Load	[4] e(1)	[4] e(2)	[4] e(3)	[4] e(max)	[4] e(min)	[4] gamma	[4] s(max)	[4] s(min)	[4] tau
1	334.2	0.00	-1.680183449		1.817215	0	0	0	0	0	0
2	382.8	5.1	24.36328185		9.08614	0	0	0	0	0	0
3	418.1	10	51.24825344		17.71812	0	0	0	0	0	0
4	440.7	15.3	79.81508811		25.89593	0	0	0	0	0	0
5	466.7	20	107.1231165		34.07386	0	0	0	0	0	0
6	500.1	25	137.3737157		41.79758	0	0	0	0	0	0
7	527.4	30	163.8444612		47.70404	0	0	0	0	0	0
8	560.7	35	194.0984234		56.33668	0	0	0	0	0	0
9	594.1	40	225.6148749		65.42382	0	0	0	0	0	0
10	619.7	45	257.5535314		74.05676	0	0	0	0	0	0
11	646	50	292.0159029		84.96173	0	0	0	0	0	0
12	670.9	55	329.8431361		96.32132	0	0	0	0	0	0
13	701.9	60	371.8766838		109.0444	0	0	0	0	0	0
14	729.2	65	416.015635		122.6766	0	0	0	0	0	0
15	762.5	70.6	471.5100185		138.1268	0	0	0	0	0	0
16	786.5	75.4	531.6357435		151.3053	0	0	0	0	0	0
17	812.7	80.4	594.7122975		168.1198	0	0	0	0	0	0
18	845.2	85.4	665.7878868		185.8438	0	0	0	0	0	0
19	876.4	90.2	743.6038728		200.387	0	0	0	0	0	0
20	896.3	92.9	794.5061502		210.3857	0	0	0	0	0	0
21	908	94.6	830.2669832		216.7486	0	0	0	0	0	0
22	921.7	96.3	875.7078901		224.4751	0	0	0	0	0	0

ID	Seconds Elapsed	Load	[5] e(1)	[5] e(2)	[5] e(3)	[5] e(max)	[5] e(min)	[5] gamma	[5] s(max)	[5] s(min)	[5] tau
1	334.2	0.00	1.888384856	1.246180513	1.770065271	2.415263	1.243186815	1.172076497	0.09	0.06	0.01
2	382.8	5.1	36.63591323	38.63301112	50.0067118	51.48677	35.15585273	16.33091957	2.01	1.64	0.19
3	418.1	10	68.74171043	74.77621795	95.59232836	97.49226	66.84178313	30.65047254	3.81	3.11	0.35
4	440.7	15.3	102.360533	111.7529521	146.0510686	149.3512	99.0604401	50.29072149	5.8	4.66	0.57
5	466.7	20	134.092689	145.8237754	192.5306465	197.3642	129.2591333	68.10506886	7.66	6.11	0.77
6	500.1	25	167.3380158	183.6367422	242.5562639	248.1742	161.7200735	86.45413255	9.62	7.66	0.98
7	527.4	30	203.2302877	226.4394146	299.2283842	305.252	197.2066663	108.0453393	11.81	9.36	1.23
8	560.7	35	239.8807903	268.4144531	355.0211605	361.9292	232.9727168	128.9565172	14	11.07	1.46
9	594.1	40	278.0454503	312.4711767	413.0344146	420.7001	270.3797852	150.3202944	16.27	12.86	1.71
10	619.7	45	317.3466955	356.5317033	468.3967322	476.6847	309.0586793	167.6260691	18.46	14.65	1.9
11	646	50	359.2965548	404.3375195	530.8526464	540.0345	350.114699	189.9198032	20.91	16.6	2.15
12	670.9	55	405.78556	457.1369714	596.4174441	606.0682	396.134799	209.9334061	23.5	18.74	2.38
13	701.9	60	454.5468695	514.5157957	667.7508923	677.5045	444.7932474	232.7112671	26.29	21.01	2.64
14	729.2	65	505.2030833	575.2279499	742.1964409	751.727	495.6725015	256.0545213	29.19	23.38	2.91
15	762.5	70.6	562.2918541	645.9292824	833.9389473	843.6194	552.611357	291.0080874	32.72	26.12	3.3
16	786.5	75.4	606.1524633	695.0100817	928.8012192	944.3298	590.6238341	353.7060143	36.36	28.33	4.01
17	812.7	80.4	660.9835225	772.3843116	1024.124552	1037.212	647.8962806	389.3155135	39.92	31.09	4.42
18	845.2	85.4	717.7115031	863.9173543	1130.109551	1138.66	709.1613286	429.4983973	43.81	34.06	4.87
19	876.4	90.2	775.580535	967.9520929	1251.642478	1255.982	771.24087	484.7412729	48.22	37.22	5.5
20	896.3	92.9	810.7590328	1037.042868	1336.821499	1339.376	808.2044967	531.1715388	51.28	39.23	6.03
21	908	94.6	834.5910048	1084.496163	1398.05271	1399.845	832.7991103	567.0454939	53.48	40.61	6.43
22	921.7	96.3	865.2337454	1145.692446	1484.143801	1485.499	863.878218	621.6211101	56.56	42.45	7.05

ID	Seconds Elapsed	Load	[6] e(1)	[6] e(2)	[6] e(3)	[6] e(max)	[6] e(min)	[6] gamma	[6] s(max)	[6] s(min)	[6] tau
1	334.2	0.00	6.747876009	3.832398894	4.538246903	7.764172983	3.52195	4.242223053	0.29	0.19	0.05
2	382.8	5.1	-26.14717356	-13.79639749	-7.838694978	-7.296649189	-26.6892	19.39257016	-0.5	-0.94	0.22
3	418.1	10	-53.55808896	-24.90989061	-16.08982268	-13.62828567	-56.0196	42.39134031	-0.99	-1.95	0.48
4	440.7	15.3	-77.59413692	-35.25671817	-22.69062871	-18.91448159	-81.3703	62.45580245	-1.4	-2.82	0.71
5	466.7	20	-98.25579606	-43.68731128	-27.64117717	-22.72910105	-103.168	80.43877112	-1.74	-3.57	0.91
6	500.1	25	-117.6516914	-51.73456556	-33.82929515	-27.44108238	-124.04	96.59882179	-2.1	-4.29	1.1
7	527.4	30	-126.0844585	-39.85524078	-30.9415161	-17.21481247	-139.811	122.5963497	-1.92	-4.7	1.39
8	560.7	35	-144.6360538	-45.22013141	-34.65437187	-18.95164561	-160.339	141.3871345	-2.17	-5.38	1.6
9	594.1	40	-164.4517827	-52.5009641	-40.01733804	-22.58273459	-181.886	159.3036516	-2.5	-6.12	1.81
10	619.7	45	-182.1588018	-58.24891646	-42.90506569	-24.24520363	-200.819	176.5734602	-2.74	-6.75	2
11	646	50	-206.1887695	-67.44550543	-49.09299844	-28.68001335	-226.602	197.9217413	-3.13	-7.62	2.25
12	670.9	55	-226.4236507	-73.57647258	-54.04329058	-31.27521017	-249.192	217.916521	-3.44	-8.38	2.47
13	701.9	60	-250.8730574	-79.70736599	-59.40605283	-33.25879942	-277.02	243.7615114	-3.77	-9.3	2.77
14	729.2	65	-278.271857	-87.7540517	-65.59378535	-36.30813404	-307.558	271.2493742	-4.17	-10.32	3.08
15	762.5	70.6	-313.2558693	-99.24909666	-74.66899055	-41.64191207	-346.283	304.6410357	-4.72	-11.63	3.46
16	786.5	75.4	-349.9232732	-112.2765009	-73.43147208	-41.40564188	-381.949	340.5434615	-5.06	-12.78	3.86
17	812.7	80.4	-384.0595125	-120.3226726	-80.44403704	-43.64182504	-420.862	377.2198995	-5.51	-14.07	4.28
18	845.2	85.4	-423.6715332	-128.3687172	-89.10648414	-45.74087073	-467.037	421.2962758	-6.02	-15.59	4.78
19	876.4	90.2	-466.2299441	-137.1809061	-101.4811533	-49.81736621	-517.894	468.0763649	-6.65	-17.27	5.31
20	896.3	92.9	-494.4597948	-141.3953773	-109.3182884	-51.20655074	-552.572	501.3649818	-7.03	-18.41	5.69
21	908	94.6	-516.3684488	-145.9929426	-116.7428316	-53.84516792	-579.266	525.4209446	-7.38	-19.3	5.96
22	921.7	96.3	-544.5955142	-152.1229651	-128.2919062	-58.4125779	-614.475	556.0622646	-7.87	-20.49	6.31

ID	Seconds Elapsed	Load	[7] e(1)	[7] e(2)	[7] e(3)	[7] e(max)	[7] e(min)	[7] gamma	[7] s(max)	[7] s(min)	[7] tau
1	334.2	0.00	1.605325307	0.831878644	0	1.605856845	-0.000531538	1.606388	0.05	0.02	0.02
2	382.8	5.1	26.8898649	26.62079037	43.49992493	47.13176186	23.25802798	23.87373	1.75	1.21	0.27
3	418.1	10	47.76058721	46.17131917	78.38868587	85.88345599	40.26581709	45.61764	3.18	2.14	0.52
4	440.7	15.3	70.2377041	65.72259822	112.8490653	125.0194215	58.06734789	66.95207	4.62	3.1	0.76
5	466.7	20	89.90599332	83.61059585	143.4346033	159.2058358	74.13476083	85.07107	5.88	3.95	0.97
6	500.1	25	111.5821286	101.9152436	175.3144411	195.7975488	91.09902095	104.6985	7.23	4.86	1.19
7	527.4	30	134.062056	107.3235608	198.1485232	233.0534819	99.15709725	133.8964	8.52	5.48	1.52
8	560.7	35	155.3386135	123.1328172	226.5848476	267.5761414	114.3473197	153.2288	9.79	6.31	1.74
9	594.1	40	177.0175274	141.8549395	255.0227582	299.8156164	132.2246693	167.5909	11.01	7.2	1.9
10	619.7	45	199.5003366	160.99382	282.6004289	331.2471652	150.8536002	180.3936	12.21	8.11	2.05
11	646	50	221.181126	178.4690778	308.4558499	361.5678548	168.0691211	193.4987	13.36	8.96	2.2
12	670.9	55	246.4765442	200.1059418	336.0364108	392.8126815	189.7002734	203.1124	14.58	9.97	2.3
13	701.9	60	273.7809417	223.824329	362.3255216	422.1643346	213.9421287	208.2222	15.77	11.04	2.36
14	729.2	65	301.8899351	247.5438202	386.4609807	449.6540758	238.69684	210.9572	16.9	12.11	2.39
15	762.5	70.6	338.8355373	277.9230267	412.7526914	480.4109687	271.17726	209.2337	18.21	13.46	2.37
16	786.5	75.4	379.3984618	314.1307479	442.4941294	512.7722063	309.1203849	203.6518	19.63	15.01	2.31
17	812.7	80.4	424.3828989	345.3463655	462.7537833	543.6464989	343.4901833	200.1563	20.96	16.42	2.27
18	845.2	85.4	473.7900166	373.2339344	474.823747	575.3811508	373.2326128	202.1485	22.28	17.7	2.29
19	876.4	90.2	529.6298306	394.8790694	476.1169743	614.1329297	391.6138752	222.5191	23.72	18.67	2.52
20	896.3	92.9	567.7972452	405.7019817	473.0994489	644.5799164	396.3167777	248.2631	24.75	19.12	2.82
21	908	94.6	594.7170319	409.448428	467.9265899	668.6974837	393.946138	274.7513	25.51	19.27	3.12
22	921.7	96.3	629.6746934	410.2809753	454.5636135	700.3824713	383.8558356	316.5266	26.44	19.26	3.59

ID	Seconds Elapsed	Load	[8] e(1)	[8] e(2)	[8] e(3)	[8] e(max)	[8] e(min)	[8] gamma	[8] s(max)	[8] s(min)	[8] tau
1	334.2	0.00	2.408706983	4.381814288	1.822059303	4.400716599	-0.169950314	4.570666913	0.14	0.04	0.05
2	382.8	5.1	26.49640242	15.93405062	34.16469589	45.22886621	15.4322321	29.79663411	1.62	0.94	0.34
3	418.1	10	47.77481294	27.08818231	66.5093849	88.62199647	25.66220137	62.9597951	3.12	1.69	0.71
4	440.7	15.3	70.66013191	39.43768413	102.9565643	136.8557726	36.76092369	100.0948489	4.79	2.52	1.14
5	466.7	20	92.34190753	52.58425664	137.5837989	181.316425	48.60928141	132.7071436	6.35	3.34	1.51
6	500.1	25	116.4338502	66.52796148	176.7700855	232.1704306	61.03350511	171.1369255	8.12	4.24	1.94
7	527.4	30	142.9363014	81.6672727	226.4407544	295.848896	73.5281598	222.3207362	10.31	5.26	2.52
8	560.7	35	168.6369629	96.40861285	268.3683883	350.3872822	86.61806902	263.7692131	12.2	6.22	2.99
9	594.1	40	196.748544	112.3456762	316.224793	412.5163746	100.4569624	312.0594122	14.35	7.27	3.54
10	619.7	45	226.0665573	129.0801286	363.1740122	473.793823	115.4467465	358.3470765	16.48	8.35	4.07
11	646	50	256.5912106	145.4166714	412.862846	539.5284375	129.9256191	409.6028184	18.75	9.46	4.65
12	670.9	55	292.3395078	165.3399929	468.9395477	613.3427362	147.9363193	465.4064169	21.32	10.76	5.28
13	701.9	60	332.9108345	187.2565454	530.0382586	694.8321691	168.1169239	526.7152452	24.16	12.21	5.98
14	729.2	65	378.7080889	210.3695665	594.7926438	783.4985428	190.0021899	593.4963529	27.25	13.78	6.73
15	762.5	70.6	435.7595412	240.6571796	674.1507786	891.0962253	218.8140945	672.2821308	31.02	15.76	7.63
16	786.5	75.4	490.0045132	269.7509226	747.1346754	990.3268346	246.812354	743.5144806	34.5	17.63	8.44
17	812.7	80.4	569.9761357	309.2094722	846.5920459	1130.64607	285.9221114	844.7239587	39.43	20.26	9.58
18	845.2	85.4	676.4904681	362.6228762	969.3436996	1305.940387	339.8937808	966.046606	45.64	23.72	10.96
19	876.4	90.2	818.0080369	431.1915627	1130.928072	1539.825538	409.1105715	1130.714966	53.9	28.24	12.83
20	896.3	92.9	929.4003054	485.4151891	1256.031344	1721.592618	463.8390318	1257.753586	60.32	31.78	14.27
21	908	94.6	1019.497029	527.282961	1355.13125	1868.345519	506.2827606	1362.062758	65.49	34.58	15.45
22	921.7	96.3	1157.086093	591.486885	1506.786792	2092.750606	571.1222789	1521.628327	73.4	38.87	17.26

ID	Seconds Elapsed	Load	[9] e(1)	[9] e(2)	[9] e(3)	[9] e(max)	[9] e(min)	[9] gamma	[9] s(max)	[9] s(min)	[9] tau
1	334.2	0.00	-0.40514152	0	-0.830623269	0.035598541	-1.271363331	1.306961871	-0.01	-0.04	0.01
2	382.8	5.1	26.33488952	13.6659605	19.10470857	32.46868982	12.97090827	19.49778155	1.18	0.74	0.22
3	418.1	10	54.29187632	27.33228774	39.4561636	67.77626604	25.97177388	41.80449216	2.45	1.5	0.47
4	440.7	15.3	83.87122719	41.43984891	60.63915276	105.1872043	39.32317569	65.86402857	3.79	2.3	0.75
5	466.7	20	111.0209091	55.10692147	80.16151002	138.9161816	52.26623745	86.64994418	5.01	3.05	0.98
6	500.1	25	141.8193134	67.89257946	100.9307955	178.6318694	64.11823954	114.5136299	6.41	3.82	1.3
7	527.4	30	169.7826341	82.00126422	120.454695	212.8838298	77.35349935	135.5303304	7.65	4.58	1.54
8	560.7	35	200.9898898	96.99217004	143.7181893	252.9730403	91.73503874	161.2380016	9.09	5.43	1.83
9	594.1	40	236.2523343	111.5425888	168.6445391	299.4359445	105.4609289	193.9750155	10.73	6.33	2.2
10	619.7	45	273.5440092	127.4162471	195.2339883	348.3024942	120.4755033	227.8269908	12.46	7.29	2.58
11	646	50	313.2707501	142.4084897	223.0713029	401.7756699	134.5663832	267.2092867	14.33	8.27	3.03
12	670.9	55	358.2711032	157.4011736	255.0653168	464.6033446	148.7330754	315.8702692	16.51	9.34	3.58
13	701.9	60	410.5738007	176.8041256	291.216812	534.9313406	166.8592721	368.0720685	18.96	10.61	4.18
14	729.2	65	466.9369756	193.1208164	332.3578367	616.8595569	182.4352554	434.4243015	21.77	11.91	4.93
15	762.5	70.6	539.9345171	215.171229	386.8020705	723.1069499	203.6296376	519.4773123	25.42	13.63	5.89
16	786.5	75.4	621.8664233	239.8688244	443.3304757	838.6366899	226.5602092	612.0764807	29.39	15.5	6.94
17	812.7	80.4	715.1712537	271.1835688	518.9885825	976.6160005	257.5438357	719.0721647	34.16	17.85	8.16
18	845.2	85.4	830.0001856	309.9988815	618.7746673	1152.022693	296.7521602	855.2705326	40.23	20.82	9.7
19	876.4	90.2	976.9215215	361.6101846	751.853139	1379.604568	349.1700924	1030.434476	48.12	24.74	11.69
20	896.3	92.9	1089.77934	400.8735665	856.2608537	1556.958769	389.0814247	1167.877344	54.26	27.75	13.25
21	908	94.6	1180.733298	433.080622	943.2142525	1701.981917	421.9656329	1280.016284	59.28	30.23	14.52
22	921.7	96.3	1315.976068	481.6156471	1077.209728	1921.468618	471.7171773	1449.751441	66.88	33.98	16.45

ID	Seconds Elapsed	Load	[10] e(1)	[10] e(2)	[10] e(3)	[10] e(max)	[10] e(min)	[10] gamma	[10] s(max)	[10] s(min)	[10] tau
1	334.2	0.00	28.70179656	2.06119922	2.503801431	34.44314563	-3.237547644	37.68069328	1.09	0.23	0.43
2	382.8	5.1	58.67157556	16.90207964	22.95197299	70.65546705	10.9680815	59.68738556	2.4	1.04	0.68
3	418.1	10	87.37667975	31.74339215	42.98362948	105.3137168	25.04659245	80.26712432	3.66	1.84	0.91
4	440.7	15.3	116.9277422	48.64652434	64.26812615	140.127517	41.06835134	99.05916561	4.94	2.69	1.12
5	466.7	20	140.992017	63.9010516	85.13614163	169.6058603	56.52229835	113.0835619	6.05	3.48	1.28
6	500.1	25	165.9018502	80.80525012	106.839783	199.2962814	73.4453518	125.8509296	7.17	4.32	1.43
7	527.4	30	193.3462975	101.8332062	133.135816	231.6314773	94.85063614	136.7808412	8.43	5.33	1.55
8	560.7	35	217.8364378	119.9756692	156.093778	260.7256929	113.2045228	147.5211701	9.55	6.21	1.67
9	594.1	40	242.3277558	136.8817271	179.4702187	291.3124332	130.4855413	160.8268918	10.71	7.06	1.82
10	619.7	45	263.4419064	153.7883458	204.1001271	319.079805	148.4622285	170.6175765	11.79	7.92	1.94
11	646	50	285.8238619	171.5202798	228.7312242	347.6611727	166.8939134	180.7672593	12.89	8.79	2.05
12	670.9	55	304.8281811	190.4900084	256.2860636	373.8371808	187.2770639	186.5601169	13.94	9.71	2.12
13	701.9	60	325.1002366	209.8728513	285.5125189	402.7710114	207.8417441	194.9292673	15.08	10.65	2.21
14	729.2	65	341.9942326	228.4315829	314.7406479	429.2280621	227.5068184	201.7212437	16.13	11.55	2.29
15	762.5	70.6	356.3545698	249.4656288	351.9045431	458.8171318	249.4419811	209.3751507	17.3	12.55	2.38
16	786.5	75.4	347.0625407	252.3527224	388.6535271	485.2204193	250.4956485	234.7247708	18.17	12.84	2.66
17	812.7	80.4	347.9072636	272.5628355	426.6581	508.571868	265.9934956	242.5783723	19.07	13.57	2.75
18	845.2	85.4	341.9942326	292.7737497	468.8423128	534.6908429	276.1457025	258.5451404	20.02	14.15	2.93
19	876.4	90.2	326.789611	312.985465	515.2072013	564.3235348	277.6732774	286.6502574	20.99	14.49	3.25
20	896.3	92.9	310.3184498	323.2978733	546.5372126	586.5484624	270.3072	316.2412624	21.64	14.47	3.59
21	908	94.6	293.003188	327.4228951	569.0960114	603.6627674	258.4364319	345.2263355	22.08	14.25	3.92
22	921.7	96.3	267.6648416	328.2479034	597.9225937	628.2351998	237.3522355	390.8829644	22.67	13.8	4.44

ID	Seconds Elapsed	Load	[11] e(1)	[11] e(2)	[11] e(3)	[11] e(max)	[11] e(min)	[11] gamma	[11] s(max)	[11] s(min)	[11] tau
1	334.2	0.00	2.311317886	2.888722504	3.324288629	3.329229666	2.306376849	1.022852817	0.13	0.11	0.01
2	382.8	5.1	-5.084862359	-1.238018915	-19.11423839	0.830210393	-25.02931114	25.85952154	-0.22	-0.8	0.29
3	418.1	10	-9.245166459	-7.01540073	-40.30527254	-1.18298116	-48.36745784	47.18447667	-0.51	-1.58	0.54
4	440.7	15.3	-11.5564318	-17.33199097	-62.74187671	-4.780845641	-69.51746287	64.73661723	-0.83	-2.3	0.73
5	466.7	20	-12.01868361	-26.82306944	-84.34656101	-6.181896602	-90.18334802	84.00145141	-1.08	-2.98	0.95
6	500.1	25	-12.94318597	-37.13925848	-105.1194313	-8.008010924	-110.0546063	102.0465954	-1.33	-3.65	1.16
7	527.4	30	-5.547120051	-48.28050794	-130.4611851	-2.506800967	-133.5015042	130.9947033	-1.38	-4.35	1.49
8	560.7	35	-6.933890607	-60.24676368	-152.0629957	-4.423537592	-154.5733487	150.1498111	-1.65	-5.05	1.7
9	594.1	40	-10.16967386	-71.80012315	-175.3254588	-7.554235037	-177.9408976	170.3866626	-1.98	-5.84	1.93
10	619.7	45	-12.480935	-83.35322052	-197.3407393	-10.00026007	-199.8214143	189.8211542	-2.27	-6.57	2.15
11	646	50	-16.17893097	-95.31865224	-222.2625494	-13.44302869	-224.9984517	211.555423	-2.62	-7.42	2.4
12	670.9	55	-20.8013881	-107.2838028	-247.5984722	-17.65076781	-250.7490925	233.0983246	-3.01	-8.3	2.64
13	701.9	60	-24.03708308	-118.4235179	-273.3484457	-20.41468305	-276.9708457	256.5561626	-3.36	-9.18	2.91
14	729.2	65	-29.12170502	-131.2132607	-302.4194307	-24.81979921	-306.7213365	281.9015373	-3.79	-10.18	3.2
15	762.5	70.6	-33.28181241	-141.1147765	-333.9803346	-27.38595898	-339.876188	312.490229	-4.19	-11.28	3.55
16	786.5	75.4	-30.04617627	-126.6750017	-354.7430198	-17.24872917	-367.5404669	350.2917377	-4.13	-12.08	3.97
17	812.7	80.4	-36.05519843	-134.5137874	-388.79199	-19.61345699	-405.2337314	385.6202745	-4.58	-13.33	4.38
18	845.2	85.4	-44.83748765	-144.4152389	-429.4816738	-23.64306991	-450.6760916	427.0330216	-5.15	-14.84	4.85
19	876.4	90.2	-56.39290022	-154.316498	-474.3195982	-28.72255014	-501.9899482	473.2673981	-5.81	-16.55	5.37
20	896.3	92.9	-64.71263462	-157.6168749	-504.2093531	-30.7312718	-538.1907159	507.4594441	-6.23	-17.75	5.76
21	908	94.6	-70.72124701	-158.4419658	-524.5499879	-31.43080132	-563.8404335	532.4096322	-6.5	-18.58	6.04
22	921.7	96.3	-81.35169494	-159.2670554	-553.191544	-33.32857407	-601.2146649	567.8860908	-6.93	-19.81	6.44

ID	Seconds Elapsed	Load	[12] e(1)	[12] e(2)	[12] e(3)	[12] e(max)	[12] e(min)	[12] gamma	[12] s(max)	[12] s(min)	[12] tau
1	334.2	0.00	1.773617335		2.435703417	0	0	0	0	0	0
2	382.8	5.1	26.16148267		33.12656553	0	0	0	0	0	0
3	418.1	10	47.44639315		58.94729607	0	0	0	0	0	0
4	440.7	15.3	70.50605099		83.307677	0	0	0	0	0	0
5	466.7	20	92.23630034		105.7202575	0	0	0	0	0	0
6	500.1	25	114.4109808		129.595614	0	0	0	0	0	0
7	527.4	30	139.2477702		145.1882881	0	0	0	0	0	0
8	560.7	35	160.5374117		165.1671002	0	0	0	0	0	0
9	594.1	40	182.7150687		188.0706059	0	0	0	0	0	0
10	619.7	45	205.3372747		211.9498264	0	0	0	0	0	0
11	646	50	226.6296813		231.9312596	0	0	0	0	0	0
12	670.9	55	249.6974605		255.8125383	0	0	0	0	0	0
13	701.9	60	275.4281401		277.2579067	0	0	0	0	0	0
14	729.2	65	298.4981313		298.7041789	0	0	0	0	0	0
15	762.5	70.6	326.8934022		323.0760397	0	0	0	0	0	0
16	786.5	75.4	355.7339709		353.786246	0	0	0	0	0	0
17	812.7	80.4	385.9073919		376.6982418	0	0	0	0	0	0
18	845.2	85.4	415.19507		397.1736638	0	0	0	0	0	0
19	876.4	90.2	448.0347738		414.2371448	0	0	0	0	0	0
20	896.3	92.9	470.2249623		424.9630541	0	0	0	0	0	0
21	908	94.6	484.8710167		428.8634408	0	0	0	0	0	0
22	921.7	96.3	503.0682167		431.7887505	0	0	0	0	0	0

ID	Seconds Elapsed	Load	[13] e(1)	[13] e(2)	[13] e(3)	[13] e(max)	[13] e(min)	[13] gamma	[13] s(max)	[13] s(min)	[13] tau
1	334.2	0.00	0.396769815	26.46266024	-0.532166492	26.46672565	-26.60212233	53.06884799	0.6	-0.6	0.6
2	382.8	5.1	35.71052154	48.11495266	48.42948503	50.84407993	33.29592664	17.5481533	1.97	1.57	0.2
3	418.1	10	71.02672225	74.58011844	93.66998868	96.07879191	68.61791902	27.46087289	3.78	3.16	0.31
4	440.7	15.3	106.7422249	102.4903317	142.1084062	152.6003969	96.25023417	56.35016272	5.88	4.6	0.64
5	466.7	20	141.6664716	125.5895984	189.4867114	212.1668635	118.9863195	93.18054407	8.04	5.92	1.06
6	500.1	25	180.5622016	158.3153567	241.6611933	272.1094457	150.1139492	121.9954965	10.28	7.51	1.38
7	527.4	30	221.0486672	187.67408	302.360701	346.1643908	177.2449774	168.9194134	12.95	9.11	1.92
8	560.7	35	262.7292731	215.5905044	357.7420171	416.1344555	204.3368347	211.7976208	15.48	10.67	2.4
9	594.1	40	308.7803843	246.3966142	418.9880015	493.6522971	234.1160887	259.5362084	18.28	12.39	2.94
10	619.7	45	357.61499	281.0557195	481.8393821	571.67356	267.7808122	303.8927478	21.14	14.24	3.45
11	646	50	411.6164272	317.1614672	550.5586859	659.1268797	303.0482335	356.0786462	24.31	16.23	4.04
12	670.9	55	471.5806122	362.8990959	630.4765401	755.2458141	346.8113382	408.4344759	27.86	18.59	4.63
13	701.9	60	540.289977	417.7896827	724.2628489	865.6560647	398.8967613	466.7593034	31.94	21.35	5.3
14	729.2	65	617.3508079	481.8361917	831.9252875	990.0872764	459.1888189	530.8984574	36.56	24.51	6.02
15	762.5	70.6	717.4678484	567.5651982	971.067461	1148.639861	539.895448	608.7444134	42.49	28.67	6.91
16	786.5	75.4	817.2071556	660.0531422	1114.514392	1305.884605	625.8369428	680.0476617	48.42	32.99	7.72
17	812.7	80.4	955.1259207	783.3965729	1316.68862	1532.070984	739.7435565	792.3274276	56.86	38.88	8.99
18	845.2	85.4	1139.208229	945.8122568	1592.607401	1843.268245	888.547385	954.7208604	68.4	46.73	10.83
19	876.4	90.2	1384.622131	1146.855404	1960.553991	2272.020461	1073.155661	1198.864801	84.09	56.89	13.6
20	896.3	92.9	1575.625525	1293.46932	2244.305505	2611.28626	1208.64477	1402.64149	96.41	64.58	15.91
21	908	94.6	1728.877878	1406.352232	2469.923338	2885.277917	1313.523299	1571.754617	106.31	70.64	17.83
22	921.7	96.3	1960.63511	1565.588651	2806.397209	3304.295064	1462.737255	1841.557809	121.34	79.55	20.89

ID	Seconds Elapsed	Load	[14] e(1)	[14] e(2)	[14] e(3)	[14] e(max)	[14] e(min)	[14] gamma	[14] s(max)	[14] s(min)	[14] tau
1	334.2	0.00	12.0944368	2.606848065	2.189784639	13.85732784	0.426893602	13.43043424	0.45	0.15	0.15
2	382.8	5.1	44.75085155	25.20009044	36.35164418	56.46648287	24.63601286	31.83047002	2.07	1.35	0.36
3	418.1	10	78.2157708	46.05628102	71.82984689	104.1647844	45.88083328	58.28395114	3.82	2.5	0.66
4	440.7	15.3	113.6990518	69.52051668	108.1866184	152.4567508	69.42891944	83.02783136	5.62	3.73	0.94
5	466.7	20	147.1685038	89.94397238	143.2317461	200.491326	89.90892392	110.5824021	7.37	4.86	1.25
6	500.1	25	184.2697448	113.4102307	180.9079478	251.7878801	113.3898126	138.3980675	9.27	6.12	1.57
7	527.4	30	219.7604184	137.3121612	218.5869365	301.0372964	137.3100585	163.7272379	11.09	7.38	1.86
8	560.7	35	259.6903834	161.2152137	261.9650374	360.4466996	161.2087212	199.2379784	13.25	8.73	2.26
9	594.1	40	304.0606842	187.2925508	308.4143719	425.2024231	187.272633	237.9297901	15.61	10.21	2.7
10	619.7	45	351.2587931	216.4138222	358.3740436	493.2647312	216.3681056	276.8966256	18.09	11.81	3.14
11	646	50	405.7235861	245.5367591	415.3515787	575.6086163	245.4665485	330.1420678	21.05	13.56	3.75
12	670.9	55	468.6679359	280.3125969	480.6644375	669.1123152	280.2200582	388.8922569	24.42	15.59	4.41
13	701.9	60	544.5342857	320.3077463	558.261735	782.5901832	320.2058374	462.3843458	28.48	17.99	5.25
14	729.2	65	633.7320539	366.3930087	650.7801702	918.2508788	366.2613453	551.9895335	33.33	20.8	6.26
15	762.5	70.6	755.6474788	429.0060843	771.8249055	1098.564017	428.9083672	669.6556498	39.78	24.59	7.6
16	786.5	75.4	894.957436	491.626858	899.4793004	1302.81618	491.6205565	811.1956235	47.02	28.61	9.2
17	812.7	80.4	1072.683392	582.9626218	1069.734904	1559.457901	582.9603962	976.4975046	56.22	34.06	11.08
18	845.2	85.4	1311.49925	704.7691199	1298.001716	1904.769801	704.7311652	1200.038636	68.6	41.37	13.62
19	876.4	90.2	1625.24135	863.1611172	1594.901412	2357.135682	863.00708	1494.128602	84.81	50.9	16.95
20	896.3	92.9	1868.362492	982.4227474	1822.084875	2708.334835	982.1125322	1726.222302	97.35	58.18	19.59
21	908	94.6	2067.071649	1076.458893	2005.839112	2996.939952	1075.970809	1920.969142	107.62	64.03	21.8
22	921.7	96.3	2363.458021	1214.061557	2282.034512	3432.178207	1213.314326	2218.863881	123.06	72.71	25.18

ID	Seconds Elapsed	Load	[15] e(1)	[15] e(2)	[15] e(3)	[15] e(max)	[15] e(min)	[15] gamma	[15] s(max)	[15] s(min)	[15] tau
1	334.2	0.00	2.107516917	1.801859348	1.416052299	2.109831752	1.413737464	0.696094288	0.08	0.07	0.01
2	382.8	5.1	15.0538833	13.21378322	18.76301259	21.04244812	12.77444777	8.26800035	0.81	0.62	0.09
3	418.1	10	27.69948861	25.82725964	37.17267808	40.56700459	24.3051621	16.26184249	1.55	1.18	0.18
4	440.7	15.3	42.45309102	39.94271069	55.93706057	60.64324677	37.74690482	22.89634195	2.33	1.81	0.26
5	466.7	20	54.79826992	52.55684891	72.57775188	77.93337022	49.44265159	28.49071863	3.01	2.36	0.32
6	500.1	25	68.95042792	66.37269198	90.28121201	96.61967324	62.61196669	34.00770655	3.74	2.97	0.39
7	527.4	30	86.41533432	83.49284338	111.5261767	118.900742	79.04076894	39.8599731	4.62	3.72	0.45
8	560.7	35	100.8695021	98.51099371	129.230991	136.8364899	93.26400327	43.57248661	5.34	4.35	0.49
9	594.1	40	115.0229383	113.5295867	146.9364209	154.6254686	107.3338907	47.29157787	6.06	4.98	0.54
10	619.7	45	128.5744686	128.2482374	164.9965937	172.7715669	120.7994953	51.97207159	6.78	5.6	0.59
11	646	50	142.427516	143.267707	183.0574069	190.8842999	134.6006231	56.28367683	7.5	6.22	0.64
12	670.9	55	157.1844369	159.1888282	202.1813192	210.116181	149.249575	60.866606	8.26	6.88	0.69
13	701.9	60	172.5441344	176.6125121	222.7226175	230.3648097	164.9019421	65.46286758	9.07	7.59	0.74
14	729.2	65	185.4948269	192.2342525	241.8480194	249.0758418	178.2670045	70.80883732	9.81	8.2	0.8
15	762.5	70.6	199.9518022	210.2599327	264.8702891	271.7083011	193.1137901	78.59451101	10.69	8.9	0.89
16	786.5	75.4	201.1565686	222.8782882	286.1225387	290.9241618	196.3549456	94.56921617	11.34	9.19	1.07
17	812.7	80.4	211.6983962	240.9050525	307.7299017	311.282498	208.1458	103.136698	12.12	9.77	1.17
18	845.2	85.4	219.5296092	258.6319926	329.6924232	331.9633534	217.2586789	114.7046745	12.87	10.27	1.3
19	876.4	90.2	225.8549074	277.56144	351.6558917	352.6441829	224.8666162	127.7775667	13.62	10.72	1.45
20	896.3	92.9	225.8549074	287.4771455	365.4721072	365.9504701	225.3765445	140.5739255	14.06	10.87	1.59
21	908	94.6	223.1440557	292.5853115	375.037399	375.3155092	222.8659455	152.4495637	14.33	10.87	1.73
22	921.7	96.3	216.216389	297.3930439	385.6657117	385.7399689	216.1421318	169.5978371	14.61	10.76	1.92

APPENDIX C

COUPON TEST RESULTS

Table A- 5: HSS Coupon Results Specimen 1

Sample 1 P1		
Area =	0.65	in^2
Load (lbs.)	Stress (psi)	Strain
500	763.94	2.10E-05
1000	1527.88	6.00E-05
1500	2291.83	8.20E-05
2000	3055.77	1.13E-04
2500	3819.71	1.36E-04
3000	4583.65	1.63E-04
3500	5347.59	1.83E-04
4000	6111.54	2.11E-04
4500	6875.48	2.33E-04
5000	7639.42	2.57E-04
5500	8403.36	2.81E-04
6000	9167.30	3.05E-04
6500	9931.25	3.32E-04
7000	10695.19	3.60E-04
7600	11611.92	3.82E-04
8000	12223.07	4.34E-04
9000	13750.95	4.83E-04
10000	15278.84	5.38E-04
11000	16806.72	5.97E-04
12000	18334.61	6.51E-04
13000	19862.49	7.03E-04
14000	21390.37	7.67E-04
15000	22918.26	8.25E-04
16000	24446.14	8.89E-04
17000	25974.03	9.51E-04
18000	27501.91	1.02E-03
19000	29029.79	1.09E-03
20000	30557.68	1.17E-03
21000	32085.56	1.25E-03
22000	33613.45	1.34E-03
23000	35141.33	1.42E-03
24000	36669.21	1.54E-03
25000	38197.10	1.67E-03
26000	39724.98	1.82E-03
27000	41252.86	2.03E-03
28000	42780.75	2.32E-03
29000	44308.63	2.86E-03
30000	45836.52	4.47E-03
30600	46753.25	4.99E-03
31000	47364.40	5.55E-03
31600	48281.13	5.41E-03
31800	48586.71	5.67E-03
31900	48739.50	5.90E-03
32000	48892.28	6.14E-03
32200	49197.86	6.45E-03
32300	49350.65	6.60E-03
32400	49503.44	7.12E-03
32600	49809.01	7.59E-03

Sample 2 P1		
Area =	0.79	in^2
Load (lbs.)	Stress (psi)	Strain
500	631.67	2.10E-05
1000	1263.34	4.20E-05
1500	1895.01	6.30E-05
2000	2526.68	8.60E-05
2500	3158.34	1.11E-04
3000	3790.01	1.34E-04
3500	4421.68	1.53E-04
4000	5053.35	1.79E-04
4500	5685.02	2.00E-04
5000	6316.69	2.24E-04
5500	6948.36	2.48E-04
6000	7580.03	2.71E-04
6500	8211.69	2.95E-04
7000	8843.36	3.20E-04
7500	9475.03	3.47E-04
8000	10106.70	3.70E-04
8500	10738.37	3.96E-04
9000	11370.04	4.22E-04
9500	12001.71	4.52E-04
10000	12633.38	4.77E-04
11000	13896.71	5.06E-04
12000	15160.05	5.35E-04
13000	16423.39	5.88E-04
14000	17686.73	6.47E-04
15000	18950.07	7.13E-04
16000	20213.40	7.75E-04
17000	21476.74	8.47E-04
18000	22740.08	9.16E-04
19000	24003.42	9.87E-04
20000	25266.75	1.07E-03
21000	26530.09	1.16E-03
22000	27793.43	1.25E-03
23000	29056.77	1.37E-03
24000	30320.10	1.48E-03
25000	31583.44	1.60E-03
26000	32846.78	1.76E-03
27000	34110.12	1.95E-03
28000	35373.46	2.19E-03
29000	36636.79	2.48E-03
30000	37900.13	2.87E-03
31000	39163.47	3.35E-03
32000	40426.81	4.11E-03
32300	40805.81	5.02E-03
32500	41058.47	6.51E-03
32700	41311.14	7.00E-03
32800	41437.48	7.52E-03
33200	41942.81	8.02E-03
33500	42321.81	9.02E-03

32700	49961.80	9.27E-03
32900	50267.38	1.00E-02
33200	50725.74	1.20E-02
33800	51642.48	1.40E-02
34100	52100.84	
34700	53017.57	
34900	53323.15	
42800		

E =	**2.21E+07**

34100	43079.82	1.00E-02
34600	43711.48	1.20E-02
42200		1.40E-02

Table A- 6: HSS Coupon Results Specimen 2

Sample 3 P2		
Area =	0.617733	in^2
Load (lbs.)	Stress (psi)	Strain
500	809.4111857	1.50E-05
1000	1618.822371	3.50E-05
1500	2428.233557	5.20E-05
2000	3237.644743	7.00E-05
2500	4047.055929	9.30E-05
3000	4856.467114	1.13E-04
3500	5665.8783	1.38E-04
4000	6475.289486	1.61E-04
4500	7284.700672	1.86E-04
5000	8094.111857	2.07E-04
5500	8903.523043	2.30E-04
6000	9712.934229	2.52E-04
6500	10522.34541	2.82E-04
7000	11331.7566	3.09E-04
7500	12141.16779	3.36E-04
8000	12950.57897	3.59E-04
9000	14569.40134	4.15E-04
10000	16188.22371	4.78E-04
11000	17807.04609	5.31E-04
12000	19425.86846	5.95E-04
13000	21044.69083	6.62E-04
14000	22663.5132	7.27E-04
15000	24282.33557	7.96E-04
16000	25901.15794	8.64E-04
17000	27519.98032	9.42E-04
18000	29138.80269	1.03E-03
19000	30757.62506	1.10E-03
20000	32376.44743	1.18E-03
21000	33995.2698	1.27E-03
22000	35614.09217	1.37E-03
23000	37232.91454	1.47E-03
24000	38851.73692	1.59E-03
25000	40470.55929	1.73E-03
26000	42089.38166	1.89E-03
27000	43708.20403	2.16E-03
28000	45327.0264	2.74E-03
29000	46945.84877	3.54E-03
30000	48564.67114	4.95E-03
30500	49374.08233	6.02E-03
30700	49697.8468	6.52E-03
30900	50021.61128	7.01E-03
31100	50345.37575	7.55E-03
31300	50669.14023	8.04E-03
31600	51154.78694	9.01E-03
31900	51640.43365	1.00E-02
32500	52611.72707	1.22E-02
33000	53421.13826	1.40E-02
33600	54392.43168	1.60E-02
34000	55039.96063	1.81E-02
34400	55687.48958	2.00E-02
40600		

E =	2.10E+07

Sample 4 P2		
Area =	0.6285	in^2
Load (lbs.)	Stress (psi)	Strain
0	0	-1.30E-04
500	795.5449483	-8.00E-05
1000	1591.089897	-5.50E-05
1500	2386.634845	-3.10E-05
2000	3182.179793	-7.00E-06
2510	3993.63564	1.80E-05
3000	4773.26969	4.10E-05
3510	5584.725537	6.60E-05
4000	6364.359586	8.90E-05
4500	7159.904535	1.14E-04
5000	7955.449483	1.39E-04
5520	8782.816229	1.65E-04
6000	9546.539379	1.89E-04
6520	10373.90613	2.15E-04
7000	11137.62928	2.41E-04
7520	11964.99602	2.68E-04
7960	12665.07558	2.89E-04
8540	13587.90772	3.22E-04
9520	15147.17582	3.76E-04
10000	15910.89897	4.04E-04
10500	16706.44391	4.32E-04
11000	17501.98886	4.60E-04
11500	18297.53381	4.90E-04
12000	19093.07876	5.18E-04
13000	20684.16866	5.80E-04
14040	22338.90215	6.40E-04
15020	23898.17025	7.03E-04
16000	25457.43835	7.71E-04
17000	27048.52824	8.40E-04
18120	28830.54893	9.21E-04
19000	30230.70804	9.91E-04
20000	31821.79793	1.08E-03
21000	33412.88783	1.17E-03
22000	35003.97772	1.26E-03
23000	36595.06762	1.40E-03
24000	38186.15752	1.55E-03
25020	39809.06921	1.73E-03
26000	41368.33731	1.98E-03
27000	42959.42721	2.31E-03
28000	44550.5171	2.78E-03
29000	46141.607	3.63E-03
30000	47732.6969	5.05E-03
30260	48146.38027	5.51E-03
30470	48480.50915	6.01E-03
30690	48830.54893	6.51E-03
30920	49196.4996	7.02E-03
31140	49546.53938	7.60E-03
31330	49848.84646	8.22E-03
31600	50278.44073	9.01E-03
31800	50596.65871	9.63E-03
32040	50978.52029	1.05E-02
32330	51439.93636	1.15E-02
32600	51869.53063	1.26E-02
32840	52251.3922	1.35E-02
33070	52617.34288	1.45E-02
33320	53015.11535	1.56E-02
33510	53317.42243	1.65E-02
33710	53635.64041	1.75E-02
33960	54033.41289	1.85E-02
40310		

Table A- 7: Flange Coupon Results Specimen 1

Sample 5 B1		
Area =	0.76	in^2
Load (lbs)	**Stress (psi)**	**Strain**
500	661.37	0.00E+00
1000	1322.74	2.60E-05
1500	1984.10	4.90E-05
2000	2645.47	7.20E-05
2500	3306.84	9.50E-05
2800	3703.66	1.18E-04
3000	3968.21	1.32E-04
3500	4629.57	1.41E-04
4000	5290.94	1.63E-04
4510	5965.54	1.85E-04
5000	6613.68	2.10E-04
6000	7936.41	2.30E-04
6590	8716.83	2.77E-04
7000	9259.15	3.02E-04
8000	10581.88	3.22E-04
9000	11904.62	3.67E-04
10000	13227.36	4.12E-04
11000	14550.09	4.56E-04
12000	15872.83	5.00E-04
13000	17195.56	5.45E-04
14000	18518.30	5.88E-04
15160	20052.67	6.32E-04
16000	21163.77	6.81E-04
17000	22486.50	7.20E-04
18000	23809.24	7.64E-04
19000	25131.98	8.09E-04
20000	26454.71	8.52E-04
21000	27777.45	8.95E-04
22000	29100.18	9.39E-04
23000	30422.92	9.82E-04
24000	31745.65	1.03E-03
25000	33068.39	1.07E-03
26000	34391.12	1.11E-03
27000	35713.86	1.15E-03
28000	37036.60	1.20E-03
29000	38359.33	1.24E-03
30000	39682.07	1.29E-03
31000	41004.80	1.33E-03
32000	42327.54	1.37E-03
33000	43650.27	1.42E-03
34090	45092.06	1.46E-03
35020	46322.20	1.51E-03
36000	47618.48	1.55E-03
38000	50263.95	1.59E-03
40030	52949.11	1.68E-03
42000	55554.89	1.77E-03

Sample 6 B1		
Area =	0.76 in^2	
Load (lbs)	**Stress (psi)**	**Strain**
500	662.24	2.50E-05
1000	1324.49	5.40E-05
1500	1986.73	8.30E-05
2000	2648.98	1.10E-04
2500	3311.22	1.40E-04
3000	3973.47	1.58E-04
3500	4635.71	1.82E-04
4000	5297.96	2.02E-04
4500	5960.20	2.25E-04
5000	6622.45	2.44E-04
5500	7284.69	2.72E-04
6000	7946.94	2.93E-04
6500	8609.18	3.15E-04
7000	9271.42	3.37E-04
7500	9933.67	3.60E-04
8000	10595.91	3.83E-04
8500	11258.16	4.06E-04
9000	11920.40	4.28E-04
10000	13244.89	4.71E-04
11000	14569.38	5.15E-04
12000	15893.87	5.57E-04
13000	17218.36	6.00E-04
14000	18542.85	6.44E-04
15000	19867.34	6.86E-04
16000	21191.83	7.31E-04
17000	22516.32	7.75E-04
18000	23840.81	8.20E-04
19000	25165.30	8.64E-04
20000	26489.79	9.12E-04
21000	27814.27	9.53E-04
22000	29138.76	9.98E-04
23000	30463.25	1.04E-03
24000	31787.74	1.09E-03
25000	33112.23	1.13E-03
26000	34436.72	1.17E-03
27000	35761.21	1.22E-03
28000	37085.70	1.27E-03
29000	38410.19	1.30E-03
30000	39734.68	1.35E-03
31000	41059.17	1.39E-03
32000	42383.66	1.44E-03
33000	43708.15	1.48E-03
34000	45032.64	1.53E-03
35000	46357.12	1.57E-03
36000	47681.61	1.62E-03
38200	50595.49	1.71E-03
39100	51787.53	1.75E-03
40000	52979.57	1.78E-03
51800		

Sample 7, B1		
Area =	0.76	in^2
Load (lbs)	**Stress (psi)**	**Strain**
1000	1320.13	5.90E-05
1500	1980.20	8.00E-05
2000	2640.26	9.90E-05
2500	3300.33	1.25E-04
3500	4620.46	1.66E-04
4000	5280.53	1.86E-04
4500	5940.59	2.08E-04
5000	6600.66	2.29E-04
5500	7260.73	2.53E-04
6000	7920.79	2.73E-04
6500	8580.86	2.93E-04
7000	9240.92	3.17E-04
8000	10561.06	3.59E-04
8500	11221.12	3.82E-04
9000	11881.19	4.03E-04
10000	13201.32	4.45E-04
11000	14521.45	4.88E-04
12000	15841.58	5.32E-04
13000	17161.72	5.76E-04
14000	18481.85	6.18E-04
15000	19801.98	6.59E-04
16000	21122.11	7.03E-04
17100	22574.26	7.49E-04
18000	23762.38	7.99E-04
19000	25082.51	8.37E-04
20000	26402.64	8.75E-04
21000	27722.77	9.18E-04
22000	29042.90	9.62E-04
23000	30363.04	1.01E-03
24000	31683.17	1.05E-03
25000	33003.30	1.10E-03
26000	34323.43	1.13E-03
27000	35643.56	1.18E-03
28000	36963.70	1.22E-03
29000	38283.83	1.26E-03
30000	39603.96	1.31E-03
31000	40924.09	1.36E-03
32000	42244.22	1.40E-03
33000	43564.36	1.44E-03
34000	44884.49	1.49E-03
35000	46204.62	1.53E-03
36000	47524.75	1.57E-03
37000	48844.88	1.62E-03
38000	50165.02	1.67E-03
39000	51485.15	1.73E-03
40000	52805.28	2.39E-03
40400	53333.33	2.41E-03
39800	52541.25	3.18E-03
39400	52013.20	7.45E-03
39100	51617.16	1.11E-02
39200	51749.17	1.61E-02
39400	52013.20	1.93E-02
39600	52277.23	
52000		

	E =	30500000.00

Table A- 8: Flange Coupon Results Specimen 2

Sample 8, B2,1		
Area =	0.75	In^2
Load (lbs)	Stress (psi)	Strain
500	663.13	2.70E-05
1000	1326.25	5.20E-05
1500	1989.38	7.70E-05
2000	2652.50	9.90E-05
2500	3315.63	1.24E-04
3000	3978.75	1.44E-04
3500	4641.88	1.65E-04
4000	5305.00	1.86E-04
4500	5968.13	2.10E-04
5000	6631.26	2.31E-04
5500	7294.38	2.53E-04
6000	7957.51	2.71E-04
6500	8620.63	2.97E-04
7000	9283.76	3.18E-04
8000	10610.01	3.61E-04
9000	11936.26	4.05E-04
10000	13262.51	4.48E-04
11000	14588.76	4.92E-04
12000	15915.01	5.33E-04
13000	17241.26	5.75E-04
14000	18567.52	6.20E-04
15000	19893.77	6.61E-04
16000	21220.02	7.02E-04
17000	22546.27	7.43E-04
18000	23872.52	7.84E-04
19000	25198.77	8.23E-04
20000	26525.02	8.64E-04
21000	27851.27	9.04E-04
22000	29177.53	9.44E-04
23000	30503.78	9.85E-04
24000	31830.03	1.03E-03
25000	33156.28	1.06E-03
26000	34482.53	1.10E-03
27000	35808.78	1.14E-03
28000	37135.03	1.18E-03
29000	38461.28	1.22E-03
30000	39787.53	1.25E-03
31000	41113.79	1.29E-03
32000	42440.04	1.33E-03
33000	43766.29	1.38E-03
34000	45092.54	1.41E-03
35000	46418.79	1.45E-03
36000	47745.04	1.49E-03
37000	49071.29	1.54E-03
38000	50397.54	1.59E-03
39000	51723.79	1.63E-03
40000	53050.05	1.68E-03
41000	54376.30	1.73E-03
40600	53845.80	7.50E-03
42600	56498.30	4.50E-03
44300	58752.93	5.00E-03
45300	60079.18	5.35E-03
46900	62201.18	5.40E-03
47600	63129.55	5.50E-03
52500		

Sample 9, B2,2		
Area =	0.76	In^2
Load (lbs)	Stress (psi)	Strain
500	660.50	2.60E-05
1000	1320.99	4.50E-05
1500	1981.49	6.70E-05
2000	2641.98	8.60E-05
2500	3302.48	1.10E-04
3000	3962.97	1.29E-04
3500	4623.47	1.52E-04
4000	5283.96	1.70E-04
4500	5944.46	1.92E-04
5000	6604.95	2.13E-04
5500	7265.45	2.35E-04
6000	7925.94	2.56E-04
6500	8586.44	2.78E-04
7000	9246.93	2.98E-04
8000	10567.92	3.38E-04
9000	11888.91	3.81E-04
10000	13209.90	4.24E-04
11000	14530.89	4.65E-04
12000	15851.88	5.08E-04
13000	17172.87	5.49E-04
14000	18493.86	5.96E-04
15000	19814.85	6.35E-04
16000	21135.84	6.80E-04
17000	22456.83	7.21E-04
18000	23777.82	7.64E-04
19000	25098.81	8.08E-04
20000	26419.80	8.52E-04
21000	27740.79	8.91E-04
22000	29061.78	9.05E-04
23000	30382.77	9.80E-04
24000	31703.76	1.02E-03
25000	33024.75	1.06E-03
26000	34345.74	1.10E-03
27000	35666.73	1.15E-03
28000	36987.72	1.19E-03
29000	38308.71	1.23E-03
30000	39629.70	1.27E-03
31000	40950.69	1.31E-03
32000	42271.68	1.36E-03
33000	43592.67	1.40E-03
34000	44913.66	1.44E-03
35000	46234.65	1.48E-03
36000	47555.64	1.53E-03
37000	48876.63	1.56E-03
38000	50197.62	1.61E-03
39000	51518.61	1.64E-03
39100	51650.71	8.00E-03
38900	51386.51	1.00E-02
39000	51518.61	1.40E-02
39000	51518.61	1.20E-02
38900	51386.51	9.00E-03
51700		

Sample 16, B2,3		
Area =	0.75	In^2
Load (lbs)	Stress (psi)	Strain
500	662.69	2.70E-05
1000	1325.37	4.80E-05
1500	1988.06	7.10E-05
2000	2650.74	9.10E-05
2500	3313.43	1.18E-04
3000	3976.11	1.38E-04
3500	4638.80	1.61E-04
4000	5301.48	1.80E-04
4500	5964.17	2.02E-04
5000	6626.85	2.23E-04
5500	7289.54	2.46E-04
6000	7952.22	2.66E-04
6500	8614.91	2.89E-04
7000	9277.59	3.10E-04
8000	10602.96	3.52E-04
9000	11928.33	3.94E-04
10000	13253.71	4.39E-04
11000	14579.08	4.83E-04
12000	15904.45	5.25E-04
13000	17229.82	5.68E-04
14000	18555.19	6.11E-04
15000	19880.56	6.53E-04
16000	21205.93	6.96E-04
17000	22531.30	7.40E-04
18000	23856.67	7.79E-04
19000	25182.04	8.15E-04
20000	26507.41	8.59E-04
21000	27832.78	9.42E-04
22000	29158.15	9.87E-04
23000	30483.52	1.02E-03
24000	31808.89	1.07E-03
25000	33134.26	1.11E-03
26000	34459.63	1.15E-03
27000	35785.00	1.20E-03
28000	37110.37	1.23E-03
29000	38435.74	1.27E-03
30000	39761.12	1.31E-03
31000	41086.49	1.34E-03
32000	42411.86	1.39E-03
33000	43737.23	1.42E-03
34000	45062.60	1.47E-03
35000	46387.97	1.51E-03
36000	47713.34	1.55E-03
37000	49038.71	1.58E-03
38000	50364.08	1.65E-03
39000	51689.45	1.72E-03
40200	53279.89	2.26E-03
39400	52219.60	3.96E-03
39400	52219.60	5.56E-03
39500	52352.14	7.39E-03
39500	52352.14	8.68E-03
39500	52352.14	1.01E-02
39500	52352.14	1.09E-02
39400	52219.60	1.16E-02
39300	52087.06	1.23E-02
39200	51954.52	1.38E-02
39200	51954.52	1.45E-02
39200	51954.52	1.62E-02
39400	52219.60	1.75E-02

39400	52219.60	1.84E-02
39400	52219.60	1.94E-02
39300	52087.06	1.99E-02
39200	51954.52	
52000		

E =	**3.05E+07**

Table A- 9: Web Coupon Results Specimen 1

Sample 10, U1,1		
Area =	0.76	in^2
Load (lbs)	Stress (psi)	Strain
500	662.25	2.50E-05
1000	1324.49	4.70E-05
1500	1986.74	7.10E-05
2000	2648.98	9.10E-05
2500	3311.23	1.18E-04
3000	3973.48	1.38E-04
3500	4635.72	1.59E-04
4000	5297.97	1.80E-04
4500	5960.22	2.01E-04
5000	6622.46	2.23E-04
5500	7284.71	2.46E-04
6000	7946.95	2.67E-04
6500	8609.20	2.89E-04
7000	9271.45	3.09E-04
8000	10595.94	3.51E-04
9000	11920.43	3.96E-04
10000	13244.92	4.37E-04
11000	14569.42	4.84E-04
12000	15893.91	5.28E-04
13000	17218.40	5.71E-04
14000	18542.89	6.20E-04
15000	19867.39	6.59E-04
16000	21191.88	7.04E-04
17000	22516.37	7.45E-04
18000	23840.86	7.89E-04
19000	25165.35	8.33E-04
20000	26489.85	8.81E-04
21000	27814.34	9.20E-04
22000	29138.83	9.63E-04
23000	30463.32	1.01E-03
24000	31787.82	1.06E-03
25000	33112.31	1.10E-03
26000	34436.80	1.14E-03
27000	35761.29	1.19E-03
28000	37085.79	1.23E-03
29000	38410.28	1.27E-03
30000	39734.77	1.32E-03
31000	41059.26	1.36E-03
32000	42383.76	1.41E-03
33000	43708.25	1.45E-03
34000	45032.74	1.49E-03
35000	46357.23	1.54E-03
36000	47681.72	1.58E-03
37000	49006.22	1.63E-03
38000	50330.71	1.67E-03
39000	51655.20	1.72E-03
40000	52979.69	1.76E-03
41000	54304.19	1.81E-03
42000	55628.68	1.85E-03
43000	56953.17	1.90E-03
41200	54569.08	1.51E-02
41000	54304.19	1.75E-02
42600	56423.37	9.66E-03
42800	56688.27	9.80E-03
43000	56953.17	1.00E-02
43600	57747.87	1.02E-02
44100	58410.11	1.10E-02
44500	58939.91	1.13E-02

Sample 11, U1,2		
Area =	0.75	in^2
Load (lbs)	Stress (psi)	Strain
500	663.13	2.30E-05
1000	1326.25	4.70E-05
1500	1989.38	6.90E-05
2000	2652.50	9.20E-05
2500	3315.63	1.16E-04
3000	3978.75	1.40E-04
3500	4641.88	1.59E-04
4500	5968.13	1.99E-04
5100	6763.88	2.27E-04
6000	7957.51	2.65E-04
10000	13262.51	4.72E-04
13000	17241.26	5.77E-04
15000	19893.77	6.56E-04
16000	21220.02	7.09E-04
18000	23872.52	7.92E-04
19000	25198.77	8.38E-04
20000	26525.02	8.89E-04
21000	27851.27	9.28E-04
22100	29310.15	9.74E-04
23000	30503.78	1.01E-03
24000	31830.03	1.06E-03
25000	33156.28	1.10E-03
26000	34482.53	1.15E-03
27000	35808.78	1.19E-03
28000	37135.03	1.24E-03
29000	38461.28	1.28E-03
30000	39787.53	1.33E-03
31000	41113.79	1.38E-03
32000	42440.04	1.42E-03
33000	43766.29	1.47E-03
34000	45092.54	1.51E-03
35000	46418.79	1.56E-03
36000	47745.04	1.60E-03
37000	49071.29	1.65E-03
38000	50397.54	1.69E-03
39000	51723.79	1.74E-03
40000	53050.05	1.78E-03
41000	54376.30	1.83E-03
39800	52784.80	1.06E-02
39700	52652.17	1.85E-02
39600	52519.55	1.93E-02
40700	53978.42	1.99E-02
52400	69495.56	

Sample 12, U1,3		
Area=	0.74	in^2
Load (lbs)	Stress (psi)	Strain
500	672.06	2.60E-05
1000	1344.11	4.40E-05
1500	2016.17	6.90E-05
2000	2688.23	8.80E-05
2500	3360.28	1.15E-04
3000	4032.34	1.36E-04
3500	4704.40	1.57E-04
4000	5376.45	1.78E-04
4500	6048.51	1.98E-04
5000	6720.57	2.22E-04
6000	8064.68	2.65E-04
7000	9408.79	3.05E-04
8000	10752.90	3.48E-04
9000	12097.02	3.94E-04
10000	13441.13	4.37E-04
11000	14785.24	4.82E-04
12000	16129.36	5.28E-04
13000	17473.47	5.71E-04
14000	18817.58	6.15E-04
15000	20161.70	6.59E-04
16000	21505.81	7.05E-04
17000	22849.92	7.47E-04
18000	24194.04	7.94E-04
19000	25538.15	8.37E-04
20000	26882.26	8.80E-04
21000	28226.38	9.24E-04
22000	29570.49	9.68E-04
23000	30914.60	1.01E-03
24000	32258.71	1.06E-03
25000	33602.83	1.10E-03
26000	34946.94	1.15E-03
27000	36291.05	1.19E-03
28000	37635.17	1.24E-03
29000	38979.28	1.28E-03
30000	40323.39	1.33E-03
31000	41667.51	1.37E-03
32000	43011.62	1.42E-03
33000	44355.73	1.46E-03
34000	45699.85	1.50E-03
35000	47043.96	1.55E-03
36000	48388.07	1.60E-03
37000	49732.19	1.64E-03
38000	51076.30	1.68E-03
39000	52420.41	1.73E-03
40000	53764.52	1.77E-03
41000	55108.64	1.81E-03
39900	53630.11	9.03E-03
40200	54033.35	1.74E-02
52400	70431.53	

E =	3.03E+07

44800	59337.26	1.19E-02
45500	60264.40	1.20E-02
46100	61059.10	1.22E-02
46600	61721.34	1.23E-02
47200	62516.04	1.24E-02
47600	63045.84	1.26E-02
48000	63575.63	1.28E-02
48600	64370.33	1.30E-02
49300	65297.47	1.32E-02
49700	65827.27	1.33E-02
50000	66224.62	1.35E-02
53000	70198.09	

Table A- 10: Web Coupon Results Specimen 2

Sample 13 U2,1		
Area =	0.76	in^2
Load (lbs)	Stress (psi)	Strain
500	662.03	2.60E-05
1000	1324.06	4.70E-05
2000	2648.11	7.30E-05
3000	3972.17	1.25E-04
4000	5296.23	1.47E-04
5000	6620.28	1.76E-04
6000	7944.34	2.24E-04
7000	9268.40	2.65E-04
8000	10592.46	2.91E-04
9000	11916.51	3.17E-04
10000	13240.57	3.40E-04
11000	14564.63	3.62E-04
12000	15888.68	3.82E-04
13000	17212.74	4.24E-04
14000	18536.80	4.66E-04
15000	19860.85	5.12E-04
16000	21184.91	5.58E-04
17000	22508.97	6.01E-04
18000	23833.03	6.44E-04
19100	25289.49	6.88E-04
20000	26481.14	7.30E-04
21000	27805.20	7.70E-04
22000	29129.25	8.10E-04
23000	30453.31	8.54E-04
24000	31777.37	8.94E-04
25000	33101.42	9.33E-04
26000	34425.48	9.78E-04
27000	35749.54	1.01E-03
28000	37073.60	1.06E-03
29000	38397.65	1.10E-03
30000	39721.71	1.14E-03
31000	41045.77	1.18E-03
32000	42369.82	1.21E-03
33000	43693.88	1.25E-03
34000	45017.94	1.29E-03
35000	46341.99	1.32E-03
36000	47666.05	1.37E-03
37000	48990.11	1.40E-03
38000	50314.17	1.44E-03
39000	51638.22	1.48E-03
40000	52962.28	1.52E-03
41000	54286.34	1.57E-03
42000	55610.39	1.60E-03
39600	52432.66	1.64E-03
52400		1.68E-03
		1.72E-03
		1.76E-03
		4.45E-03

Sample 14 U2,2		
Area =	0.75	in^2
Load (lbs)	Stress (psi)	Strain
600	796.81	3.10E-05
1000	1328.02	4.70E-05
1500	1992.03	6.70E-05
2000	2656.04	8.80E-05
2500	3320.05	1.10E-04
3000	3984.06	1.31E-04
3500	4648.07	1.52E-04
4000	5312.08	1.73E-04
4500	5976.10	1.97E-04
5000	6640.11	2.18E-04
5500	7304.12	2.41E-04
6000	7968.13	2.61E-04
6700	8897.74	2.93E-04
8000	10624.17	3.48E-04
9000	11952.19	3.91E-04
10000	13280.21	4.38E-04
11000	14608.23	4.83E-04
12000	15936.25	5.25E-04
13000	17264.28	5.67E-04
14000	18592.30	6.10E-04
15000	19920.32	6.50E-04
16000	21248.34	6.99E-04
17000	22576.36	7.40E-04
18000	23904.38	7.82E-04
19000	25232.40	8.27E-04
20000	26560.42	8.70E-04
21000	27888.45	9.12E-04
22000	29216.47	9.54E-04
23000	30544.49	9.97E-04
24000	31872.51	1.04E-03
25000	33200.53	1.08E-03
26000	34528.55	1.13E-03
27000	35856.57	1.17E-03
28000	37184.59	1.21E-03
29000	38512.62	1.25E-03
30000	39840.64	1.30E-03
31000	41168.66	1.34E-03
32000	42496.68	1.38E-03
33000	43824.70	1.42E-03
34000	45152.72	1.47E-03
35000	46480.74	1.51E-03
36000	47808.76	1.55E-03
37000	49136.79	1.59E-03
38000	50464.81	1.63E-03
39000	51792.83	1.68E-03
40000	53120.85	1.72E-03
40600	53917.66	1.75E-03
38600	51261.62	7.12E-03
38700	51394.42	1.49E-02
50700		

Sample 15 U2,3		
Area =	0.75	in^2
Load (lbs)	Stress (psi)	Strain
500	662.46	2.40E-05
1000	1324.93	4.50E-05
1500	1987.39	6.80E-05
2000	2649.86	9.10E-05
2500	3312.32	1.17E-04
3100	4107.28	1.41E-04
3500	4637.25	1.59E-04
4000	5299.72	1.80E-04
5000	6624.65	2.21E-04
6000	7949.58	2.66E-04
7000	9274.51	3.10E-04
8000	10599.44	3.56E-04
9000	11924.37	3.98E-04
10000	13249.30	4.42E-04
11000	14574.23	4.86E-04
12000	15899.16	5.32E-04
13000	17224.09	5.73E-04
14000	18549.02	6.13E-04
15000	19873.95	6.55E-04
16000	21198.88	6.97E-04
17000	22523.81	7.40E-04
18000	23848.74	7.90E-04
19000	25173.67	8.34E-04
20000	26498.59	8.71E-04
21000	27823.52	9.16E-04
22000	29148.45	9.61E-04
23000	30473.38	1.01E-03
24000	31798.31	1.04E-03
25000	33123.24	1.09E-03
26000	34448.17	1.14E-03
27000	35773.10	1.17E-03
28000	37098.03	1.22E-03
29000	38422.96	1.27E-03
30000	39747.89	1.30E-03
31000	41072.82	1.34E-03
32000	42397.75	1.39E-03
33000	43722.68	1.43E-03
34000	45047.61	1.48E-03
35000	46372.54	1.52E-03
36000	47697.47	1.55E-03
37000	49022.40	1.60E-03
38000	50347.33	1.65E-03
39000	51672.26	1.69E-03
40000	52997.19	1.74E-03
41000	54322.12	1.78E-03
42000	55647.05	1.82E-03
43000	56971.98	1.86E-03
41400	54852.09	1.91E-03
41200	54587.11	2.35E-03
41000	54322.12	7.23E-03
41000	54322.12	1.21E-02
41000	54322.12	1.73E-02
52500		

E =	3.08E+07

BIBLIOGRAPHY

1. ABAQUS, (2003) *ABAQUS Theory Manual,* Hibbitt, Karlsson & Sorensen, Inc., Pawtucket, Rhode Island, USA.

2. AASHTO (2001) Standard Specifications for Structural Supports for Highway Signs, Luminaires and Traffic Signals, 4th Edition, *American Association of State Highway and Transportation Officials, Inc.*, Washington D.C.

3. AISC (2000) Load and Resistance Factor Design Specification for Steel Hollow Structural Sections, *American Institute of Steel Construction*, Chicago, Illinois, November 10.

4. AISC (2001) Manual of Steel Construction - Load and Resistance Factor Design 3rd Edition, *American Institute of Steel Construction*, Chicago, Illinois, November.

5. AISC (1997a) Hollow Structural Sections Connections Manual, *American Institute of Steel Construction*, Chicago, Illinois.

6. AISC (1997b) Specification for the Design of Steel Hollow Structural Sections, *American Institute of Steel Construction*, Chicago, Illinois, April 15.

7. AWS (2004) D1.1 Structural Welding Code – Steel 19th Edition, *American Welding Society*, Miami, Florida, October 15.

8. Bathe, K.J. (1996) *Finite Element Procedures,* Prentice-Hall, Inc., Upper Saddle River, New Jersey.

9. Boyle, R., Earls, C.J., (2004) "Full-Scale Testing of Tri-Chord Sign Structure Connections" *Report No. CE/ST 28*, Department of Civil and Environmental Engineering, University of Pittsburgh, Pittsburgh, Pennsylvania.

10. Chen, W.F., Ross, D.A. (1977), "Tests of Fabricated Tubular Columns," *Journal of the Structural Division*, ASCE, Volume 103, No. ST3.

11. Clough, R.W., (1965), The Finite Element Method in Structural Mechanics, in O.C. Zienkiewicz et al. (1st Ed), Stress Analysis, John Wiley and Sons, London.

12. Dieter, G. E. (1986), Mechanical Metallurgy 3rd Ed., McGraw Hill, ISBN 0-07-016893-8.

13. Galambos, T. (1998), Guide to Stability Design Criteria for Metal Structures, 5th Ed., Wiley, ISBN 0471127426.

14. Greco, N., Earls, C.J., (2003) "Structural Ductility in Hybrid High Performance Steel Beams," *Journal of Structural Engineering,* Vol. 129, No. 12, American Society of Civil Engineers, Reston, Virginia, pp.1584-1595.

15. Kosteski, N., Packer, J.A., (2003) "Longitudinal Plate and Through Plate-to-Hollow Structural Section Welded Connections," *Journal of Structural Engineering,* Vol. 129, No. 4, American Society of Civil Engineers, Reston, Virginia.

16. Kurobane, K., Makino, Y., Mitsui, Y. (1976) "Ultimate Strength Formulae for Simple Tubular Joints." IIW Doc. XV-385-76. Dept. of Architecture, Kumamoto Univ.

17. Kurobane, K., Makino, Y., Mitsui, Y. (1980) "Re-Analysis of Ultimate Strength Data For Truss Connections in Circular Hollow Sections." IIW Doc. XV-461-80. Dept. of Architecture, Kumamoto Univ.

18. Kurobane, K. (1981), "New Developments and Practices in Tubular Joint Design." IIW Doc. XV-488-81. Dept. of Architecture, Kumamoto Univ.

19. Li, Y., Earls, C.J. (2002), "Design Recommendations for the Proportioning and Detailing of Long-Span Tri-Chord Sign Structures, Phase I," *Report No. CE/ST 24,* Department of Civil and Environmental Engineering, University of Pittsburgh, Pittsburgh, Pennsylvania.

20. Marshall, P.W. (1992), Design of Welded Tubular Connections – Basis and Use of AWS Code Provisions, Elsevier, Amsterdam, ISBN 0 444 88201 4.

21. Packer, J.A., Henderson, J.E. (1997), Hollow Structural Section Connections and Trusses, second edition, *Design Guide,* Canadian Institute of Steel Construction, Willowdale, Ontario, Canada, June.

22. Prion, H.G.L., Birkemoe, P.C. (1988), "Experimental Behaviour of Unstiffened Fabricated Tubular Steel Beam-Columns," *Publ. No. 88-3*, Department of Divil Engineering, University of Toronto, Toronto, Ontario, Canada.

23. PENNDOT (2003a) "Overhead Sign Structures – 2-Post & 4-Post Tri-chord Truss Spans From 18 288 to 73 152 (60' to 240') Notes and Design Criteria", *Standard Drawings for Bridge Design - BD 644-M,* Commonwealth of Pennsylvania Department of Transportation, Harrisburg, Pennsylvania.

24. PENNDOT (2003b) "Overhead Sign Structures – 2-Post & 4-Post Tri-chord Truss Spans From 18 288 to 73 152 (60' to 240') Notes and Design Criteria", *Standard Drawings for Bridge Construction - BC 744-M,* Commonwealth of Pennsylvania Department of Transportation, Harrisburg, Pennsylvania.

25. Popov, E.P., Zayas, V.A., Mahin, S.A. (1979), "Cyclic Inelastic Buckling of Thin Tubular Columns," *Journal of the Structural Division*, ASCE, Volume 105, No. ST11.

26. Soh, C.K., Chan, T.K., Yu, S.K., (2000) "Limit Analysis of Ultimate Strength of Tubular X-Joints," *Journal of Structural Engineering,* Vol. 126, No. 7 American Society of Civil Engineers, Reston, Virginia.

27. Stamenkovic, A., Sparrow, K. (1983), "Load Interaction in T-Joints of Steel Circular Hollow Sections," *Journal of Structural Engineering*, ASCE, Volume 109, No. 9.

28. Thomas, S., Earls, C.J., (2003) "Cross Sectional Compactness and Bracing Requirements for HPS483W Girders," *Journal of Structural Engineering,* Vol. 129, No. 12 American Society of Civil Engineers, Reston, Virginia, pp. 1569-1583.

29. Toma, S., Chen, W.F. (1979), "Analysis of Fabricated Tubular Columns," *Journal of the Structural Division*, ASCE, Volume 105, No. ST11.

30. Wardenier, J. (1982), Hollow Section Joints, Delft University Press, Delft, ISBN 90.6275.084.2.

31. Wardenier, J., Kurobane, Y., Packer, J.A., Dutta, D., and Yeomans, N. (1991) Design Guide for Circular Hollow Section (CHS) Joints Under Predominantly Static Loading. CIDECT (ed.) and Verlag TUV Rheinland GmbH, Koln, Federal Republic of Germany.

32. Young, W. (1989), Roark's Formulas for Stress and Strain 6th Edition, McGraw-Hill, New York, ISBN 0-07-072541-1.

Pennsylvania Department of Transportation
PENNDOT

DATE: December 13, 2004

SUBJECT: Buckling Strength of Circular Tubes in Sign Structures
Report No CE/ST 29

TO: Tom Macioce, P.E.
Assistant Chief Bridge Engineer
Bureau of Design
Bridge Quality Assurance Division

FROM: Christopher J. Earls, Ph.D.
Associate Professor and William Kepler
Whiteford Faculty Fellow
University of Pittsburgh

I have reviewed your comments and offer the following responses:

Non-editorial

1. The report should describe the basis of selecting the capacity equations such as lower bound strength, best fit of the data or a certain confidence limit.
Since the capacity equations are developed based on curved fitting to analytical data, there is no scatter to the results for statistical analysis. The equations describe the nominal capacity with no variability in material and geometric properties. Mean, standard deviation, confidence limits, etc. do not apply in this case. This is clarified in the final version of the report.

2. The design capacity equations appear to predict the ultimate strength of the tube/connection. Per the scope of work, a recommended Factor of Safety is to be provided since sign structures are currently designed with the allowable stress approach. The recommended Factor of Safety should be consistent with the AASHTO sign specification accounting for the failure mode of this structural component, consequences of this type of failure, etc. As a point of reference, a minimum factor of safety per the AWS D.1. Structural welding Code would be 1.4.
The nominal factor of safety (SF) prescribed by AWS D1.1 is 1.8 (see section C2.24.1.1 – Figure C2.9). This is based on the limit state of ultimate plastic collapse, which is a consistent limit state observed in the bearing connection under investigation. Thus, the same SF is recommended until further experimental testing is conducted. For this limit state, variations in yield strength (Fy) and chord wall thickness (t) will dominate the

uncertainty in the overall connection capacity. This is addressed in the final version of the report.

3. The report describes the modulus of elasticity for the pipe chord material as 22,000 ksi which is well below the standard/theoretical value of 29,000 ksi. Based on discussions with experts in the field of steel material, the reported value is an apparent value due to possible inaccuracies in the instruments used to determine the modulus and/or inaccuracies in the specimen geometry. Section 5.1 should be reworded to clarify the issue with the modulus of elasticity as the present write-up is questionable/arguable.
   Due to the extensive cold-working processes applied to the parent steel plate in the manufacturing of the round tubular member, the stress-strain behavior of the material has been altered from the well-documented linear elastic-plastic response. For tubular steels, the onset of nonlinear behavior begins at stresses well below the yield stress. To model this analytically in the context of the von Mises metal plasticity model, an "effective" elastic modulus of 21,000ksi has been utilized to approximate the nonlinear elastic behavior of the steel. This is clarified in the final version of the report.

4. At a status meeting the issue of a deflection limit was discussed as possibly limiting the capacity of the tube, yet this deflection limit was not presented in the report. A deflection limit should be provided or a write-up dismissing the deflection limit as a critical design criteria should be provided.
   No clear guidance could be found in the existing specifications or research for the defining of a deflection limit criterion, and what can be considered "excessive deflection" in tubular connections. Capacity has been defined as the first peak in the load-deflection response, which appears to be consistent with the basis of the AWS code equations.

5. Recommended capacity equations are provided for axial load capacity and moment capacity, but a capacity equation for combined bending and axial is not provided. Since the structural tees are rigidly connected to the chords, the tees carry axial forces and moments. A capacity equation for combined bending and axial should be provided.
   A quadratic interaction equation is found to fit the test data for combined axial load and moment. This is addressed in the final version of the report.

6. Another point that was discussed at the status meeting was the critical condition during erection when the truss is placed on the towers but the end cap and U-bolts have not been installed to restrain the open end of the truss chord. It would be beneficial to provide recommendations on this critical condition such as: install the end caps prior to setting the truss on the tower supports or support the truss with the crane until the U-bolts are installed.
   After a cursory review of the U-bolt connection, this may have a minor strengthening effect on the overall bearing capacity. However, it cannot be recommended to count on this component for bearing strength since it may not have a tight fit and/or it may be removed in the future. Also, the U-bolt itself is not a structural- grade fastener.

Editorial

E1. The report will have to be finalized to provide page numbers, list of figures and tables, etc.

If you have any questions, please call me at (717) 787-7504.

This has been addressed in the final version of the report.

University of Pittsburgh

School of Engineering
Department of Civil & Environmental Engineering

949 Benedum Hall
Pittsburgh, PA 15261-2294
412-624-9870
Fax: 412-624-0135

March 18, 2005

Mr. Michael Bonini
PennDOT Research
Commonwealth Keystone Building
400 North Street – 6th Floor
Harrisburg, PA 17120

Dear Mike,

Enclosed please find the final report for the ITQ project "Buckling Strength of Circular Tubes in Sign Structures." We have enjoyed working on this project and hope that the Department will find the results valuable and useful.

Sincerely Yours,

Christopher J. Earls, Ph.D., P.E.
Associate Professor and Chairman
William Kepler Whiteford Faculty Fellow
(412) 624-9575
earls@engr.pitt.edu